TABLE OF CONTENTS

LIST OF TABLES AND FIGURES

ACKNOWLEDGMENTS

This project was made possible by funding provided by the U. S. Minerals Management Service. Special appreciation is expressed to Dr. Charles Smith, Research Program Manager, Offshore Minerals Management Technology Assessment and Research Branch, Herndon, Virginia. Dr. Smith provided a number of key background references for the project and provided the overall direction for this work.

Detailed background on one of the platforms studied during this project was provided by Amoco Production Company. Appreciation is expressed to Mr. Gary Imm and Mr. James Light for providing information on this platform.

Detailed background on two of the platforms studied during this project was provided by Chevron Petroleum Technology Company. Appreciation is expressed to Mr. Dirceau Bothelo for providing information on these platforms.

The non-linear analyses performed during this project were performed using software provided by SINTEF (USFOS) and Det Norske Veritas (SESAM pre and post processors). Appreciation is expressed to SINTEF and DNV for the assistance they provided during this project. In addition, Mr. Øyvind Hellan of SINTEF provided extensive assistance during the initiation of this project by implementing the software and providing instructions on the background, use and limitations of this software.

This project was conducted in conjunction with a Joint Industry Project titled "Screening Methodologies for Use in Platform Assessments and Requalifications." Appreciation is expressed to the sponsors of this project including Arco Exploration Co., Exxon Production Co., UNOCAL Corporation, Shell Oil Co., Mobil Research and Development Co., the California State Lands Commission and the California National Sea Grant College Programs.

1.0 INTRODUCTION

Non-linear ultimate-limit-state (ULS) analysis is one of the most precise means available for determining the ultimate lateral load resisting capacity of offshore structures. While it is possible to build full scale models of the offshore platforms, it is not possible to test these models in the laboratory setting. Therefore, these models should be constructed in actual ocean conditions and subjected to actual storm, earthquake and ice loadings to obtain an accurate measure of their ultimate lateral load resistance. Since nature controls the environmental loading conditions, it may take scores of years for a significant loading condition to occur. For most engineering purposes, this time period is much too long. In addition, the cost of such an exercise is extremely prohibitive.

Scaled down tests also have many problems. First, it is nearly impossible to accurately model loadings from extreme waves and storms in a laboratory setting. Second, even scaled down tests are extremely expensive and take considerable time to perform. Hence, non-linear computer simulations using appropriate loading and behavior analyses are a worthy substitution for actual platform testing.

Currently, in the United States, the building code for new offshore structures prescribes linear-elastic design procedures (API, 1993). Non-linear performance is taken into account by load reduction factors. However, as computers become more powerful and non-linear software becomes more user-friendly, the trend toward performing non-linear

analyses is increasing. Several other countries have made significant advances in using non-linear Ultimate Limit State (ULS) analyses for design of new platforms and requalification of existing platforms. (Hellan, 1994). While the United States has continued to use linear-elastic methods for new design, it has begun to realize the benefit of non-linear analyses for requalification of existing platforms (API, 1994). Non-linear analysis has allowed engineers to analytically examine the ultimate limit of structures, which has helped to decrease the reliance on conservative assumptions concerning non-linear behavior.

Construction of new offshore platforms is leveling off or even declining, but there are over 6,000 existing platforms, over 3,800 of which are in the Gulf of Mexico (Oceanweather, 1992). The majority of these existing platforms were designed to much lower wave heights and load levels than are prescribed in current codes for design of new platforms. Therefore, these platforms rarely satisfy current design code regulations for new platforms. However, meeting current code requirements for new structures is not the aim of most requalification efforts.

Of primary concern to regulatory agencies and platform owners is the safety of platform personnel, the protection of the environment and the preservation of financial resources (not necessarily in that order). It is possible to meet these goals even if a platform does not comply with current code regulations.

"Failure" for platform requalifications can be broadly defined as the occurrence of an undesirable event, such as global collapse, unrepairable damage, unacceptable displacements, significant spillage or loss of life. The load at which failure occurs in a platform can be estimated using non-linear computer simulations, which account for geometric and material non-linearity and force redistribution.

Although ULS simulations are very powerful, they are notoriously complicated. They also require detailed input information and are very sensitive to some parameters used to create the non-linear structural models and their loading conditions. Thus, depending on the specific combination of model input and solution procedure, ULS analysis results can be suspect. Therefore, at the present state of development, ULS analyses cannot accurately mimic reality and should be verified against actual platform performance whenever possible.

2.0 PURPOSE AND SCOPE

2.1 Ultimate Limit State Performance of Offshore Platforms

The field of offshore engineering has greatly advanced from the early days of using wooden oil derricks near the water's edge. The fields of oceanography, hydrodynamics and structural analysis have all made significant progress since that time. Unfortunately, along with these advancements comes the knowledge that previously built structures often fall short when evaluated using more advanced and recent criteria. This is not to say that structural sufficiency is always inversely proportional to structural age. This fact has been made clearly evident during recent hurricanes and earthquakes both onshore and offshore, where in some instances older structures performed better than their younger neighbors (PMB, 1993) (Bothelo et al., 1993b). As a general rule, older platforms have less lateral wave load resisting capacity than do recently designed platforms. This fact is primarily due to the low (25-year return period) wave heights used in design of many platforms until the mid-1960's.

The majority of existing offshore structures are at least fifteen to twenty years old, and some platforms are more than thirty years old. However, storms that are considered to be significant have design level forces with return periods of one hundred years or more. Therefore, while the occurrence of significant storms usually causes some degree of structural failure, these storms present valuable opportunities to verify the applicability of

theoretical models and to gain new insights into the ULS performance of offshore structures.

Hurricane Andrew provided the offshore industry with the latest, albeit costly, learning opportunity. Andrew was the costliest natural disaster in United States history, with the most severe damage occurring in southern Florida (Oceanweather, 1992). At least 249 of the 3,800 Gulf of Mexico Platforms were negatively affected by this storm between August 24 to 26 1992 (Oceanweather, 1992). Hindcast studies suggest a maximum significant wave height, H_s, of 43.5 feet and a maximum individual wave height of 72.3 feet in deep water. Andrew's path over the Gulf is shown in figure 2.1-1 (PMB, 1993). Although many platforms were affected, considering Andrew's intensity, relatively few platforms experienced severe damage.

Even more amazing was the lack of environmental impact and loss of life. Reportedly, less than five hundred barrels of oil were spilled leaving almost no residual pollution, and there were no deaths recorded offshore (Oceanweather, 1992). This fact is truly a testament to the reliability of downhole shutoff devices and to the skills of the oil company employees involved. However, the good fortune experienced during Andrew should not be used as justification of the adequacy of existing platforms.

Hurricane Andrew did not significantly load the majority of the platforms in the Gulf. Although Andrew was quite large, the Gulf is capable of developing storms as large or

larger than Andrew. Therefore, Andrew should be viewed as a wake up call to re-evaluate our current theoretical models and to requalify older existing platforms whose ULS is not known.

One such study that partially accomplished both of these tasks was the joint industry project (JIP) headed by PMB Engineering Inc. (PMB, 1993). This project's goals were to provide documentation on the offshore structures affected and perform a calibration of current procedures for assessing existing platforms (caissons excluded). Table 2.1-1 summarizes the significant damage to steel jacket platforms recorded by the PMB project team (PMB, 1993).

Of most significance were the project's findings concerning the comparability of current analytical results and actual platform performance. It was determined that ULS pushover procedures, on average, have a bias of 1.19 with an associated uncertainty of ten percent. While this bias factor should not be directly applied to requalifications, it does provide evidence for the high value of ULS procedures and useful information for technical decision makers. The results of other important related studies can be found in references Bothelo et al. (1993a, 1993b), Imm et al. (1994) and Nair et al. (1994). Particularly of interest is the effort by Bothelo et al. (1993a) to quantify the probability of failure for a platform.

Table 2.1-1: Summary of Damaged Steel Jacket Platforms During Hurricane Andrew (PMB, 1993)

Gulf of Mexico Area	Year Installed	Water Depth (ft)	Distance From Hurricane Eye (miles)	Number of Platforms	Condition of Platforms
South Timbalier (ST)	1948 - 1969	up to 100	12	2	5 toppled 6 extensively damaged 5 with minor to heavy damage 1 with deck severely damaged - being repaired
		101 - 150	1 to 5	2	
			14 - 21	10	
	1970 - 1977	up to 100	24	1	
	1978 - 1981	101 - 150	5, 18	2	
Ship Shoal (SS)	1948 - 1969	up to 50	8	2	4 toppled 3 with moderate to heavy damage 2 with unknown damage
		51 - 100	4 to 12	3	
		101 - 150	14, 18	2	
	1970 - 1977	43	3, 24	2	
South Pass (SP)	1962	61	70	1	unknown damage
South Pelto (PL)	1967	unknown	unknown	1	unknown damage
			Total	28	

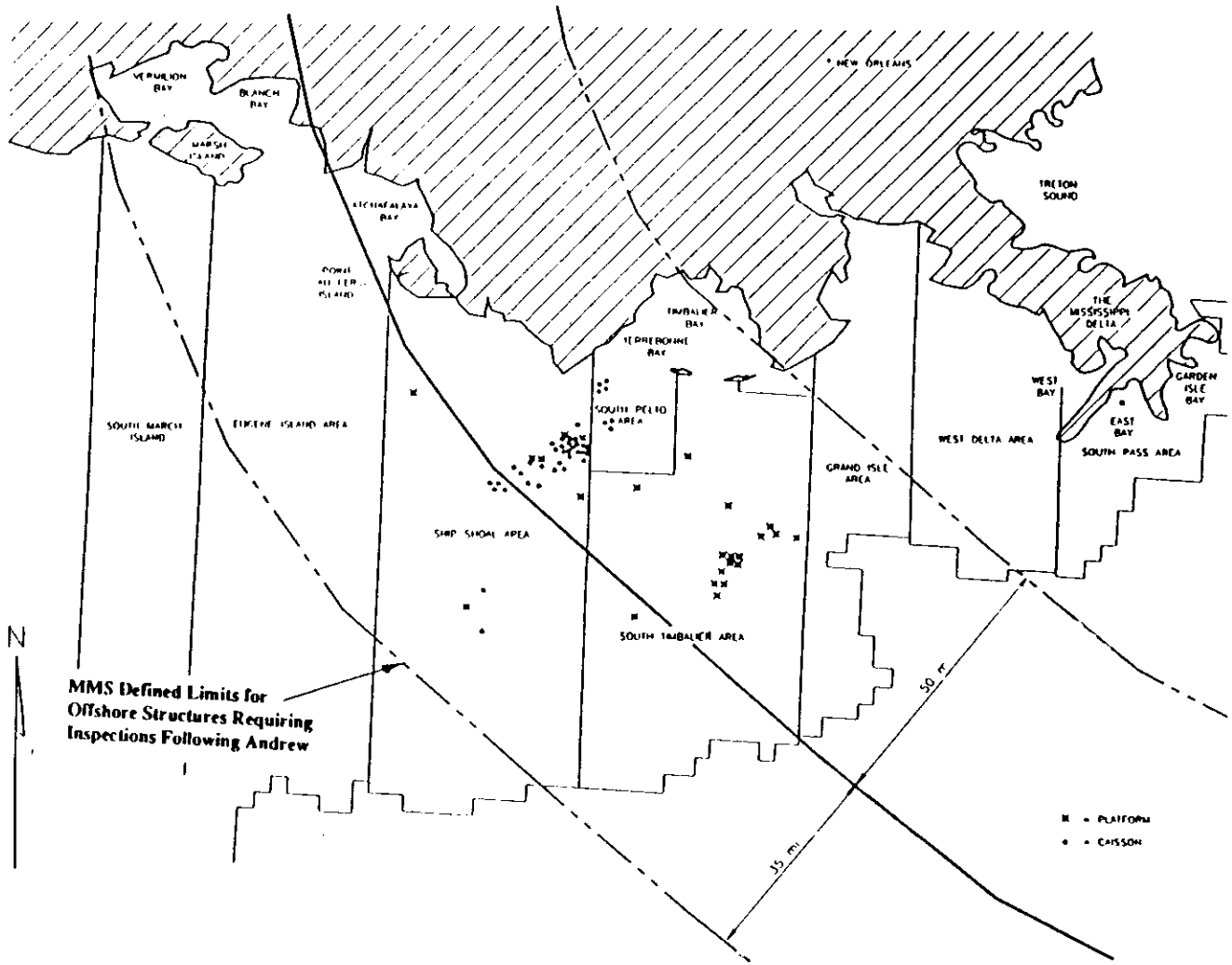

Figure 2.1-1: Path of Hurricane Andrew in the Gulf of Mexico (PMB, 1993)

2.2 Research Purpose

The purpose of this research is three-fold. First, the validity of ULS results will be verified by comparison to actual platform performance during Hurricane Andrew and Hurricane Hilda. Second, the sensitivity of the results to loading, structure and foundation parameters will be investigated and discussed. Finally, the methods and procedures used in ULS analyses will be assessed, with particular attention being paid to potential pitfalls and oversights.

2.3 Research Scope

This report addresses the static pushover analyses of four offshore platforms located in the Gulf of Mexico. All four platforms are steel template type platforms with piled foundations. The results of two platform analyses are compared to actual platform performance during Hurricane Andrew and Hurricane Hilda to further evaluate the validity of ULS analyses in predicting platform survival during severe storm conditions. One of these two platforms survived Hurricane Andrew with only minor damage, while the other platform experienced global failure. In addition, one platform was analyzed as part of a JIP lead by PMB Incorporated to determine the variation in results of ULS analyses (PMB, 1994).

Detailed platform information was supplied by their respective owners, without whose support this research would not have been possible. The results of the platform analyses

are also being used to verify the results of a simplified ULS screening procedure currently being developed at U. C. Berkeley (Bea and Mortazavi, 1995).

The platforms were modeled using DNV's PREFRAME program (DNV, 1994a). Only the main structural components were included in the computer models. The contribution of the platform appurtenances and non-structural components to the overall platform capacity was taken to be insignificant. However, the loads induced in the platform due to non-structural components were taken into account. The jacket and conductor wave loads were generated using another DNV SESAM program, specifically WAJAC (DNV, 1994b). Deck loads were calculated by hand using the method outlined by API RP 2A section 17 (API, 1994).

The static pushover analyses were performed using a state-of-the-art non-linear analyses program, SINTEF's USFOS (SINTEF, 1988). Both the loading and analysis programs were run using a IBM RISC 6000 computer, which uses AIX, IBM's version of UNIX, as its operating system.

It should be noted that there are many important and related issues that are not addressed in this report. Of most significance to the authors is the area of dynamics (Bea and Young, 1993). All analyses performed for this research were static pushover analyses. In an effort to remain focused, no attempt was made to include the effects of both the linear and non-linear dynamic properties of the platforms when determining their ultimate

capacity. While this subject was not addressed in this research, it can be of extreme importance and can be very complimentary to the results presented here (Bea and Young, 1993).

Dynamics considerations can increase or decrease both the load a platform experiences and its capacity to resist that load (Young, 1993). It is well known that dynamic amplification factors up to 2.0 can be experienced depending on the loading frequency to structure frequency ratio (Clough and Penzien, 1993). This could be of extreme importance when considering wave in deck loads, where the loads resemble more of an dynamic impact than a static force. Linear and non-linear dynamic loading and capacity effects are clearly presented by Young and Bea (1993). It is the authors' opinion that the results from a static pushover analysis should, as a minimum, be scrutinized in light of these known dynamic effects.

Another important issue not discussed here is the areas of materials and material imperfections. Recent seismic events have shown that welded structures can exhibit extremely brittle behavior in and around their heat effected zones (Astaneh, 1994, Zarghamee and Ojdrovic, 1995 and Campbell, 1995). In addition, other minor imperfections, e.g., micro cracks, can lead to local member failure (SINTEF, 1988b). These types of material problems can be especially important in the offshore environment where corrosion and fatigue loading are highly present. The discovery of brittle zones in the 1980's led directly to the adoption of API RP2Z, Recommended Practice for

Preproduction Qualification for Steel Plates for Offshore Structures (Peterson and Rosenberg, 1994).

Material imperfections are highly localized and are thus, difficult to include in large scale structural models. Moreover, such imperfections are stochastic in nature. Therefore, probabilistic tools are required for analysis. Consequently, while material behavior is extremely important in determining all potential failure modes and hence, a structure's true ultimate capacity, material behavior and material imperfections are outside the scope of this research.

2.4 Organization of Report

This report is divided into eight sections. The first two sections provide an introduction to the focus of the report and the scope of the research performed. Sections three through five lay the foundation for the theories and methodologies used to perform static pushover analyses. Section six summarizes the analysis results for the three platforms studied. Appendix B contains more detailed information concerning the platforms, the development of their models, the development of their loading profiles and their pushover analyses results. Section seven discusses the sensitivity of the results to certain loading, structure and foundation parameters. Section eight summarizes the finding of this research and includes recommendations for further study in this area. Finally, Appendix A contains a discussion of the pitfalls and potential problems with using ULS analyses.

3.0 HURRICANE CONDITIONS AND KINEMATICS

3.1 Essential Storm Components

Ocean storms and hurricanes are highly complex phenomena. By nature, they are difficult to study with any degree of precision. However, the seemingly random components of such storms interact with each other in notable ways. The main storm components of concern to the offshore engineer are wind, waves, current and surge.

While each of these components can be very important in the design or requalification of offshore structures, wave loading is of primary significance for most fixed template style platforms. Wind and current loads can sometimes be very large, but usually the vast majority of the lateral load experienced by the platform is due to wave loading. Storm surge can be very important particularly when wave crests reach the platform decks. However, except for possibly increasing the buoyancy force on the jacket, storm surge alone does not play a major role in storm loading. Surge becomes important due to its effect of increasing the mean water level, which in turn raises the wave crest elevation.

Therefore, the majority of the following discussion of storms and hurricanes will focus on waves and the loads they induce on offshore platforms. This section also addresses currents and their loads. Since wind loads occur almost exclusively in the deck portions of a platform, discussion of wind loads is deferred until section 4.5. Although different types

of storms can occur, from this point forward, the term storm will represent storm and hurricane conditions as would be expected to occur in the Gulf of Mexico.

3.2 Loading Determination Approaches

There are several important procedural steps that are usually necessary to establish the structural storm loading. Sarpkaya and Isaacson (1981) suggest the following sequence of calculation procedures:

(a) establish the wave climate in the vicinity of a structure, either on the basis of recorded wave data, or by hindcasting from available meteorological data;

(b) estimate the design wave conditions for the structure;

(c) select and apply a wave theory to determine the corresponding fluid particle kinematics;

(d) use a wave force formulation to determine the hydrodynamic forces on the structure;

(e) calculate the structural response; and

(f) calculate the structural loading, which includes base shear and moment, stresses and bending moments.

These steps are not a complete list for every structure, but they can serve as a general guide when calculating structural loads.

There are two distinct approaches one may take when following the above procedures. One is a deterministic approach and the other is a stochastic approach. The deterministic approach has two approaches within its classification, these being pseudo-static and time-dependent. The pseudo-static approach is the simplest of the three approaches. In this

approach a static analysis uses the maximum storm loads and does not account for the time dependent properties of the load or the structure. The time-dependent approach uses a time record of the wave motion to calculate time-dependent loads, which then are applied to the structure while accounting for the structure's dynamic response. Whereas, the stochastic approach describes the wave motion by its spectral density (Bea, 1994). Therefore, the time-dependent deterministic approach uses the time domain, while the stochastic approach uses the frequency domain. Figure 3.2-1 graphically illustrates these three approaches (Bea, 1994). As previously discussed in section 2, this research does not attempt to account for dynamic platform properties and the effect they have on the platform's effective load and capacity. Therefore, all analyses performed for this research used the pseudo-static approach to wave force determination.

The typical method of performing a pushover analysis is to determine a reference wave/wind load pattern and then to incrementally increase this load pattern on the platform. While this procedure may be valid for some engineering purposes, it is not a valid approach for determining a platform's ultimate limit state. Using this approach, the loading pattern is linearly increased up to or beyond the full reference load. The problem arises from the fact that in reality the load pattern changes with increasing load. This fact becomes clearly evident when wave-in-deck forces are included. A better approach would be to increase the load magnitude and change the load pattern to be consistent with the imposed wave height. This can best be done by tying the load magnitude and load pattern to an expected return period wave height.

The load magnitude and load pattern which causes the platform to "fail" with a load factor of unity gives a more realistic measure of the platform's ultimate resistance capacity. In linearly increasing a reference load far beyond a load factor of unity it is possible to miss the true ultimate limit state. For example, one might determine that the jacket braces are the weak link when in reality the first failure mode occurs in the piles or in the deck legs. Thus, for this report, the preliminary analysis wave was determined using the procedures prescribed in the current U.S. design code (API, 1993). However, if the load factor at failure was significantly greater or less than 1.0, the wave height and period were adjusted to obtain a more realistic load profile causing failure.

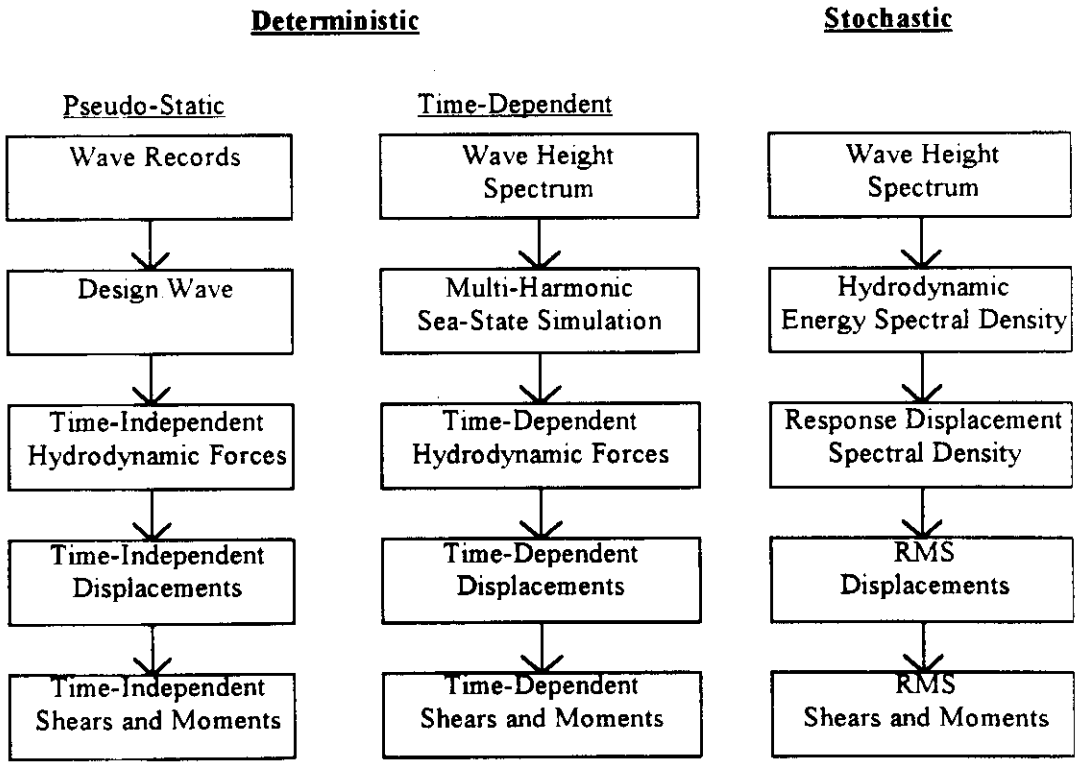

Figure 3.2-1: Summary of Wave Loading Analysis Procedures (Bea, 1994)

3.3 Wave Theory

Wave theories are mathematical models of sinusoidal fluid motion. Many different theories have been developed over the last century and a half. Linear wave theory was first introduced by Airy in 1845. About five years later, Stokes took the next step by considering higher order theories, which are valid for intermediate to deep water. After that time many other wave theories were introduced. Some of the other notable wave theories include (Sarpkaya and Isaacson, 1981):

- Cnoidal Wave Theory, developed by Korteweg and de Vries (1895), and later extended by Fenton (1979),
- Hyperbolic Wave Theory, developed by Iwagaki (1968),
- Solitary Wave Theory, developed by Keller (1948),
- Stream Function Theory, developed by Dean (1965).

All wave theories attempt to accurately model the fluid motion for varying combinations of wave shape, water depth and current profile. Some models are better than others, but each has its range of applicability. Figure 3.3-1 shows the applicable regions of Stokes V, Linear/Airy and Dean's Stream Function as a function of wave height, H, water depth, d, and apparent wave period T_{app}. T_{app} differs from the actual wave period, T, due to the lengthening and shortening effect of in-line current.

Many volumes exist which document the different wave theories and their background in fluid mechanics. In addition, the development of wave theories was not critical for this research. Therefore, the subject will not be discussed in any more detail. What is important to note is the wave theory used for the research presented herein and the reasons for choosing this theory. As previously mentioned, the results of this research are

being used to verify a simplified screening methodology currently being developed (Bea and Mortazavi, 1995). This screening method uses Stoke V in calculating wave kinematics. Therefore, to remain consistent with the screening study, this research consistently uses Stokes V wave theory. All three platforms are located in intermediate to deep water, and were checked using figure 3.3-1 to ensure that Stokes V was applicable for their environment. Also, Stokes V wave theory has become somewhat of an industry standard and is widely recognized as a robust approach. Thus, while one can argue that there are more precise theories available for the environment of the four platforms, Stokes V suits the purposes of this research well. In addition, pseudo-static pushover analyses require a reasonable approximation of the loading profile on a platform. However, the analysis uses load factors that are different from 1.0. Thus, it is the belief of the authors that ensuring an extremely precise description of the wave kinematics is not critical to the ULS analysis results.

For the sake of completeness, figure 3.3-2 shows the chief parameters included in a wave theory model. Wave speed or celerity, c, is defined as the wave length, L, divided by wave period, T. The origin indicates the point in the wave train when time, t, is zero. Therefore, the surface elevation, η, is a function of time, t, and location, x. It is important to note that the celerity is not the velocity used in calculating member forces. The celerity is a measure of the global wave train velocity across the water surface. The actual water particle velocity in the wave is much higher than the wave celerity. Even if irrotational flow is assumed, the surface particles must travel along the surface path, which is much

longer than the wave length, L. Thus, the actual water velocity and acceleration at any point inside the wave are the two parameters that wave theories attempt to determine.

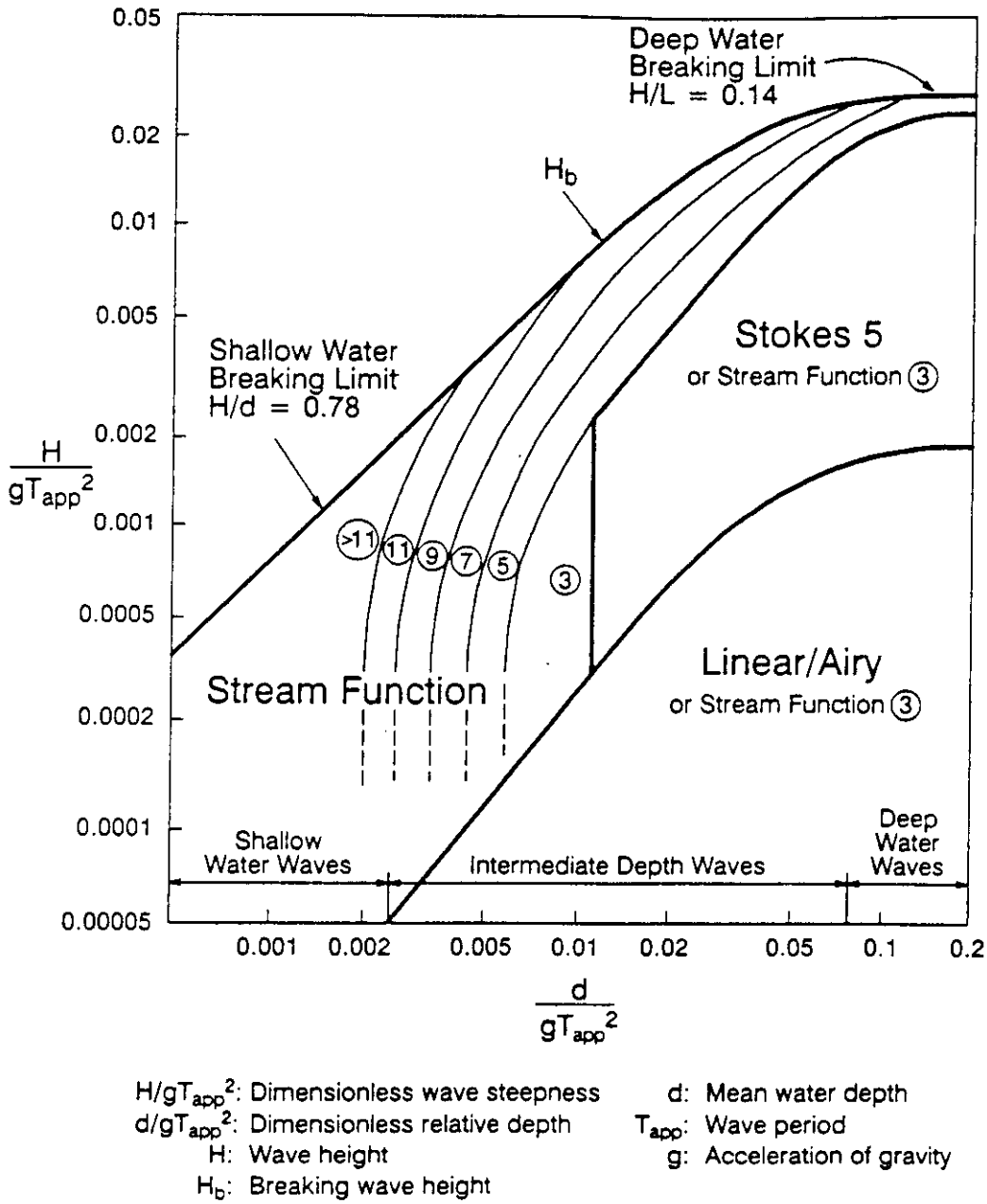

H/gT_{app}^2: Dimensionless wave steepness
d/gT_{app}^2: Dimensionless relative depth
H: Wave height
H_b: Breaking wave height
d: Mean water depth
T_{app}: Wave period
g: Acceleration of gravity

Figure 3.3-1: Regions of Applicability of Stokes V, Linear/Airy and Stream Function Wave Theories (API, 1993)

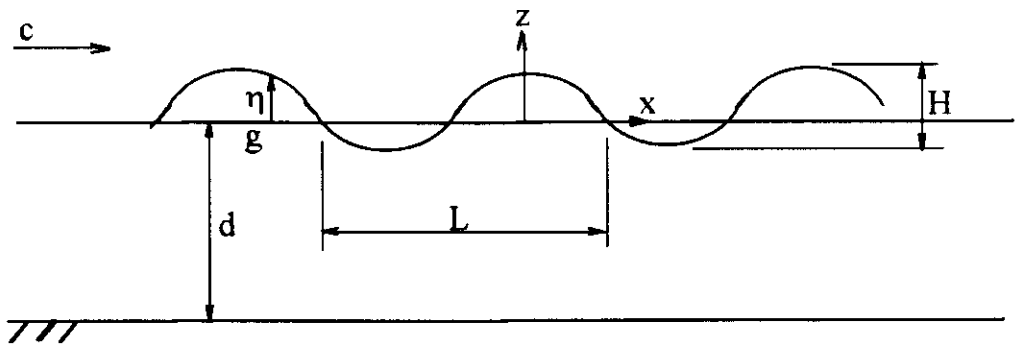

Figure 3.3-2: Wave Train Parameters

3.4 Directional Spreading

Two dimensional wave theories, including Stokes V, do not account for irregularity in wave shape. Using regular waves, the wave kinematics are determined assuming a continual uniform wave train that is very wide or "long-crested." However, most all storm sea states are extremely random phenomena with many different wave trains interacting simultaneously. Thus, the wave kinematics predicted using ordinary two dimensional wave theories do not reflect the diffusion or spreading of wave energy that occurs during ocean storms. This spreading effect tends to decrease the velocities and accelerations predicted by normal wave theory. Hence, it is necessary to decrease the predicted velocities and accelerations before calculating member forces.

Reduction of wave kinematics is usually accomplished by means of a unitless factor known as a directional spreading coefficient, or more commonly, a wave kinematics factor. Directional spreading effects depend upon the wave frequencies. Therefore, when using a pseudo-static deterministic wave, it is important to include a wave kinematics factor

associated with the most significant wave. The large waves of a storm will normally have a period that is near the "spectral peak" of the sea state. Use of a weighted average reduction factor, considering all frequencies, would most likely overestimate the spreading effect. The wave kinematics factor can be estimated as:

$$wkf = \sqrt{(n+1)/(n+2)} \tag{3.1}$$

Where n is the exponent in the $\cos^n\theta$ spreading function (API, 1993).

Measurements of spreading indicate a range of 0.85 to 1.00 depending upon location and type of storm. The current US design code recommends using a wave kinematics factor of 0.88 (API, 1993). This value was used throughout this research.

3.5 Current and Current Blockage Factor

Current, defined as the steady flow of fluid in a particular direction, can have many causes. Consequently, there is more than one type of current. The three most common types of current are tidal current, circulation current and storm-generated current. Tidal currents are associated with astronomical tides. These currents are generally weak in deeper water beyond the shelf break and rarely exceed 1 ft/s. However, certain bottom configurations in some inlets and coastal regions can significantly increase tidal current velocities. Cook Inlet is capable of producing tidal currents with surface velocities near 10 ft/s (API, 1993). Circulation currents are relatively steady currents associated with ocean scale circulation patterns. Examples of circulation currents include the Gulf Stream in the Atlantic Ocean and the Gulf Stream in the Gulf of Mexico (API, 1993). Storm generated currents are the

result of pressure changes and wind shear on the water surface during intense storms. In deep water along open coastlines, storm current surface velocities are approximately two to three percent of the associated one-hour sustained wind velocity (API, 1993). When possible, all three types of current should be accounted for during an analysis. Frequently, current measurements or hindcast results lump all the currents present into one current. In either case, a current profile that varies with water depth is developed and is used to determine member loads. For shallow water, approximately less than two hundred feet, the current profile is roughly constant with water depth.

Although most fixed offshore platforms are composed of relatively slender elements, the platform's presence affects the current profile and the associated current loads. The platform's presence causes some of the current flow to diverge and to go around the platform's extremities, which causes the portion of the current passing through the platform to have a reduced velocity. Hence the platform is not invisible to the current. The decrease in current is proportional to the density and number of members the current must pass. Consequently, the current experiences higher blockage when passing end-on through a platform than when passing through the broadside planes. The blockage effect is normally accounted for by applying a current blockage factor to the current velocity profile. The current blockage factor can be calculated as:

$$cbf = \left[1 + \sum \left(C_d A\right)_i / 4\bar{A}\right]^{-1} \tag{3.2}$$

Where $\Sigma(C_dA)_i$ equals the sum of "drag areas" of all individual members, and $\bar{A}$ represents the area within the perimeter area of the platform projected normal to the current (API, 1993).

For typical fixed template style platforms with three to eight legs, the current blockage factor falls between 0.70 and 0.90. Once a current and an associated current blockage factor have been determine, it is necessary to combine them with the wave kinematics. However, modeling the interaction of currents and waves is highly complicated due to the many possible combinations of wave and current. Currents can be non-uniform in all three global coordinates and have widely varying effects on different wave trains. However, as previously mentioned, an exact description of a wave train of wave kinematics is not necessary for the purposes of this report. Consequently, there are a limited number of interaction effects that are of interest.

Current and wave interaction is of primary importance for developing platform forces. As will be discussed in section 4.0, for most fixed offshore platforms the drag forces dominate the total base shear and are proportional to the square of the water particle velocity. Hence, an extremely simplified approach to combining current and wave effects is the direct addition of their modified velocity vectors. This new total velocity can then be used for calculating member forces. In reality, the current affects the wave shape, height, period, particle velocity, etc. Most wave load programs, including the one used for this research, take account of these effects. However, the combining of the wave and current velocity vectors is the most important interaction effect and is usually sufficient for the purposes of pushover analyses. As will be discussed in section 4.0, this simple combining of velocity vectors is the standard approach for determining deck forces.

4.0 FORCES ON STEEL FRAMED PLATFORMS

4.1 Hydrodynamic Forces

As happens for wave kinematics, the complexity of the hydrodynamic force phenomena causes empiricism to dominate over theory. Moreover, since wave kinematics produce the major hydrodynamic forces of concern to offshore engineers, the process of determining the wave induced forces on offshore platforms is doubly complex. Thus, although hydrodynamic forces have been studied in some detail (Bea et al., 1988), the current collection of knowledge and recorded data is inadequate to positively model the fluid loading on and the dynamic response of offshore structures (Sarpkaya and Isaacson, 1981). Consequently, current procedures for developing wave and current induced forces on offshore platforms represent methods that try to best match the empirical test data that has been gathered. It is important to note that much of this data has been primarily gathered under idealized laboratory conditions.

Wave and current induced forces are dependent upon the water particle kinematics at the water-structure interface. Hence, as a first step in determining hydrodynamic forces on any structure, one must determine the critical water particle kinematics at all points of interest. In general, wave generated fluid kinematics prove significant at depths under half the wave length structures (Sarpkaya and Isaacson, 1981).

As was discussed in section 3.0, many different approaches exist for determining wave induced fluid kinematics. The choice of approach depends upon a variety of factors such as water depth, structural period, availability of storm records and desired accuracy or purpose of calculation.

For rigid steel-framed platforms, one normally chooses a deterministic and time-independent approach. For longer period structures, a pseudo-static analysis cannot directly capture the important dynamic effects caused by the time-dependent non-linear response of the structure. However, certain studies show that it is possible to indirectly account for these effects even when using a pseudo-static analysis (Bea and Young, 1993). Since the platforms analyzed as part of this research were relatively rigid and located in intermediate water depths, a pseudo-static approach was used throughout.

A pseudo-static approach typically uses the kinematics of a design wave. This wave usually corresponds with the maximum wave height expected to occur in a specific area within a given period. As a rule, the offshore industry currently uses a 100-year return period to choose a design wave. Thus, after choosing an acceptable return period, the associated wave height and period may be determined using the storm statistics of the platform location. See Bea (1993) and Thoft-Christensen and Baker (1982) for further information on choosing appropriate return periods. These references contain very thorough discussions of probability and reliability concepts as they apply to offshore structures.

Design waves are normally assumed to be uniform, long-crested and propagating with a constant shape and speed. In addition, for small body structures, it is assumed that the structure is invisible to the wave. That is, the existence of the structure does not cause a global disturbance of the fluid flow. While the second assumption holds true for typical offshore platforms, anyone who has ever observed a rough sea knows that the first assumption is a theoretical simplification. However, to determine the wave kinematics using an appropriate wave theory it is necessary to define a two-dimensional wave, i.e., define the wave height, length and period.

Much time and effort can be wasted by specifying wave parameters in great detail, when in reality the sea surface and storm kinematics contain inherent randomness that cannot be captured using deterministic methods. This is just one example of why all the available theories and computing power will never replace the need for experienced engineering judgment.

Once the water particle kinematics have been modeled, a force transfer function must be developed which is capable of computing the different hydrodynamic member forces. Fundamentally, the moving fluid develops four types of forces on the members: drag, lift, inertia and diffraction. Drag and lift forces are proportional to the fluid velocity squared, while inertia and diffraction forces are proportional to the fluid acceleration. For most rigid steel framed structures, the drag and inertia forces are most critical.

Lift forces oscillate transversely to the direction of the fluid velocity due to vortex shedding around the member. Frequently, lift forces are smaller than the accompanying drag forces. Lift forces are most significant when the dynamic properties of the member in question interact with the oscillating forces to create resonant vibration. Such vibrations can greatly amplify the effective lift force experienced by the member. Thus, lift forces may be very important when considering the forces on individual members, especially for fatigue analyses. However, they normally do not contribute significantly to the low cycle failure of platform members.

If the platform or portions thereof transversely span more than approximately one fifth the wave length, the fluid flow becomes modified to produce diffraction forces in the incident wave direction (Bea, 1994). However, when diffraction is important, D/L greater than or equal to 0.2, the particle accelerations are maximum over only a portion of the member width. In addition, for cylindrical members, the fluid particle displacements relative to member diameter may be sufficiently small to significantly minimize the effects of flow separation. For a vertical cylinder where diffraction is important, the Keulegan-Carpenter number, KC, is limited to 2.2 for shallow water and approximately 1.0 for deep water structures (Sarpkaya and Isaacson, 1981). Thus, the inclusion of wave diffraction reduces the calculated wave forces from those calculated if diffraction were neglected. This means that if the variation of fluid kinematics in the x direction due to diffraction were ignored, then the inertia coefficient would necessarily be that of a slender member. This incorrect

C_m would result in a general overestimation of the inertia force structures (Sarpkaya and Isaacson, 1981).

Most members of framed offshore platforms do not have sufficient width to cause significant in line flow disturbances, i.e., a typical leg or conductor of a steel-frame platform has a diameter between two to fifteen feet. For a relatively small wave, H = 30 ft with a height to width ratio of 0.10, the significant range of effective diameter starts at 60 ft. This important range becomes even larger with increasing wave height and smaller height to length ratios. Consequently, except for very wide structures and small wave heights, diffraction effects can be neglected.

Drag forces result from the shearing of the fluid near the surface of the member. Compatibility necessitates that the fluid at the member surface has zero velocity. The velocity profile transverse to the member axis increases with distance from the member surface. Therefore, the drag force on the member surface is equal to the sum of the fluid shear forces out to the point of "constant" velocity.

Except for very small oscillations, KC < 3, the flow separates on the downside of the cylinder, which induces a change in velocity. This change in velocity is termed the local acceleration. The local acceleration has an associated fluid mass, which, when using Newton's law, produces a force known as the inertia force.

The maxima of drag and inertia forces occur out of phase with one another. For a linear wave, the maximum velocity lags the local acceleration by ninety degrees see figure 4.1-1. This phase lag accounts for the observed phase difference in the drag and inertia forces, see figure 4.1-2 (Bea, 1994). For a wave having significant skewness (non-linearity, crest height significantly greater than trough depth), the drag and inertia force maxima can have a phase angle less than ninety degrees.

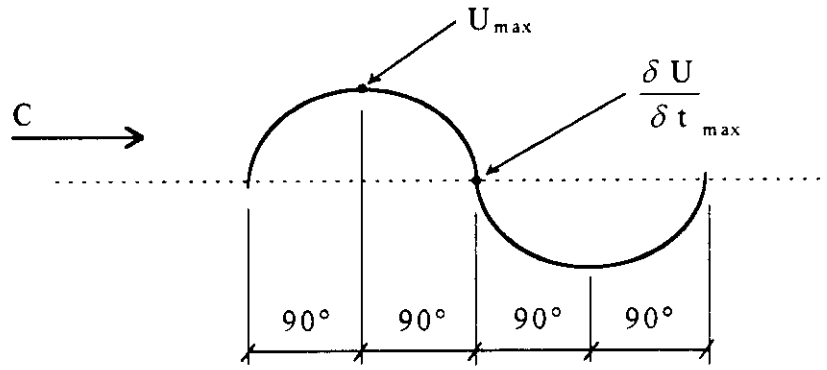

Figure 4.1-1: Maximum Velocity and Acceleration Phase Difference (Bea, 1994)

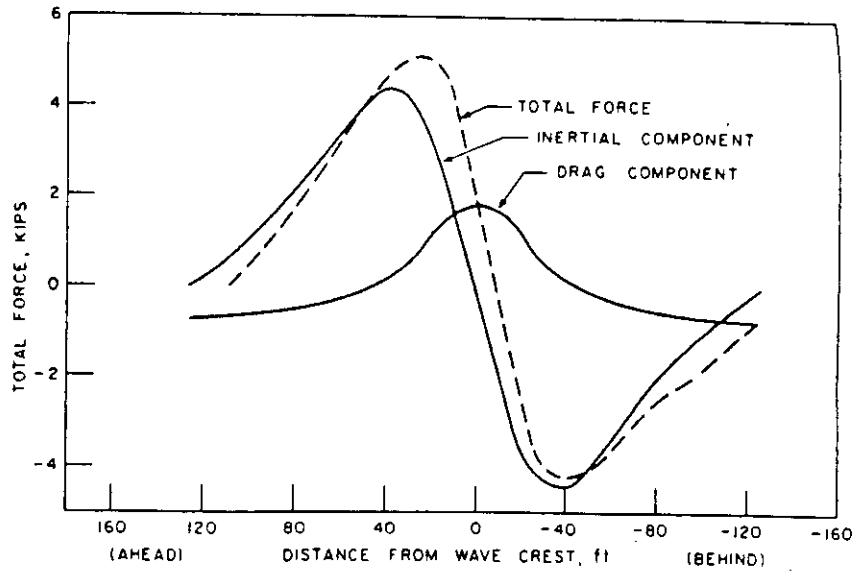

Figure 4.1-2: Theoretical Components of Total Wave Force (Bea, 1994)

4.2 Morison's Equation

If lift and diffraction forces are negligible, such as for a rigid small-body structure, then the necessary force transfer function need only consider drag and inertia related forces. Morison's equation is almost universally accepted as the most efficient transfer function that determines such forces. In its general form, Morison's equation is expressed as

$$F = F_d + F_i = C_d \times \frac{\rho}{2} \times A \times U|U| + C_m \times \rho \times V \times \frac{\delta U}{\delta t} \qquad (4.1)$$

where

F = force vector per unit length acting normal to the axis of the member

F_d = drag force vector per unit length acting normal to the axis of the member

F_i = inertia force vector per unit length acting normal to the axis of the member

C_d = drag coefficient, derived from empirical test data

ρ = mass density of sea water

A = projected area per unit length normal to member axis, D for cylindrical members

V = displaced volume of member per unit length, $\pi D^2/4$ for cylindrical members

U = component of the velocity vector that is normal to the axis of the member due to both wave and current, modified by the wave kinematics factor and current blockage factor as appropriate

$|U|$ = absolute value of U

C_m = inertia coefficient, derived from empirical test data

$\frac{\delta U}{\delta t}$ = local acceleration vector normal to the axis of the member

Note that in Morison's equation local acceleration is used rather than the total acceleration, that is, local plus convective. There are many who argue that the total acceleration should be used, but their arguments are based on the unrealistic assumption that the flow does not separate from the cylinder (API, 1993). However, as explained in the commentary API (1993), the fluid acceleration due to flow separation is much greater than that produced by the convective acceleration. In addition, the convective acceleration can be nearly in phase with the local incident velocity which leads the undisturbed far-field velocity. Thus, it can be argued that the effects of convective acceleration are captured in the empirically derived drag coefficient. Finally, the convective acceleration is typically less than fifteen percent of the local acceleration except in very steep waves where the drag forces dominate.

Morison's equation by no means represents the most accurate hydrodynamic force transfer function, but it does represent a simple yet robust approach to dealing with extremely complex phenomena. The popularity and longevity of the Morison's equation can be attributed to its simplicity and its relatively broad range of applicability. Moreover, it is sufficiently accurate for most all engineering purposes considering the large uncertainties of the input parameters. Thus, until the input uncertainties are reduced, there is little need to develop a more sophisticated force transfer function.

4.3 Drag and Inertia Coefficients

Ironically, while the Morison equation has been widely adopted for quite some time, the empirical drag and inertia force coefficients, C_d and C_m, still incite much discussion. Countless studies have been performed in an attempt to determine the optimum values of these coefficients. Yet, there is still a wide scatter in the published results structures (Sarpkaya and Isaacson, 1981) (Bea, 1994). Two principal reasons exist for such scatter: the inability to precisely measure the drag and inertia forces under realistic ocean wave conditions and the inability to precisely measure and then model the wave kinematics that caused those forces. Unfortunately, these difficulties will probably always exist to some degree due to the inherent randomness of wave kinematics and hydrodynamic forces. Hence, while further study of these coefficients is necessary and beneficial, the natural research limitations that exist must be recognized so that future studies do not result in futility or replication.

Amidst the large scatter of results concerning C_d and C_m, there exists a range of acceptable values. It is generally accepted that both C_d and C_m are proportional to the Keulegan-Carpenter number, KC, the Reynolds number, Re and the relative surface roughness e. The relative surface roughness is defined as the average peak-to-valley height of "hard" growth organisms, k, divided by the effective element diameter, $D = D_c + 2t$. D_c is the clean member diameter and t is the marine growth thickness, see figure 4.3-1 (API, 1993).

Unfortunately, determining KC, Re, or e for full scale platforms under true storm conditions can prove extremely difficult if not impossible. Therefore, not having such detailed information, general approximations or relationships for C_d and C_m are frequently used. Considering the importance of these factors, such generalizing may seem too presumptuous. However, according to structures Sarpkaya and Isaacson (1981) and Bea (1994), the uncertainty of the wave force test data can be as high as 100 percent. Thus, choosing values or relationships for C_d and C_m based on sound engineering judgment will most likely not significantly increase the uncertainty of the force calculations. Consequently, due to the lack of detailed information, this research used C_d and C_m values of 0.6 and 1.6 for smooth cylinders and 1.2 and 1.2 for rough cylinders respectively.

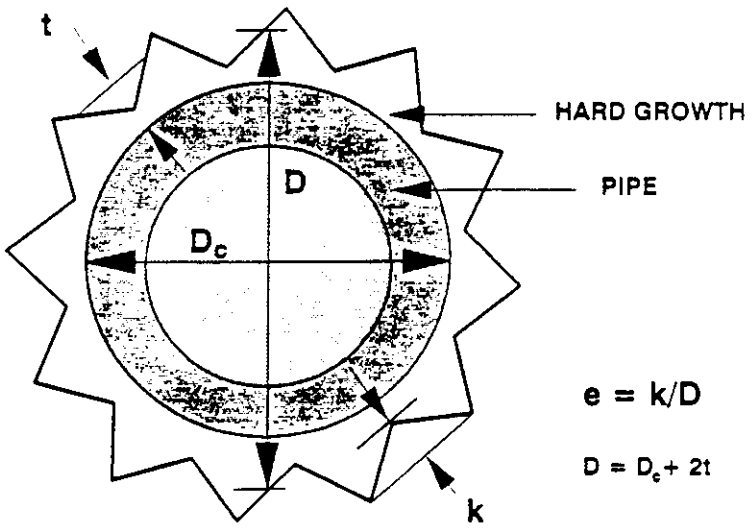

Figure 4.3-1: Surface Roughness Height and Thickness (API, 1993)

4.4 Wave-in-Deck Forces

Equipment and personnel decks are not only the heart of an offshore platform, they also play an important role in platform loading. Decks support virtually all equipment dead and live loads. What is more important, hydrodynamic forces in the decks can compose the majority of a platform's severe storm loading. Almost without exception, wave-in-deck forces have been the root cause of failures in major drilling and production platforms in the Gulf of Mexico during severe storm conditions (PMB, 1988). These failures have been primarily confined to platforms whose decks were designed using 25-year return period wave heights and tides.

Wave-in-deck forces can be so destructive that, if possible, they are best to avoid entirely. Hence, today most engineers design platforms with deck elevations above the expected maximum crest elevation associated with the design wave; for example, a 100-year return period wave. Crest heights higher than the expected maximum may still occur, but most all attempts to avoid deck forces prove beneficial.

Unfortunately, a notable portion of existing platforms were designed using less severe storm conditions and lower expected crest elevations than would be used today. Thus, for the assessment of existing platforms and for modern platforms where other design conditions necessitate using a lower deck height, wave-in-deck forces must be calculated.

Deck force calculations present even more complications than those for cylindrical jacket members. Decks are typically composed of members with a variety of shapes and orientations. The equipment supported by the decks usually have even more diversity than the deck members and are spaced with varying degrees of density. In addition, the local and global shapes and configurations of typical platform decks induce important hydrodynamic effects such as run-up, shielding and slamming.

Detailed studies show that drag and slamming forces dominate platform deck loading (McDonald et al., 1990). Horizontal inertia forces on decks are usually not significant. This is primarily because deck elevations are typically near the peak of the significant wave crest where the fluid acceleration is at a minimum and the fluid velocity is at a maximum, see figure 4.1-1. Laboratory tests indicate that slamming forces in decks can be up to two to three times larger than the steady state drag forces. Theoretical computations indicate a potential increase of six times the drag force (McDonald et al., 1990).

Due to the extreme complexity of platform decks combined with the intricate nature of the wave kinematics in the splash zone, empiricism dominates the study of wave in deck forces. Consequently, the current state of the practice dictates using an approach similar to Morison's equation. This standard method attempts to capture all the horizontal force components, predominately drag and slamming forces, in one drag force coefficient. Again, this approach may seem too simplistic, but the actual hydrodynamic force phenomena occurring in the deck regions are essentially impossible to describe

mathematically. Moreover, even the empirical test data shows considerable scatter (McDonald et al., 1990).

The simple equation for calculating deck forces prescribed in the current U.S. design code (API, 1994) is written as follows

$$F = \frac{\rho}{2} \times C_d \times \left(\alpha_{wkf} \times V + \alpha_{cbf} \times U\right)^2 \times A \qquad (4.2)$$

where

F = total horizontal force, applied midway between the lowest deck elevation and the lower of the wave crest elevation and the top of the main deck

ρ = mass density of sea water

C_d = drag coefficient, derived from empirical test data

A = total projected area of decks normal to wave direction up to wave crest height

α_{wkf} = wave kinematics factor, see section 3.4

V = fluid particle velocity due to wave motion

α_{cbf} = current blockage factor, see section 3.5

U = fluid particle velocity due to current in line with wave

The drag coefficient is chosen based on angle of attack and on the relative density of the deck's equipment. Table 4.4-1 lists values of C_d currently recommended in the U.S. design code (API, 1994) and used throughout this research.

Unfortunately, this approach makes no attempt to consider the dynamic properties of the decks or the entire platform. These properties can have a profound impact on the effective deck forces due to the short rise time of impact forces nearing the structure's resonant frequency. Relatively simple methods for incorporating such dynamic effects do exist and could potentially increase the precision of current deck force calculation procedures (Young, 1993).

This approach also does not consider the vertical forces acting on the platform decks. As a wave passes through a platform, the surface elevations at all points underneath the decks rise and fall as well as propagate in the wave direction. Consequently, this vertical motion of the wave can create severe impact loads on the bottom of the deck. This is especially true if the deck floor consists of solid steel plating rather than perforated steel grating. The effects of these vertical forces on ULS analysis results will be discussed in section 7.

Table 4.4-1: Drag Coefficients, Cd, for Wave/Current Platform Deck Forces (API, 1994)

Deck Type	Cd End-on and Broadside	Cd Diagonal
Heavily Equipped (solid)	2.5	1.9
Moderately Equipped	2.0	1.5
Bare (no equipment)	1.6	1.2

4.5 Wind Forces

Wind forces on platforms are developed in much the same way as hydrodynamic loads. Wind and wave force formulations for offshore platforms essentially differ only in their respective fluid densities. However, determination of the fluid kinematics that cause those loads is quite different for wind and wave flows.

The wind force equation can be written as (API, 1993)

$$F = \frac{\rho}{2} \times C_s \times (V)^2 \times A \qquad (4.3)$$

where

F = total horizontal force, applied midway between the wave crest elevation and the top of the main deck

ρ = effective mass density of air, which should account for the high water content of the air near the ocean surface

C_s = shape coefficient, derived from empirical test data

A = total projected area of decks normal to wind direction up to the top of the main deck

Velocity V varies with respect to elevation above mean water level. The velocity used in equation 4.3 is determined by choosing a mean velocity profile, which is then modified to account for gusting effects. The details of this procedure are outlined in API (1993).

Wind loads, while being important, do not usually represent a significant percentage of the total lateral load on a fixed offshore platform in intermediate to deep water. In addition,

the kinematics of wind are much more stable and easily describable than those of ocean storm waves. Many partial and full scale tests have been performed for wind loads, so that the wind load test "databank" is much more comprehensive than that for wave loads. Thus, no further detailed discussion of wind load will be included here. For further information on the subject, a relatively complete listing of references on the subject can be found in Bea (1994).

4.6 DNV's WAJAC Wave Load Generation Computer Program

This research used the WAJAC wave load generation program to generate hydrodynamic forces for use in its ULS analyses (DNV, 1994b). WAJAC is part of the SESAM analysis program developed by Det Norske Veritas of Norway. The program also computes selfweight gravity loads and buoyancy loads.

WAJAC is a very versatile program that allows the user many options in determining how the hydrodynamic loads are generated. As an example, WAJAC has a number of possible wave theories available. This research used Stoke's V wave theory due to its broad range of use and its general acceptance in the offshore industry. WAJAC can also perform time domain and frequency domain analyses. However, since this research concentrated on static ULS analyses, a deterministic wave approach was used throughout.

To perform a deterministic wave load analysis, WAJAC uses a complete structural model generated by PREFRAME (DNV, 1994a) and a design wave and current. For the wave,

WAJAC requires the height, period and wave direction relative to the platform. For the current, a velocity profile with direction is needed up to the expected wave crest. Using the wave and current information, WAJAC determines the fluid particle kinematics at every point throughout one wave length. Then, applying these kinematics to the PREFRAME model, the local forces on all members are generated at user defined time periods or phase angles. Thus, the position of the wave crest relative to the platform that gives the largest base shear can be found from trial and error and later used in the ULS analyses.

WAJAC was not used to directly generate wave in deck loads for the reasons discussed in section 4.4. However, the wave kinematics developed by WAJAC were used in equation 4.2 to calculate the deck loads by hand.

5.0 ULTIMATE LIMIT STATE PUSHOVER ANALYSES

5.1 Introduction

All discussion until now has focused on ocean storms and the forces they induce on offshore structures. From previous sections, given a specific structure and the important properties of a particular storm, e.g., wave, current and wind details, it is possible to determine the maximum forces that such a storm would exert on the structure. Once this load or force profile is known, one can analyze the structure's behavior or response to such forces.

This report is concerned with performing analyses to determining a structure's ultimate limit state or ultimate capacity. Thus, it is necessary to go beyond performing a purely linear elastic analysis and into the realm of modified linear or complete non-linear analysis. Currently, the state-of-the-practice (API, 1993) is to use a modified linear elastic analysis. The modification comes from applying theoretical and empirical factors to the linear results to predict local and global failure. However, the state-of-the-art approach, which is utilized in this report, is to perform a complete non-linear analysis. A non-linear analysis considers both geometric and material non-linearities to directly determine a structure's failure mode and ultimate load resisting capacity.

5.2 Defining Failure

Obviously, if the ultimate limit state is defined as the load resistance existing at the time of failure, it is first necessary to define failure. This fact may appear obvious or even rhetorical, but failure can take on many forms. For example, for the case of an offshore platform, failure could be defined as member yielding, member plastification, tensile fracture, crack rupture, weld fracture, exceeding a specified displacement, buckling or global collapse. Failure could even have a somewhat nebulous definition such as X barrels of oil spilled , Y lives lost or Z dollars in damage. This report defines failure as exceeding the maximum base shear. This event typically occurs after multiple yield events and one or more individual member failures, e.g., brace buckling.

5.3 Geometric Non-Linearity

The inclusion of geometric non-linearity in an analysis generally means that equilibrium is achieved in the deformed position versus the undeformed position. For structures with small displacements, the inclusion of geometric non-linearity may not be significant. However, for structures with large displacements or for very highly stressed members, the inclusion of such effects could produce a substantial difference in the analysis results.

There are two general types of geometric non-linearities, $P\Delta$ effects and $P\delta$ effects. $P\Delta$ effects reduce the global stiffness of frames or structures due to sidesway of the overall system. $P\delta$ effects occur at the local or member level and are not dependent on the

existence of sidesway. These two effects can be readily seen in figure 5.3-1 (White and Hajjar, 1991).

Many analysis programs available today consider PΔ effects. However, few programs perform a true or comprehensive second-order analysis by including the local Pδ effects. The reason for this simplification is the complexity involved in a Pδ analysis. For while a PΔ analysis only requires the rotation of the member chord, which is a function of the end node displacements, a Pδ analysis requires the exact or near exact description of the deformed member shape.

USFOS uses a user defined initial imperfection, single or double curvature, and the exact solution of the fourth-order differential equation for a beam subjected to end forces for its element formulation. Effects of large displacements and coupling between lateral defection and axial strain are included by using Green strain (SINTEF, 1994). In addition, The elastic tangent stiffness matrices are calculated from closed form expressions. No numerical integration is performed over either the member cross section or member length (SINTEF, 1988b).

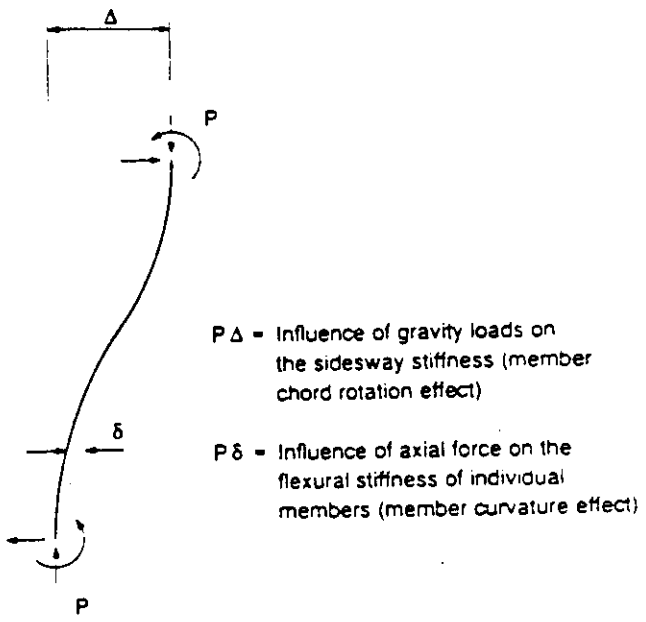

Figure 5.3-1: PΔ and Pδ Effects (White and Hajjar, 1991)

5.4 Material Non-Linearity

Linear elastic analyses assume a linear relationship between stress and strain proportional to Young's modulus for all levels of strain. Non-linear analyses consider the non-linear stress-strain behavior that usually occurs at high levels of strain. While one rarely attempts to model the exact stress-strain behavior of a material, certain key parameters exist which can be used to define a simplified multiple-linear stress-strain model. Thus, every non-linear stress-strain model needs an initial stiffness, Young's modulus, a yield criterion, a flow rule and a hardening rule.

The yield criterion determines at what stress or strain state the material begins yielding or deviates from the linear stress-strain relationship. Two popular yield criteria are the

Maximum Shear (Tresca) and Distortion Energy (von Mises) criteria (Mosaddad and Powell, 1982). The von Mises yield criterion is generally accepted as being more accurate and is defined by a single continuous function criteria (Mosaddad and Powell, 1982). In USFOS, the yield condition is defined by a plastic interaction function for the stress resultants:

$$\Gamma = f\left(\frac{N}{N_P}, \frac{Q_y}{Q_{yP}}, \frac{Q_z}{Q_{zP}}, \frac{M_x}{M_{xP}}, \frac{M_y}{M_{yP}}, \frac{M_z}{M_{zP}}\right) - 1 = 0 \tag{5.1}$$

which for a tubular section with torsion and shear forces neglected reduces to

$$\Gamma = f\left(\frac{N}{N_P}, \frac{M_y}{M_{yP}}, \frac{M_z}{M_{zP}}\right) - 1 = \cos\left(\frac{\pi}{2}\frac{N}{N_P}\right) - \frac{\sqrt{M_y^2 + M_z^2}}{M_P} = 0 \tag{5.2}$$

Once the yield criterion has been satisfied, any further increase in stress or strain will cause the stress-strain path to deviate from its original linear path.

A flow rule determines the direction of the stress-strain path once yielding has occurred. It is assumed that after yield, any strain increment can be divided into elastic and plastic parts. That is,

$$\Delta v = \Delta v_e + \Delta v_p \tag{5.3}$$

For metals, an associated flow rule is usually assumed. Graphically, the associated flow rule means that the contours of the plastic potential function are comprised of multiple curves which are geometrically similar to the yield function.

In USFOS, the flow rule is given by

$$\Delta v_p = \begin{bmatrix} g_1 & 0 \\ 0 & g_2 \end{bmatrix} \begin{bmatrix} \Delta\lambda_1 \\ \Delta\lambda_2 \end{bmatrix} = \boldsymbol{G}\Delta\lambda \tag{5.4}$$

where

$$g_i^T = \frac{\partial \Gamma}{\partial \boldsymbol{S}_i} = \left[\frac{\partial \Gamma}{\partial N}, \frac{\partial \Gamma}{\partial Q_y}, \frac{\partial \Gamma}{\partial Q_z}, \frac{\partial \Gamma}{\partial M_x}, \frac{\partial \Gamma}{\partial M_y}, \frac{\partial \Gamma}{\partial M_z} \right]_i \tag{5.5}$$

and index i refers to the beam ends (SINTEF, 1994). The direction vector of the plastic displacements at the current force state, $\boldsymbol{S}_i$, is given by the normal to the yield surface, Δg_i. The magnitude of the plastic displacements is defined by a scalar factor $\Delta\lambda$.

The hardening rule describes the progressive change of the yield surface between plastic states for strain-hardening materials. For an elastic-perfectly-plastic material, that is one with zero post-yield stiffness, the yield surface does not change for strains exceeding the yield strain. However, for strain-hardening materials, the slope of the post-yield stress-strain is not zero. Thus, the yield surface must change to account for this new stiffness.

Two widely accepted hardening rules are the kinematic rule of Prager and the isotropic rule of Hill criteria (Mosaddad and Powell, 1982). The kinematic rule, as its name implies, involves the movement of the yield surface origin while retaining the original yield surface shape. This isotropic rule involves changing the shape or size of the yield surface while keeping the original origin. These two rules are graphically illustrated in figure 5.4-1 (Mosaddad and Powell, 1982).

USFOS uses a two surface plasticity model, a yield surface and a bounding, fully plastic surface (SINTEF, 1994). In force space, when the force state contacts the yield surface, this indicates the first occurrence of yield in the cross section. At this stage a yield hinge is introduced. When the force state contacts the bounding surface, the cross section is fully plastic. Between the two events, the yield surface moves so that the force state does not leave the yield surface. The bounding surface also moves to account for strain hardening, but the bounding surface moves much slower than does the yield surface. Figure 5.4-2 illustrates this hardening process for a tubular cross section plotted in two dimensional force space criteria (SINTEF, 1994).

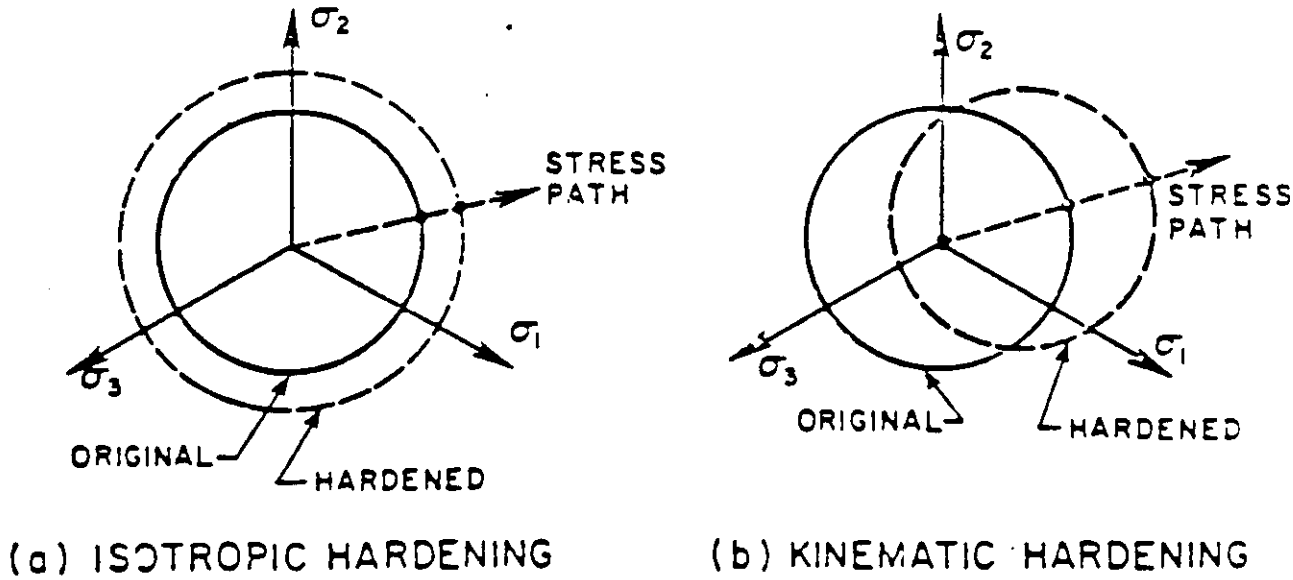

Figure 5.4-1: Strain Hardening Assumptions (Mosaddad and Powell, 1982)

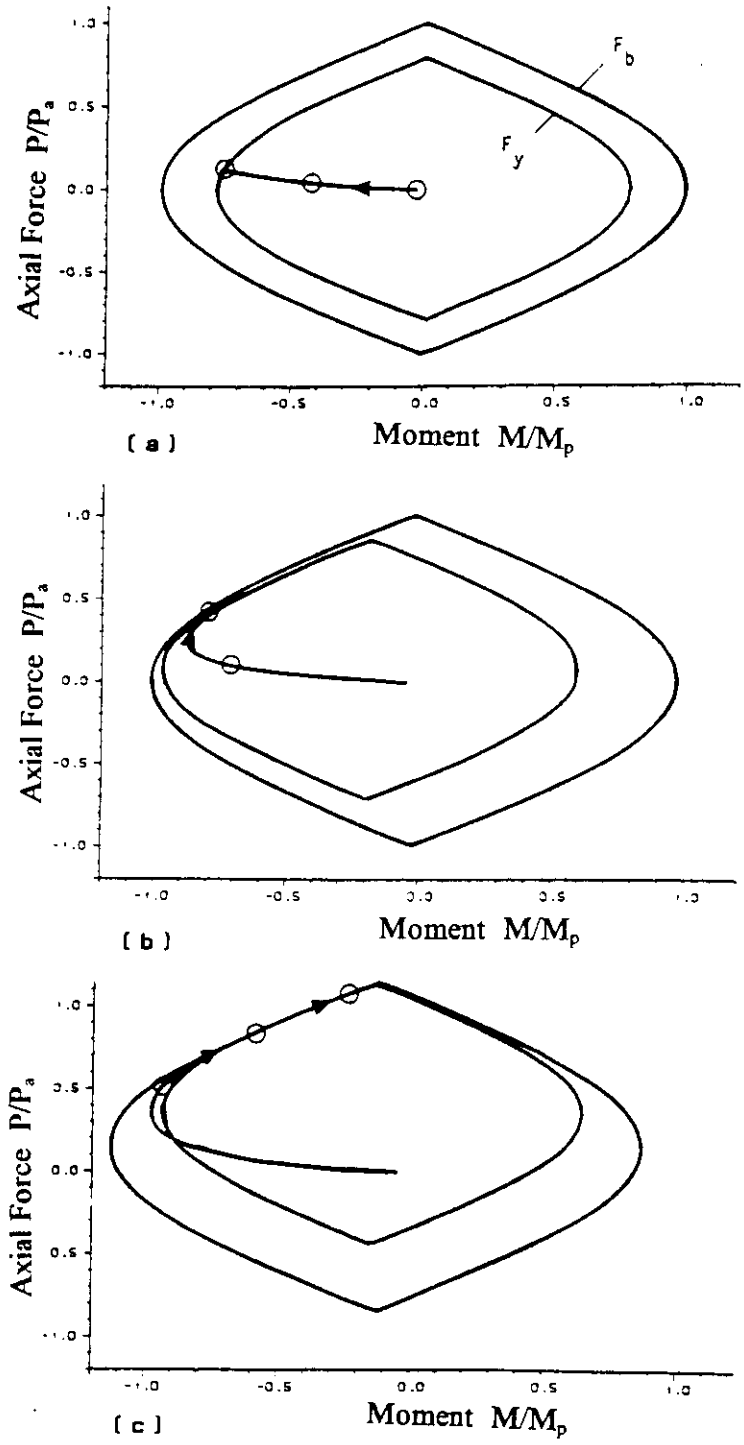

Figure 5.4-2: Two-Surface Plasticity Model With Kinematic Strain Hardening (SINTEF, 1994)

5.5 SINTEF's USFOS Collapse Analysis Computer Program

USFOS is an extremely powerful, state-of-the-art computer program design to perform progressive collapse analyses of steel offshore structures. USFOS is solely devoted to performing collapse analyses. Consequently, structure models and load profiles must be generated elsewhere. In fact, USFOS was specifically designed to be compatible with PREFRAME and WAJAC.

USFOS's solution algorithm is based on energy principles and allows for large displacements but assumes small strains. Elastic tangent stiffness matrices are calculated using closed form expressions (SINTEF, 1988b). Thus, as previously stated, no numerical integration is performed over the member cross section nor over the member length. The load is applied incrementally according to the updated Lagrangian formulation (SINTEF, 1994). The load increment is internally reversed if global instability is detected. The effects of initial imperfections and local buckling are included for beam elements. Joint flexibility and joint capacity can be included using API or DOE rules (SINTEF, 1988a).

Many of USFOS's features were not used for this research. Some of the more advanced features of USFOS are

- inclusion of globally damaged or locally dented members,
- ship collision analyses,
- dynamic collapse analyses,
- inclusion of external hydrostatic pressure
- and inclusion of temperature effects.

Finally, one of the most powerful features of USFOS is its post-processing unit, POSTFOS with its graphical interface, XFOS. Using POSTFOS, any bit of analysis information can be extracted and tabulated. This is accomplished using step and history tables. Step tables report information for a single step in the analysis, while history tables report desired information at every step in the analysis. These tables can be easily printed or imported into most spreadsheet or database programs for further manipulation or plotting. XFOS can be used to view both history plots and deformed structural model at any step in the analysis. Color fringes can also be applied to the models to graphically show normalized values of member stress, member plastification and a host of other parameters that may be of interest to the user. POSTFOS and XFOS are both extremely powerful and easy to use and help make the USFOS one of the most complete analysis packages available today.

5.6 Verification Studies of USFOS Analysis Program

While there are several different non-linear packages available for use today, there has been relatively little benchmarking of such packages against either analytical, experimental or insitu test data (Billington, 1993). However, such comparisons are extremely important not only to verify the robustness of the software but also to test the software's sensitivity to its input parameters. Non-linear analysis programs are designed with various solution schemes, e.g., conventional finite elements, phenomenological modeling or exact beam-column action modeling, which are dependent upon certain assumptions concerning material and member behavior. Thus, while a particular benchmark comparison may yield

similar results, other comparisons may uncover result discrepancies or software limitations.

USFOS has been the subject of many benchmarking tests, not including the research presented here, which attempt to validate or verify its solution scheme. Sφreide (1986) has documented several studies which compared USFOS results with "proven" FE programs and large scale frame tests.

One such test compared USFOS and FENRIS (Sφreide, 1986) results by analyzing an axially loaded simply supported beam-column with a slenderness ratio of 120. Figure 5.6-1 shows that the two programs yield very similar results. While the load deformation histories in the elastic range are nearly identical, they deviate slightly near the peak load. USFOS underestimates the capacity in the post-buckling range due to the initial out-of-straightness being simulated by lateral load (Sφreide, 1986).

Another test cited by Sφreide (1986) concerns the experimental analysis of the 2D K-braced frame shown in figure 5.6-2. The transverse beam was supported by two diagonal bracing elements and loaded by a hydraulic jack at the joint. The load-displacement history for both the experiment and the USFOS analysis are shown in figure 5.6-3. The yield stress in the transverse beam was increased from 335 MPa to 414 MPa to account for strain hardening in the large deflection range. As before, USFOS underestimates the

frame's post-buckling capacity. However, taking into account the sensitivity of the frame and its associated data recording instrumentation, the difference in results is tolerable.

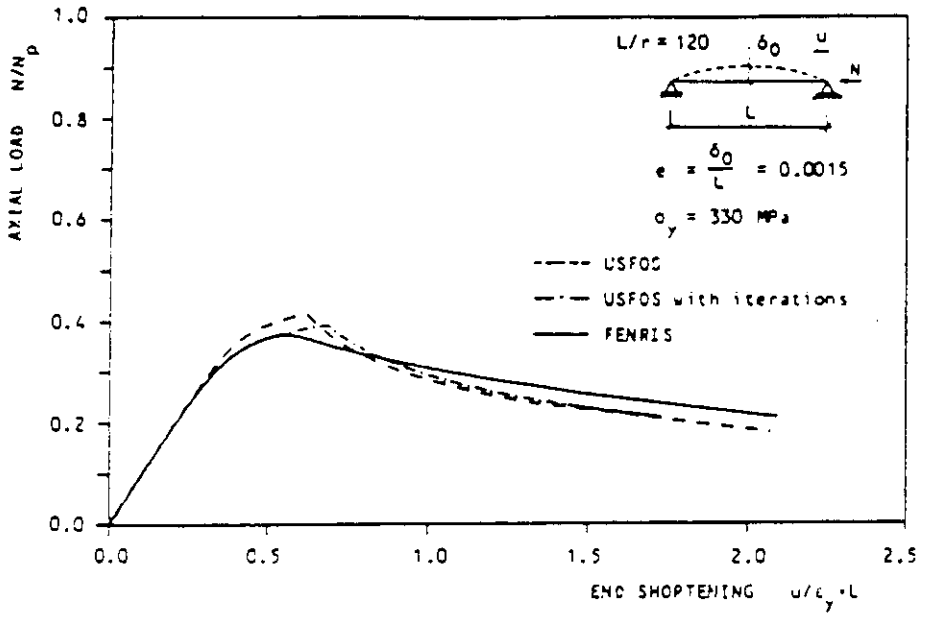

Figure 5.6-1: Comparison of USFOS and FENRIS Results (Sφreide, 1986)

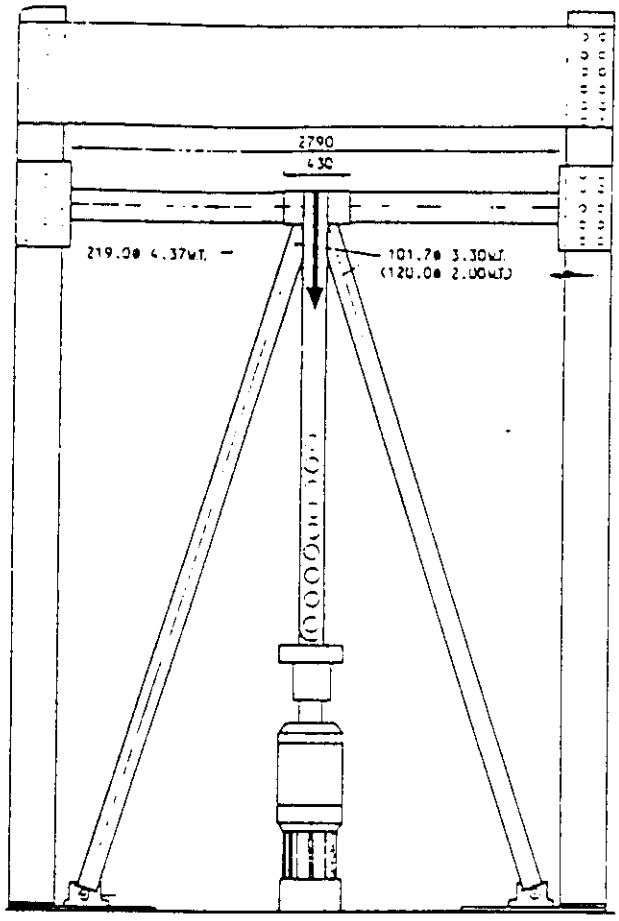

Figure 5.6-2: K-Braced Frame for USFOS Comparison Study (Søreide, 1986)

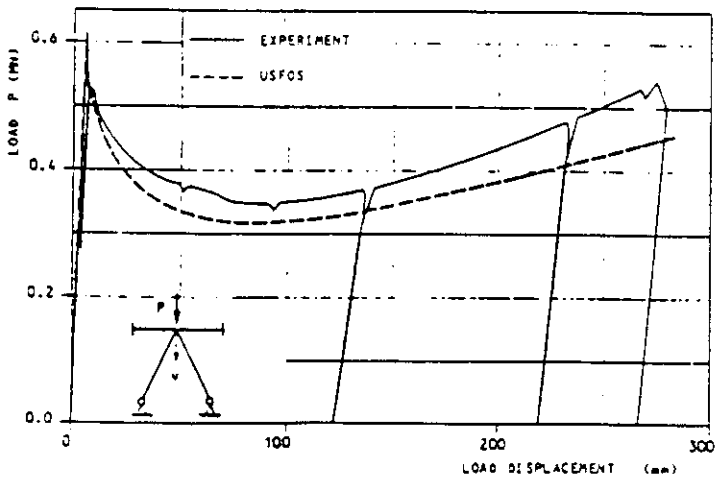

Figure 5.6-3: Load-Displacement History for K-Braced Test Frame (Søreide, 1986)

5.7 Non-Linear Foundation Modeling

The USFOS computer models used for this research contained non-linear foundations. All the platforms analyzed had tubular pipe piles extending down into primarily clay and silty clay soils. Thus, the non-linear foundations consisted of non-linear soil-springs connected along the pile length. Three types of non-linear springs were modeled: axial friction (T-Z), end bearing (Q-Z) and lateral displacement (P-Y).

In most cases, API RP 2A Section 6 was used to define the general spring properties by non-linear, force/displacement curves. Figures 5.7-1 and 5.7-2 show typical T-Z and P-Y curves respectively. For some analyses, these curves were modified to account for dynamic strain hardening effects, code biases or soil data corrections. These modifications are and their effects on the global platform capacity are discussed in section 7.3. Once T-Z and P-Y curves were defined for a section of pile, they were combined into one springs and connected to an adjacent pile node. The springs were then defined by the pile section's local degree of freedom. Hence, axial displacement was defined as the displacement of the node in the direction of the pile section's longitudinal axis. Lateral displacement was defined as displacement in both orthogonal directions perpendicular to the pile's longitudinal axis, i.e., a P-Y spring was defined for the pile section's local y and z axes.

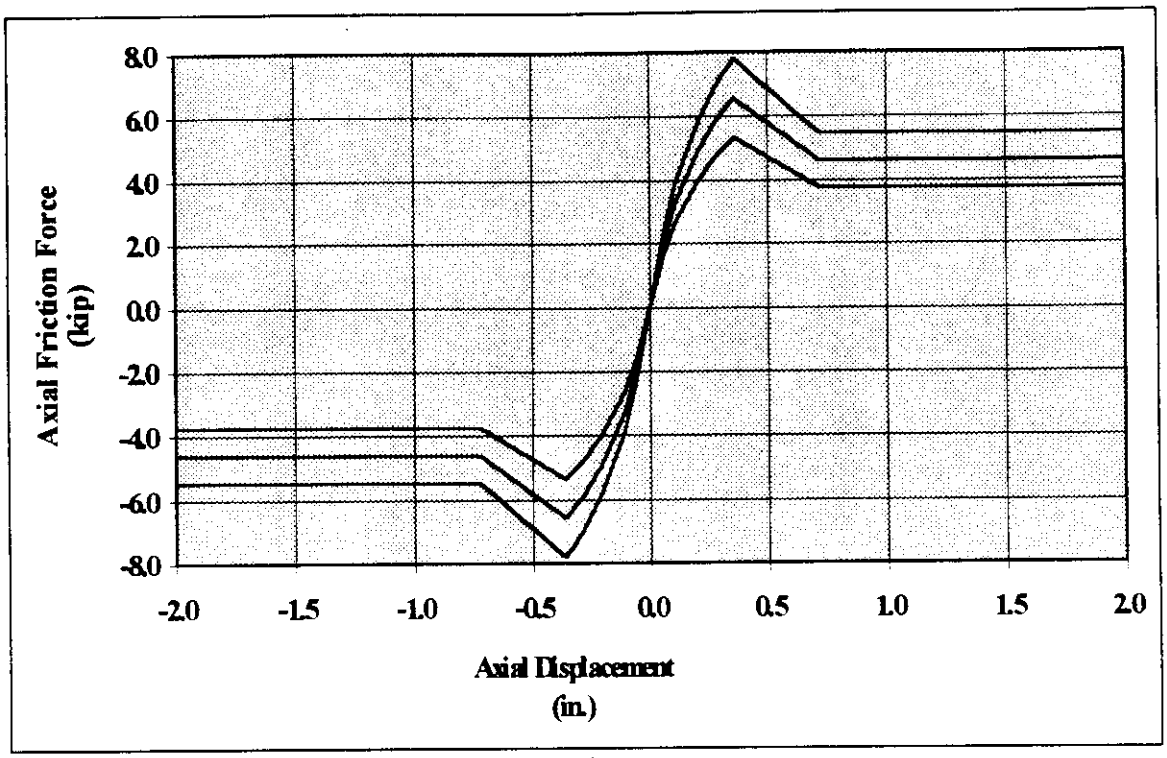

Figure 5.7-1: Typical T-Z Soil Spring Curve

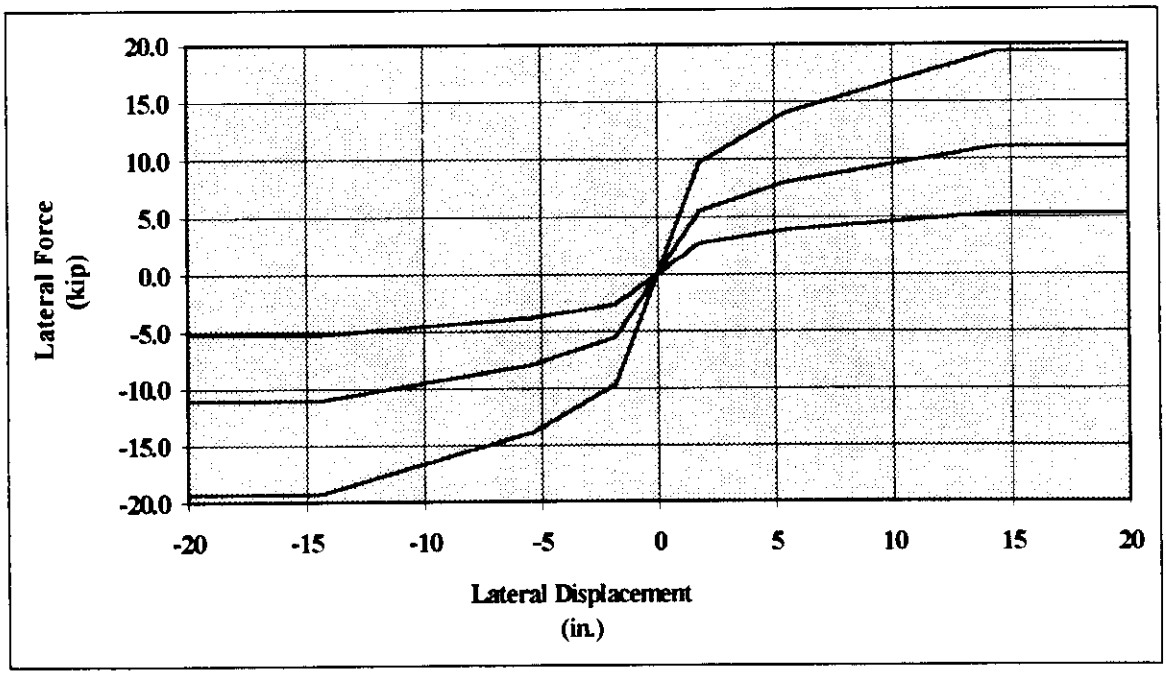

Figure 5.7-2: Typical P-Y Soil Spring Curve

6.0 RESULTS OF CASE STUDIES

This section presents the results of the four platforms analyzed as part of this report. Additional detailed information and example calculations for the platforms can be found in Appendix B. The platform names and certain platform information are withheld in this report to protect the anonymity of the platform owners.

6.1 Platform A

Platform Description

Platform A (PA) is located in the Gulf of Mexico's South Timbalier region. This region is subject to severe storm conditions. McDermott Inc. originally designed the platform using a 25 year Glenn storm (wave height of 55 feet). McDermott later fabricated and installed PA in 118 feet of water. The installation occurred in July 1964.

PA is a self contained eight pile drilling and production platform with twelve slots and nine drilled wells (figures 6.1-1 to 6.1-3). It had an original production capacity of 85 MMCFD. Cellar and main deck elevations are at + 34 ft and +47 ft respectively. The major deck framing is 43 ft x 93 ft in plan, and the jacket legs are battered at one to eight in both broadside and end-on framing. The deck legs are 36 in. in diameter and are connected to the tops of the piles. The 39 in. diameter legs have no joint cans. However, gusset plates are used with the jacket leg K-joints. The broadside braces vary from 14 in.

in the first of four jacket bays to 20 in. in the lowest jacket bay, while the end-on bracing varies from 14 in. to 16 in.

Based on coupon tests, the jacket bracing and horizontal framing are made of nominal 50 ksi steel with an average yield strength of 58 ksi. According to the platform owner, the jacket legs and piles are composed of nominal 36 ksi steel with an average yield strength of 43 ksi. The strength of the legs and piles is based on the assumption that large members, i.e., greater than 30 in., were fabricated of plate steel, while the smaller members were constructed of rolled pipe sections.

The 36 in. piles extend 190 ft below the mudline through 165 ft of soft to stiff gray clay and 25 ft of fine dense sand. At the time of design, anticipated pile loads were 770 tons in compression and 350 tons in tension. PA's piles were grouted inside its 39 in. jacket legs in 1973 as a result of its first risk assessment.

Platform History

Although the platform has survived several hurricanes, namely Carmen and Andrew, PA has sustained no significant structural damage. This is due in part to previous platform remediations. In 1974, the eye of Hurricane Carmen passed within ten miles of PA. Cellar deck damage suggests the largest waves were approximately 58 ft from the southeast. Hindcast studies predicted slightly higher wave heights. Post-hurricane analyses indicate that the +10 ft vertical diagonal joints may have experienced minor

compressive yielding. The platform was the subject of a risk analysis in 1988 that identified it as a significant risk. Consequently, in 1991 all eight conductors were removed and the cellar deck was cleared of all equipment.

In 1992, the eye of Hurricane Andrew passed within eight miles of the platform. Cellar deck damage suggests a maximum wave height between 60-64 ft from east-southeast, approximately fifteen degrees off broadside. Hindcast studies confirm this information. During this event, all four +10 ft K-joints experienced yielding, two at ultimate capacity. During the post-hurricane inspection, it was discovered that there was no grout in the pile-jacket leg annulus at +10 ft. Below the water line, the grout performed well. If all four +10 ft K-joints yield, a collapse mechanism is formed. It was estimated that ten percent more lateral load would have collapsed the structure. Post-hurricane analyses showed that the load causing the joint yielding was very close to the load experienced during Andrew. More importantly, it was estimated that removing the conductors decreased the load during Andrew by twenty percent. Analyses also showed that the platform was capable of being re-loaded to the level experienced during Andrew. However, the +10 ft K-joints were grouted as an additional safety measure.

Platform Loading

The analysis performed on PA included assumptions and estimations that do not exactly match those in API RP-2A or those of the hindcast studies for Andrew. Some of the assumptions concerning PA were made due to lack of detailed information concerning the

platform and the oceanographic conditions in the area. One example of this was the lack of information concerning the deck structures and their supported equipment. Other assumptions were made due to the desire to use as much of the owner supplied computer model as possible. The platform owner previously performed a pushover analysis using USFOS and supplied a copy of their input file as part of the platform's documentation. Therefore, some details concerning the platform and its loading were previously developed by the owner and used unmodified in this analysis.

Several trials analyses were performed to find the wave height that caused platform failure with a load factor of unity. It was assumed that the majority of the load causing failure in the platform was due to wave loads, specifically wave-in-deck loads. Therefore, no attempt was made to exactly correlate the wave height, current and wind to the same return period. Instead, current and wind data from the Andrew hindcast studies were used while the wave height was varied. The wind forces used were previously calculated by the owner. Without sufficient details to perform loading calculations, the boat landing forces were assumed to be equal to 80 kips for broadside loading case and were applied at the +10 ft horizontal framing. Since the failure mode was not expected to be in the jacket legs or the piles, the broadside and end-on loading scenarios were considered separately (Bea and Mortazavi, 1995).

Hydrodynamic coefficients were chosen based on recent test data and engineering judgment. Due to the uncertainty in the appurtenance loads, the drag coefficient for

smooth cylinders was chosen to be artificially high to conservatively increase the load above the water line. Moreover, it has been shown that surface roughness heights as little as D/1000 are large enough to create rough surface behavior in the passing fluid (Bea, 1994). Thus, the drag coefficient, C_d, was taken to be 1.2 for both rough and smooth cylinders. The inertia coefficient, C_m, was taken to be 1.2 for rough cylinders and 1.6 for smooth cylinders respectively (Bea, 1994).

A wave kinematics factor equal to 0.88 was used for both the deck and jacket loads. A current blockage factor of 0.80 for broadside loading and 0.70 for end-on loading was also included. Summaries of the loading magnitude and pattern for both broadside and end-on loading scenarios are included in figures 6.1-4 and 6.1-5 respectively. It should be noted that the wave height used for the end-on loading scenario did not create a load pattern that failed the platform with a load factor of unity. However, it was determined that this wave height was close to the realistic limit for this water depth.

Computer Model

As previously mentioned, the model used for this analysis was created by the owner after Hurricane Andrew. The model for PA contains only the main structural components of the platform. It was assumed that the main and cellar decks were not part of the first failure mode. Therefore, only the main framing members of the decks were modeled. The conductor framing was replaced with sufficiently rigid cross members to simulate their stiffness contribution. To account for a grouted pile-jacket leg annulus, the owner

doubled the leg thickness. All members were given an initial imperfection, which was calculated by using Chen's buckling curve and member information for the critical braces in the structure. Finally, since the damaged joints in the platform have all been grouted, this analysis used rigid joints.

The non-linear soil springs were developed by PMB using the PAR (Pile Analysis Routines) program assuming static loading. Since the first failure mode occurred in the upper jacket bay for both broadside and end-on loading, the exact performance of the soil springs was not critical in determining the ultimate lateral load resistance capacity of the platform. However, there are two items concerning the soil spring models that should be noted.

First, the T-Z and Q-Z springs included as part of the model are linear as defined in the input to USFOS, which means that they will exhibit elastic behavior. The owner originally defined these nodes using two force-displacement points, which translates into a straight line model. When defining nonlinear soil properties, USFOS linearly extrapolates from the last two user-defined points at both curve extremes. Therefore, since there were only two user-defined points defining the non-linear behavior of the T-Z and Q-Z springs, USFOS extrapolated along the same original user-defined line for both tension and compression behavior. The P-Y curves were defined using eight points, four points for each transverse direction. Thus the P-Y springs will exhibit non-linear behavior.

As stated above, the linear elastic model of the T-Z and Q-Z springs will not significantly effect the determination the platform's ultimate capacity. However, this fact is based on the assumption that the pile-soil interaction is not part of the first failure mode. The ultimate pile uplift and compression forces were calculated by the owner using the AXCAP computer program and were included as part of the platform's documentation. The largest tension and compression pile forces for both the broadside and end-on loading cases were lower than these previously calculated maximum values. Thus, the piles are not the weak link in the system for the load patterns used. Hence, while the ultimate capacity of the platform should not be significantly affected by the linear springs, it is assumed that the shape of the displacement dependent results will not be exactly correct.

Secondly, the manner in which the combined T-Z/P-Y springs were modeled is prone to potential error, especially for large displacements. Again, this error is assumed not to affect the ultimate capacity of the platform, but it does cause inaccuracies that are worth mentioning. In the PA model the T-Z and P-Y were combined into a two node non-linear soil spring. The combined spring has T-Z spring properties for its axial displacements and P-Y spring properties for its transverse displacements. Both axial and transverse displacements are measured relative to the original coordinates of the element's end nodes. However, when a T-Z/P-Y soil spring element becomes deformed, the relative position of the two end nodes must be considered for the deformed shape. Since this is not the case, in a deformed position the displacement transverse to the element will be

resisted by the P-Y spring and the T-Z spring. The exact spring properties for any given deformed shape can be solved using vector analysis.

Broadside Loading

The force-displacement curve for broadside loading is shown in figure 6.1-6. This curve indicates that the platform fails at 0.907 of the reference load pattern or a total base shear of 3,860 kips. From figure 6.1-6, it can be seen that the platform has no reserve strength after the first brace buckles. However, it is important to note that the platform can experience large inelastic displacement before a mechanism is formed. If the force-displacement curve were extended, it would show that eventually, the jacket legs develop sufficient resistance in bending to cause buckling of the braces in the third jacket bay.

The axial force history for the four upper braces that buckle and the outer sets of braces at this same level are shown in figures 6.1-7 and 6.1-8 respectively. The forces shown are normalized by the plastic axial capacity of the members, i.e., the actual axial force divided by the product of the member's area and yield stress. The normalized interaction curves for two of the four upper compression braces are shown in figures 6.1-9 to 6.1-10. The normalized moment values significantly beyond 1.0 are not realistic and are probably the result of very large strains at the plastic hinges, which can result in mathematical errors in the solution strategy. However, since these strains do not occur until well after the maximum capacity has been reached, the errors they cause are inconsequential.

End-On Loading

The force-displacement curve for end-on loading is shown in figure 6.1-11. This curve indicates that the uppermost compression braces buckle at 1.12 of the reference load pattern or a total base shear of 3,905 kips. Figure 6.1-11 shows that after the compression braces in the fourth jacket bay buckle, the platform has a small increase in resistance capacity until the compression braces in the third jacket bay and the horizontal framing between these two levels almost simultaneously buckle, at which point the platform is at imminent collapse. Detailed force histories for the critical braces are shown in figures 6.1-12 and 6.1-13. As in the broadside loading case, figures 6.1-14 and 6.1-15 show that the main components of the failure mode, namely the critical compression braces, have a credible interaction relationship.

Comparison of Analysis Results to Observed Performance During Andrew

The hindcast data and observed platform performance indicate that PA survived 60-64 ft waves 15 degrees off broadside during hurricane Andrew. Therefore, approximately 96 percent of Andrew's load was resisted by the end-on framing. The USFOS analysis indicates that the platform experiences first significant member failure, brace buckling, at 91 percent of the load from a 64 ft direct broadside wave.

The deck loads are very significant for this loading profile. The deck loads represent nearly 40 percent of the total load. Therefore, the hydrodynamic loads are highly sensitive to the wave height and the surge height. In addition, initial imperfection magnitude and direction are realistic but somewhat conservative. However, it is important to note that

joint behavior does influence member capacity. Consequently, the calculated brace strength would be different (most likely smaller) if flexible joints had been used.

Taking the above factors into consideration, the USFOS results indicate that PA would most likely survive the loads from Hurricane Andrew. It should be noted again that the USFOS model assumed rigid joints and that some joint deformation was observed in the ungrouted joints following Andrew. Thus, joint failure could have been the weak link in the platform. However, all platform joints are currently grouted. Consequently, the USFOS results represent a good approximation of the platform's current lateral load resistance capacity.

Previous analyses of this platform showed a broadside capacity approximately 20 percent greater than that presented here (Imm et al., 1994). In addition, the failure mode predicted was joint failure of the +10 ft K-joints. This previous analysis did not use USFOS's joint analysis feature, but rather input springs at the critical joint that had predetermined capacities. Also, the previous analysis applied only joint loads, and thus, did not consider local hydrodynamic member forces. As is shown in section 7.2, local member forces can significantly affect the capacity of slender brace members. Lastly, a different load profile was used, which can cause appreciable differences in structure behavior (Imm et al., 1994).

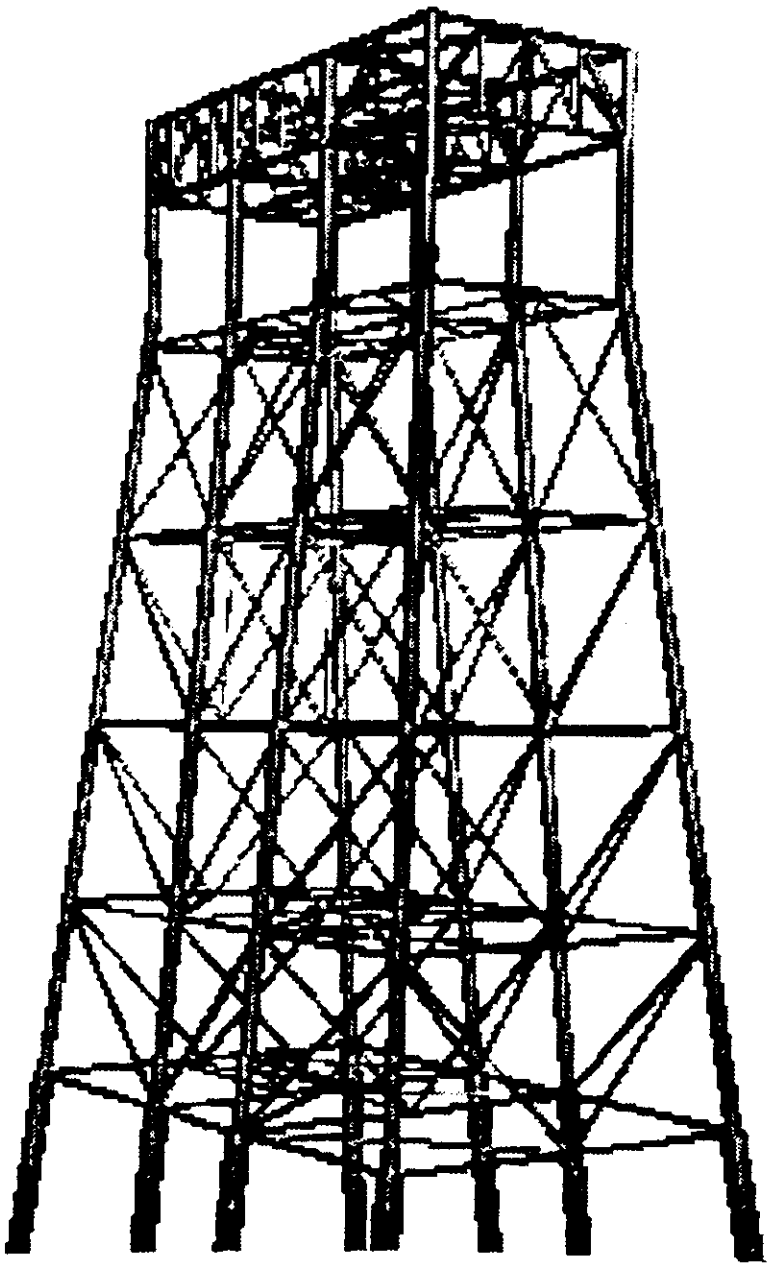

Figure 6.1-1: Platform A Isometric View

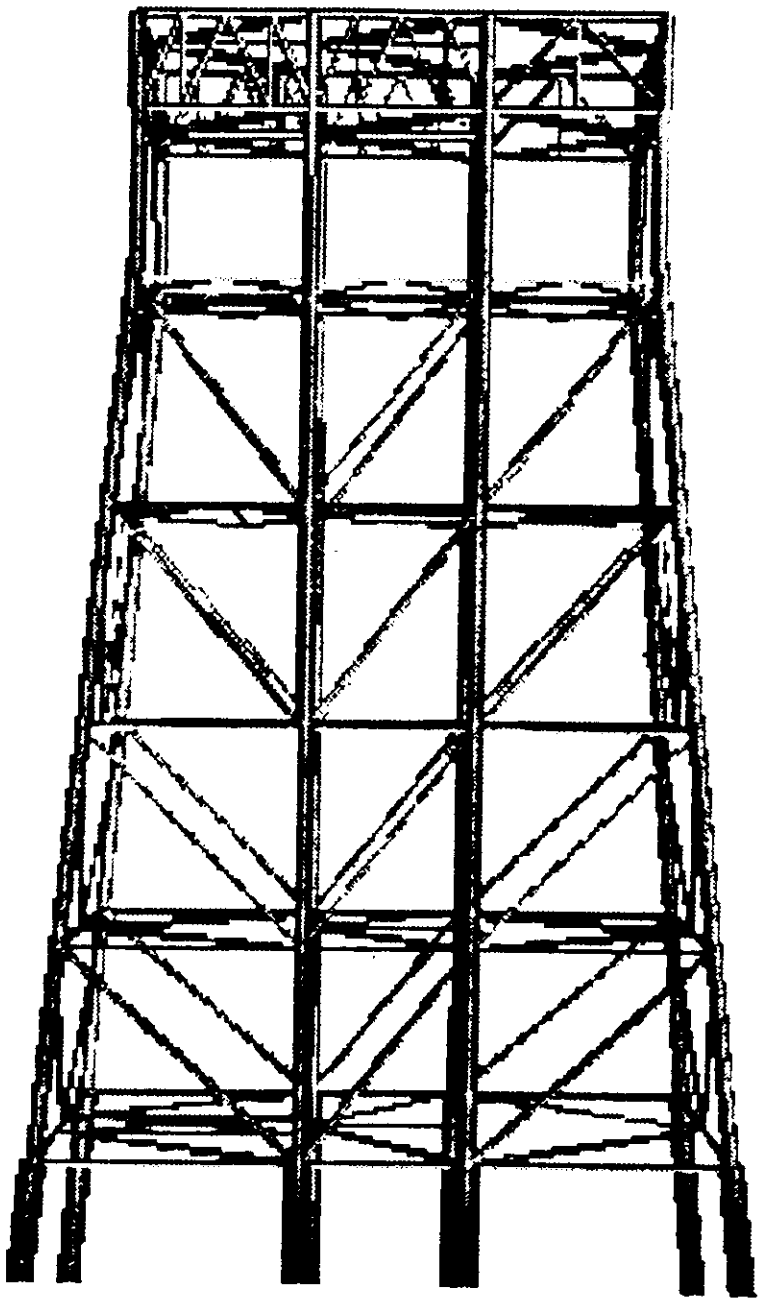

Figure 6.1-2: Platform A Broadside Elevation

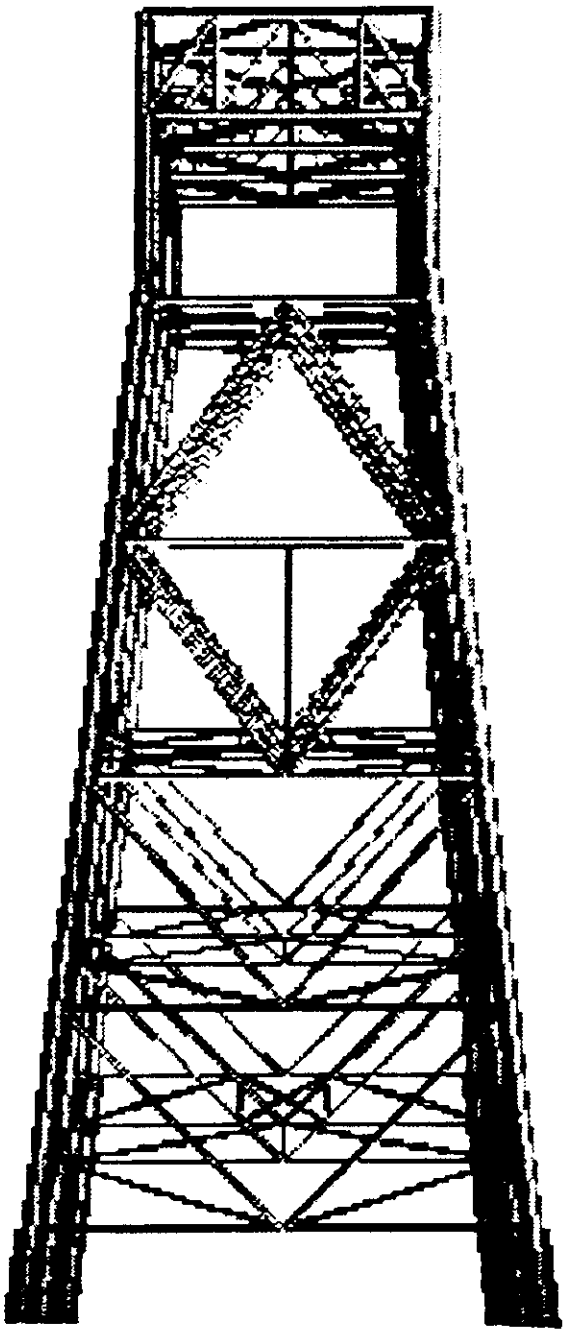

Figure 6.1-3: Platform A End-On Elevation

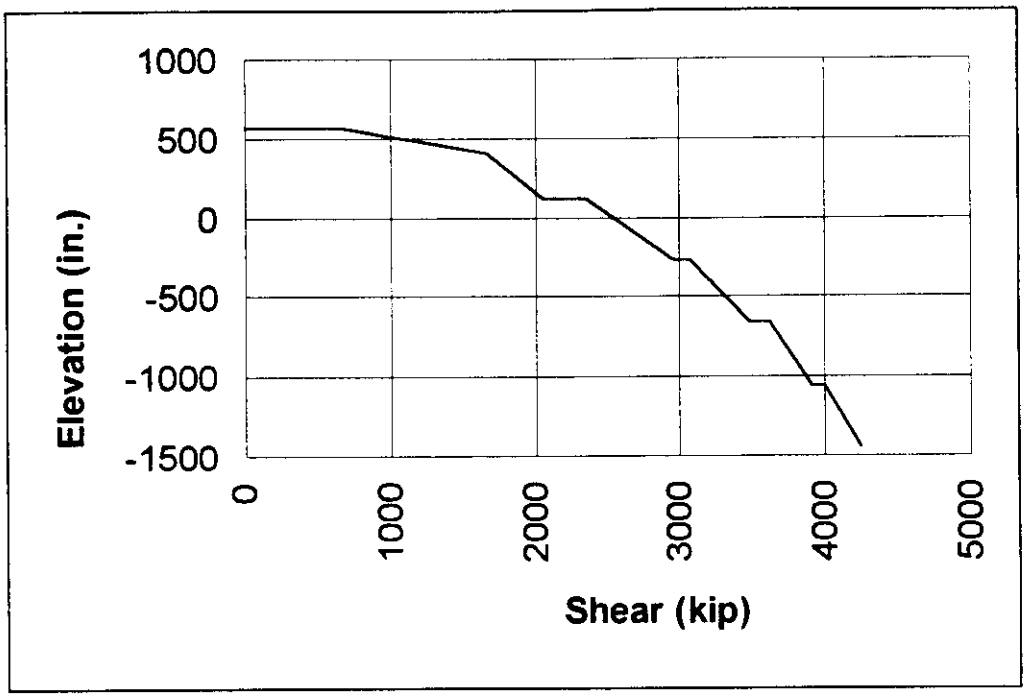

Figure 6.1-4: Platform A Broadside Shear Profile

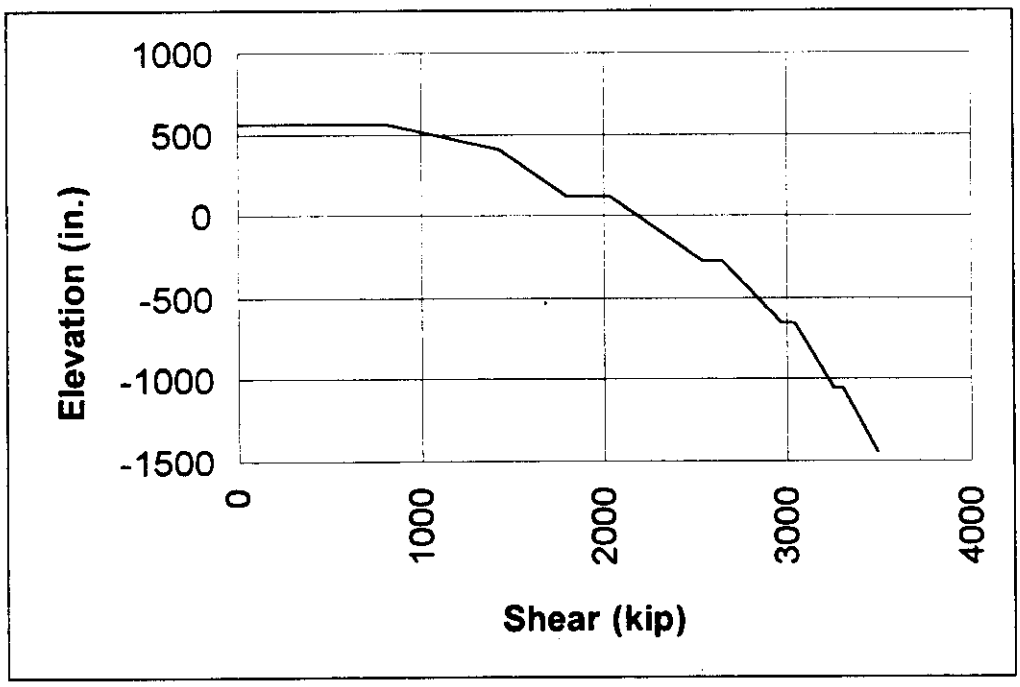

Figure 6.1-5: Platform A End-On Shear Profile

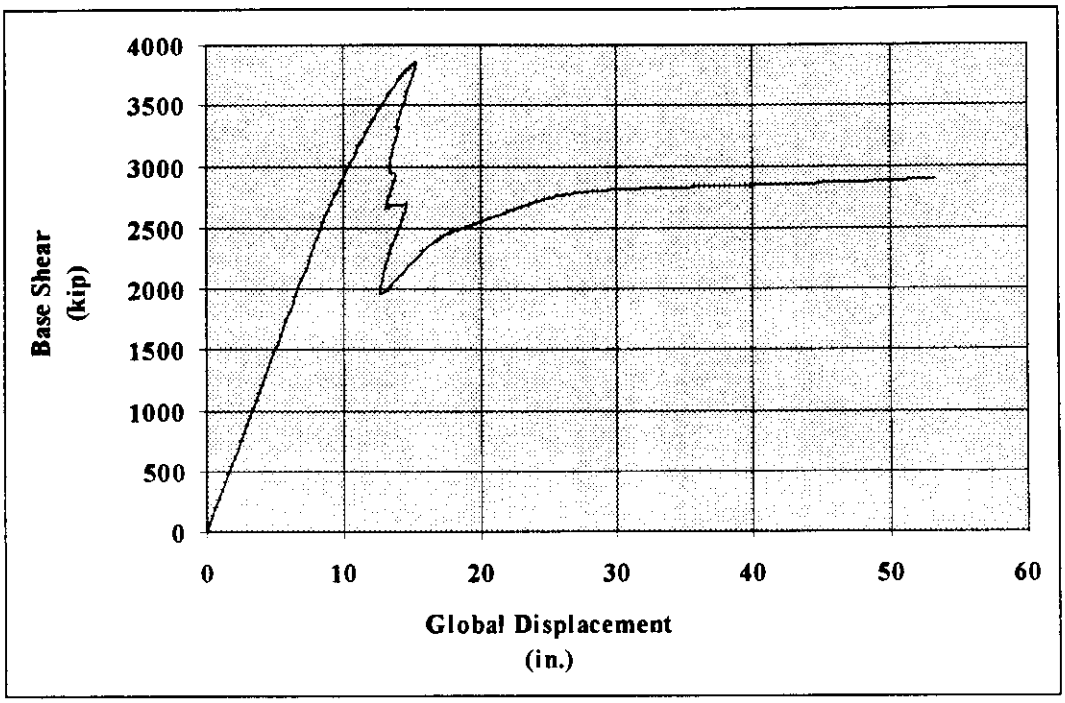

Figure 6.1-6: Platform A Broadside Force-Displacement History

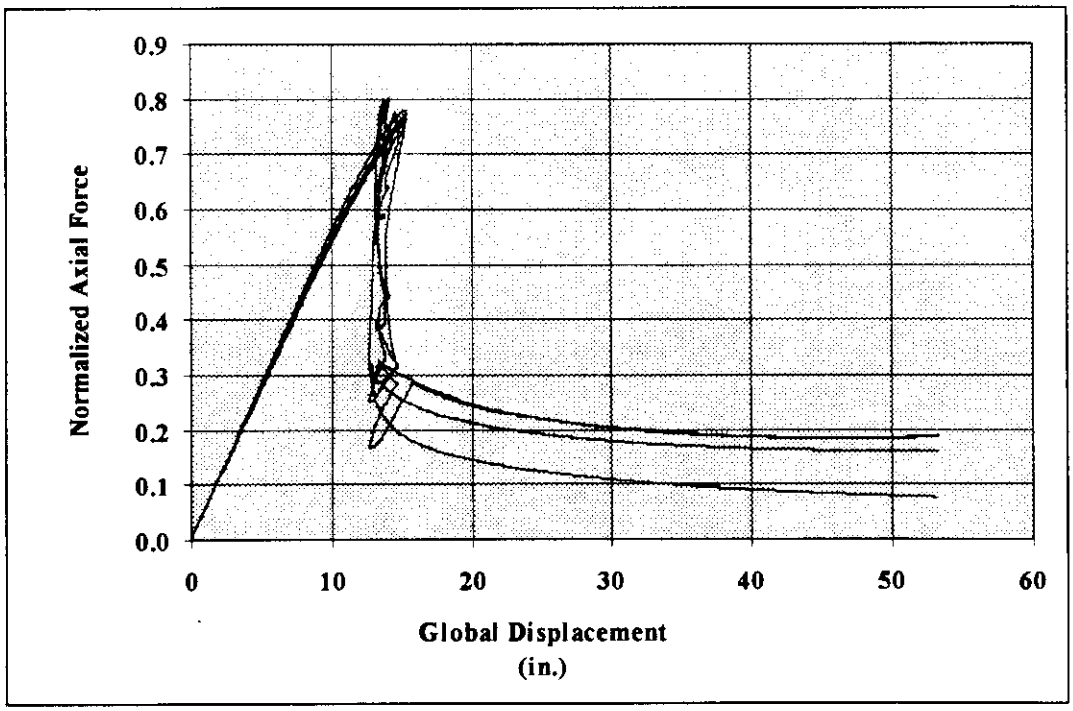

Figure 6.1-7: Platform A Broadside Fourth Bay Compression Brace Axial Force History

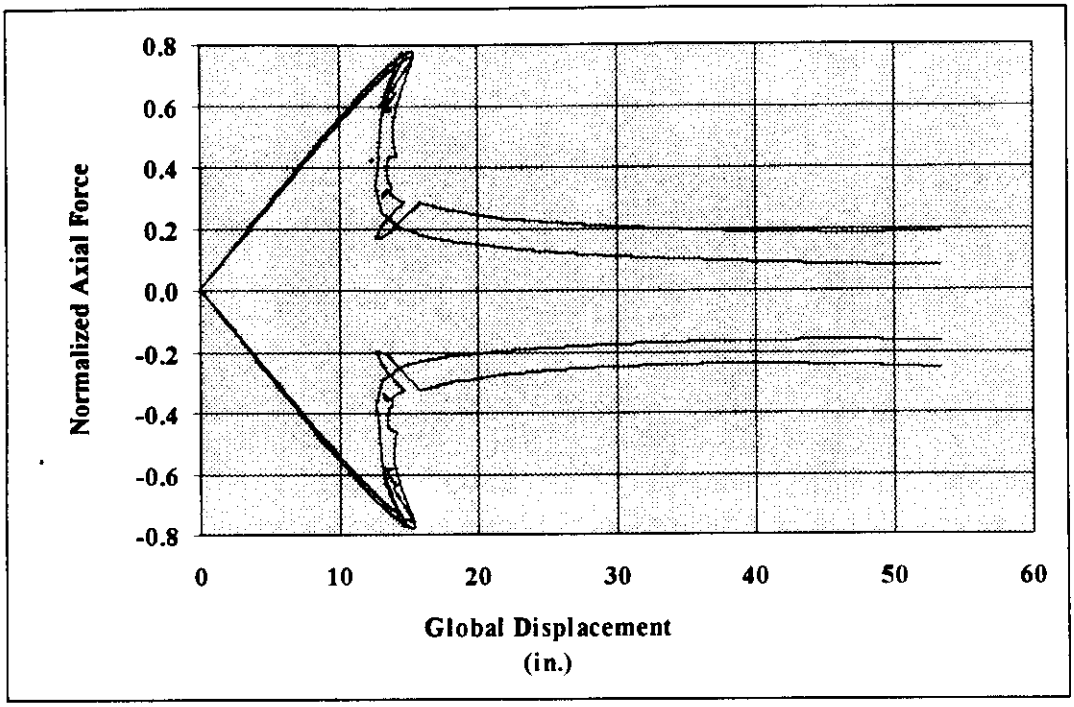

Figure 6.1-8: Platform A Broadside Fourth Bay Outer Brace Axial Force History

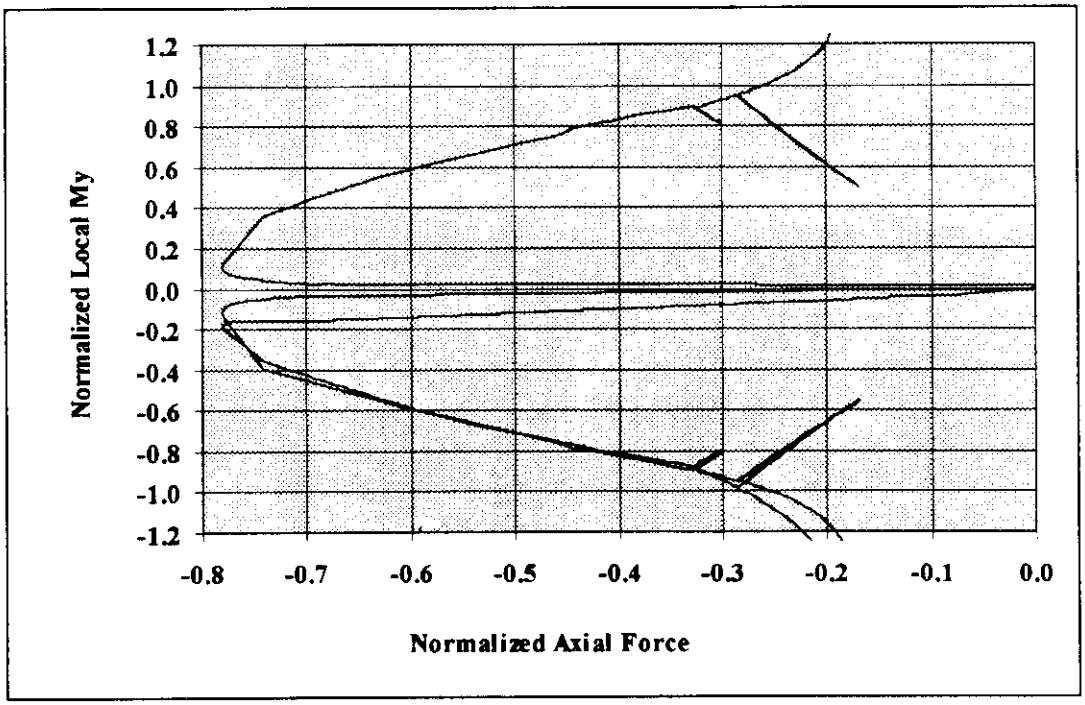

Figure 6.1-9: Platform A Broadside Fourth Bay Compression Brace 364 P-M Interaction at End Nodes and Midpoint

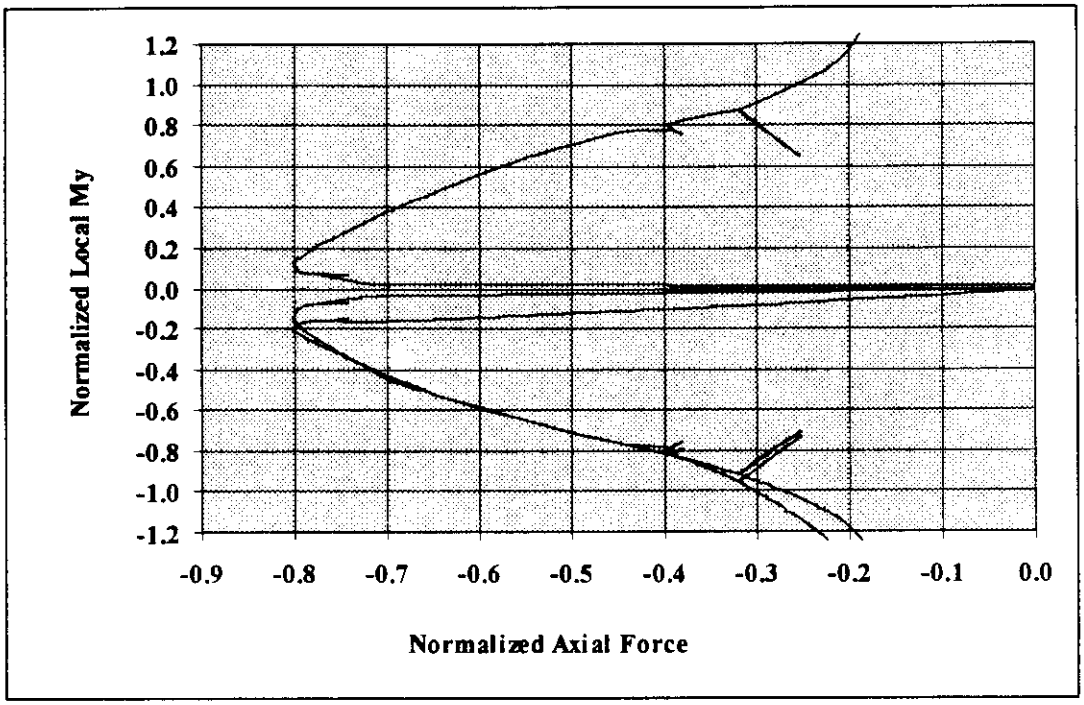

Figure 6.1-10: Platform A Broadside Fourth Bay Compression Brace 380 P-M Interaction at End Nodes and Midpoint

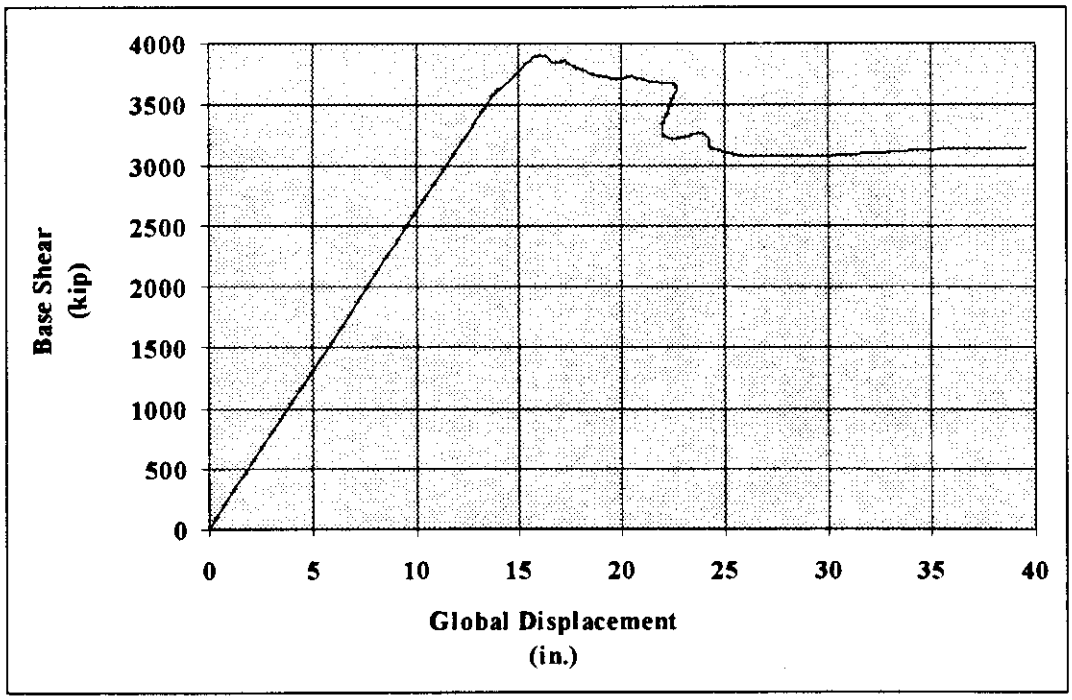

Figure 6.1-11: Platform A End-On Force-Displacement History

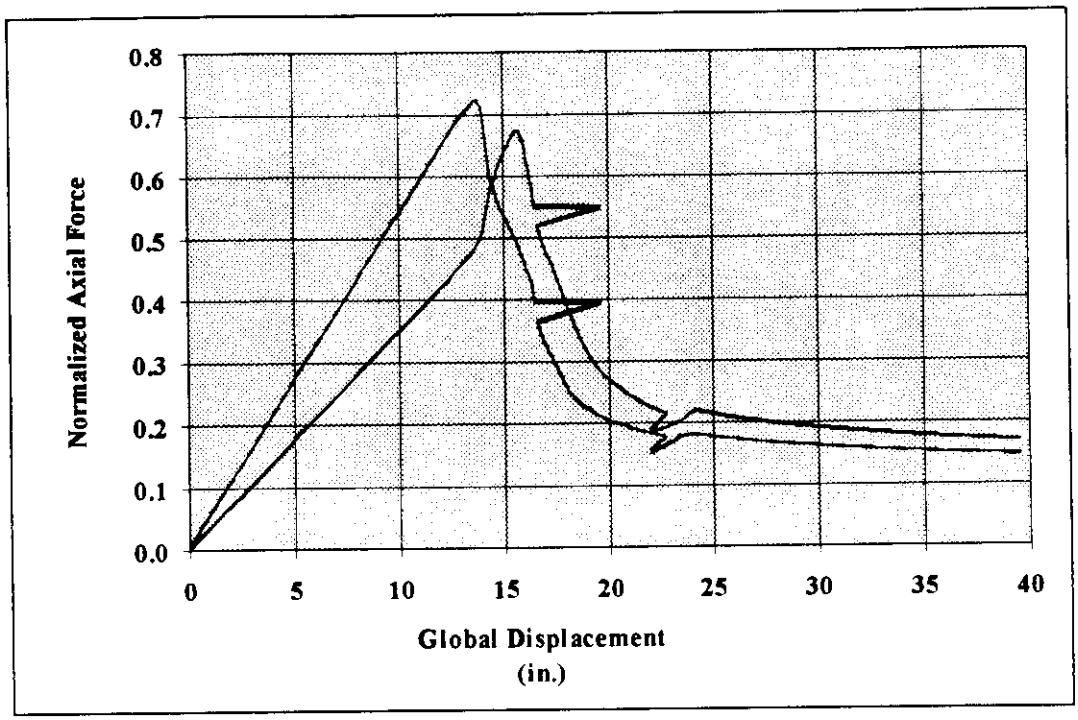

Figure 6.1-12: Platform A End-On Fourth Bay Compression Brace Axial Force History

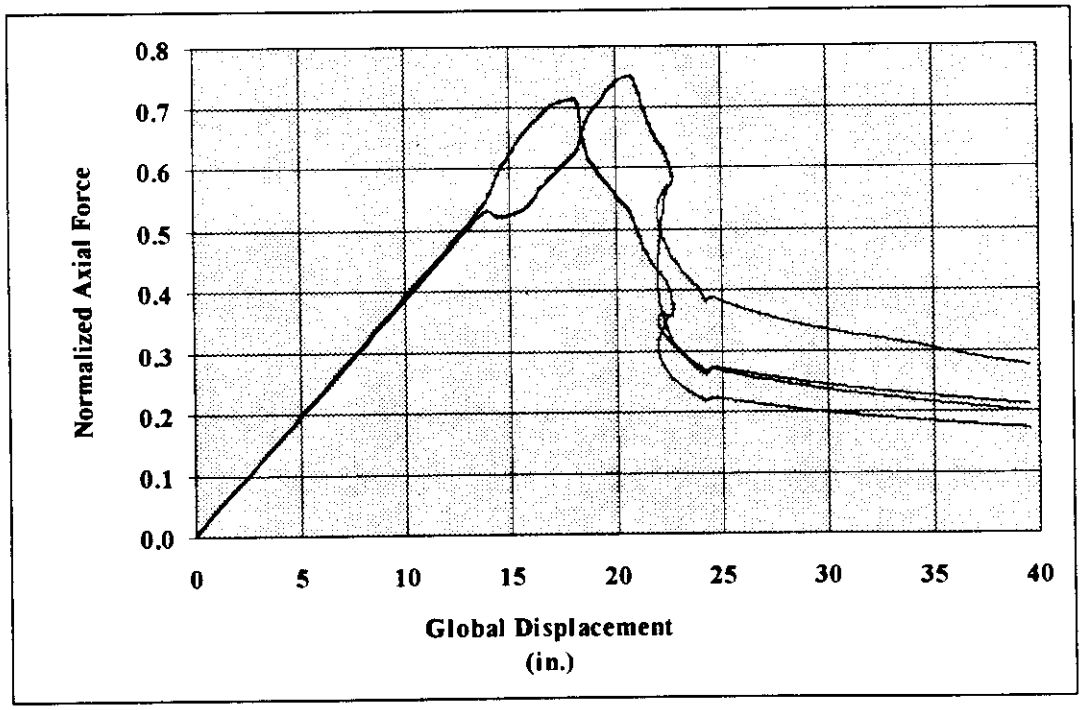

Figure 6.1-13: Platform A End-On Third Bay Compression Brace Axial Force History

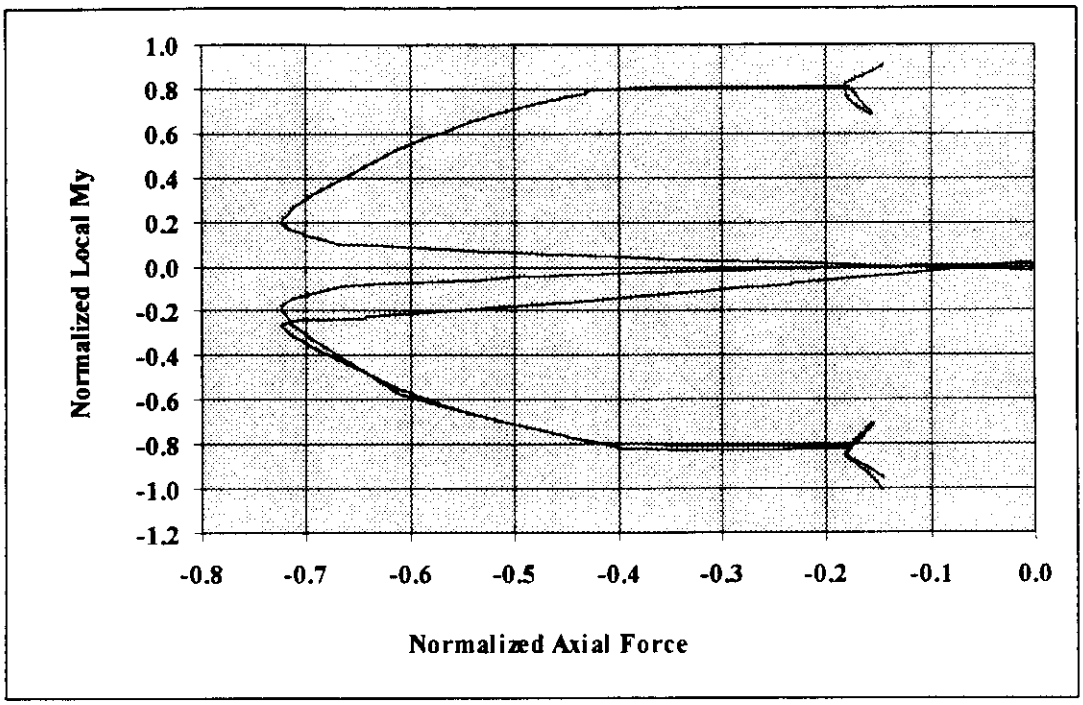

Figure 6.1-14: Platform A End-On Fourth Bay Compression Brace 317 P-M Interaction at End Nodes and Midpoint

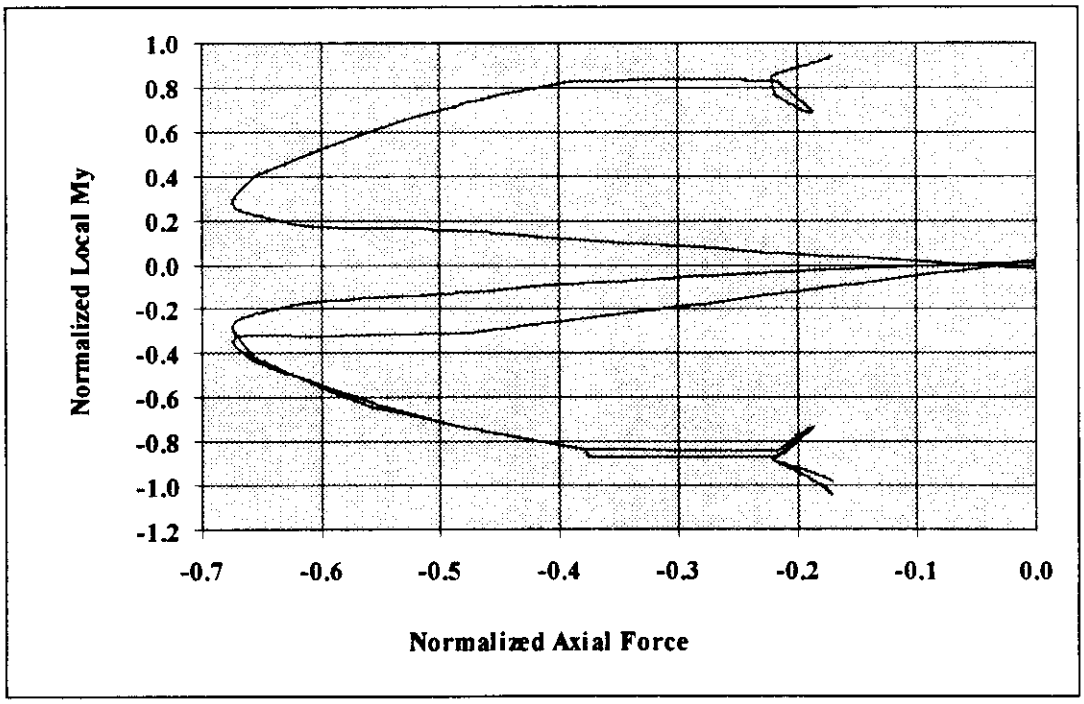

Figure 6.1-15: Platform A End-On Fourth Bay Compression Brace 318 P-M Interaction at End Nodes and Midpoint

6.2 Platform B

Prelude

At the request of the project sponsors, Platform B (PB) was added to the original list of proposed verification case studies. Many know PB as the PMB Benchmark platform (PMB, 1994). PMB used PB as the test structure for a joint industry project (JIP). The JIP's main objective was to assess the variability in the calculated ultimate capacity of a typical fixed offshore platform due to different assumptions, different code interpretations, different software packages and human error. The JIP participants were to strictly use API RP 2A (API, 1993 and 1994) to define the loading parameters of the analysis. However, the software and analysis techniques used varied between companies. Analysis results specified by PMB were submitted by all the participants. These results were then compared to assess their variability (PMB, 1994).

This study was a valuable opportunity for the UCB Marine Technology Development Group (MTDG), specifically as it related to the current research on Level 4 ULS analyses. Due to time constraints, the MTDG did not submit its USFOS analysis results for use in the study. In addition, while the majority of input parameter for the MTDG USFOS analysis were taken from API RP 2A (API, 1993 and 1994), certain loading parameters were not chosen to match those presented in API RP 2A. However, by comparing the USFOS results with those published in the study, it was possible to verify the validity of

the use of USFOS for use in Level 4 analyses. Comparison of the USFOS results with those published in the JIP report is included at the end of this section.

Platform Description

PB was installed in the Gulf of Mexico's Ship Shoal region in 1970. This platform is a self-contained four-pile drilling and production platform located in 157 ft of water. The platform has four conductors and eight risers, see figures 6.2-1 and 6.2-2. PB's decks are located at elevations of +33 ft, +43 ft, +56 ft and +71 ft. The deck legs form a 30 ft x 30 ft square in plan and the jacket legs are battered at 1:11 in both primary directions.

The piles for PB run through the jacket legs, but unlike PA, the pile-jacket leg annulus is not grouted. The 36 in. piles extend 355 ft below the mudline through 328 ft of soft to stiff gray clay and 27 ft of fine dense sand. The sand layer starts at 197 ft below mudline. The clay above the sand is generally soft and silty, while the clay below the sand is stiff.

While the pile-leg annulus is not grouted, the jacket legs and most other intersecting members have joint cans. The 39.5 in. jacket legs are 0.5 in. thick while the joint cans are 1.25 in. thick. The deck legs are 36 in. in diameter with a wall thickness of 1.25 in. and are connected to the tops of the piles. The vertical braces vary from 16 in. in the top or seventh jacket bay to 20 in. in the first jacket bay. All members are constructed of nominal 36 ksi steel with an average yield stress of 43 ksi.

Platform Loading

Several trials analyses were performed to find the wave height that caused platform failure near a load factor of unity. However, the platform was also analyzed with a fixed based. Therefore, the load profile chosen was a compromise between the fixed and free base analyses.

Wind forces were calculated using reference API RP 2A. Appurtenance and deck loads were calculated by hand using the wave kinematics developed in WAJAC. The broadside and end-on loading scenarios are essentially identical and thus, only one direction was analyzed. Diagonal loading could be critical. However, as previously discussed the Level 2 screening using these analyses results only considers the two primary orthogonal directions. More will be said about the diagonal loading direction later in this section.

As with PA, hydrodynamic coefficients were chosen based on recent test data and engineering judgment. The, the drag coefficient, C_d, was taken to be 1.2 for all cylinders. The inertia coefficient, C_m, was taken to be 1.2 for rough cylinders and 1.6 for smooth cylinders (Bea, 1994). A wave kinematics factor equal to 0.88 was used for both the deck and jacket loads. A current blockage factor of 0.80 was also included.

Computer Model

PB's computer model contains only the main structural components of the platform. It was assumed that the main and cellar decks were not part of the first failure mode. Therefore, only the main framing members of the decks were modeled. The conductors were transversely slaved to nearby nodes in the horizontal framing from the first deck down to the mudline. The piles were transversely slaved to the jacket legs that they run through except at the top, where the piles, jacket legs and deck legs are rigidly connected at all four corners. All members were given an initial imperfection, which was chosen based on the ASTM standards. Finally, since the platform contains joint cans, this analysis used rigid joints.

Single node non-linear soil springs were developed using the procedures outlined in reference (API, 1993). These procedures assume a static loading assumption. A static loading assumption can be too conservative in some cases and will indicate a false failure in the foundation. The assumptions concerning soil spring development will be discussed later in this section and in section 7.3.

Analysis Results

The force-displacement history for broadside loading is shown in figure 6.2-3. This curve indicates that platform PB fails at 0.628 of the reference load pattern or a total base shear of 1,673 kips. From figure 6.2-3 it can be seen that the platform has a constant stiffness after all the T-Z and Q-Z springs of the compression piles have reached their final

plateaus. The force-deformation relationships of four T-Z springs and one Q-Z spring for a compression pile are shown in figure 6.2-4.

Fixed Base Analysis Results

Since the foundation was shown to be the weak link in the platform, a fixed base analysis was also performed. As previously mentioned, a static assumption can indicate a false failure mode in the foundation. In addition, soil strength and non-linear spring models have exceptionally high associated uncertainty. Therefore, it is wise to also determine the first non-foundation failure mode when the foundation is the weak link. This was accomplished by analyzing the platform while rigidly fixing the piles at the mudline.

If the foundation is assumed rigid or fixed, the braces in the second jacket bay become the weak link. The force-displacement curve for this case is shown in figure 6.2-5. This figure indicates that the second bay compression braces buckle at 1.30 of the reference load pattern or a total base shear of 3,440 kips. After the compression braces in the second jacket bay buckle, the braces in the third jacket bay buckle and the jacket begins to "unzip". Detailed force histories for the critical braces are shown in figures 6.2-6 and 6.2-7. Figures 6.2-8 to 6.2-9 show that the critical braces have a credible interaction relationship.

In section 7.3, PB was reanalyzed with dynamic soil springs equal to 1.41 times the static strength, i.e., the forces on the springs' force/displacement curves were multiplied by 1.41.

Figure 7.3-7 shows the comparison between static and dynamic spring pushover results. By increasing the soil spring strength by 1.41, the pile pullout capacity increased by 1.55. This results indicates a relatively linear relationship between soil spring strength and overall foundation capacity. Thus, by increasing the soil spring strength by approximately 1.3/0.68 or 1.91 the failure mode should move from the foundation to the superstructure.

Comparison of Analysis Results JIP Published Results

The preliminary results of the PMB JIP proved very interesting and somewhat disturbing (PMB, 1994). Almost all the results compared showed large amounts of variation. Hydrodynamic loads varied on average by 25 percent. Average coefficients of variation for ultimate capacity and reserve strength ratio (RSR) were 22 percent and 38 percent respectively. These variations are relatively high, but the results become even more alarming when the unnormalized differences are considered. For instance, the average ratio of maximum to minimum RSR was 3.4.

While some may argue that the extreme outliers could or should be discarded, for this study they have as much validity as those values close to the mean. The JIP's goal was to measure variation in calculated results. As previously stated, the variation could be due to different assumptions, different code interpretations, different software packages, or human or software error. Even if the outliers represent a result of human error, the variation they cause is just as valid as that caused by the use of different wave theories. The variations published in the JIP report are those that can be expected to occur when

the API RP 2A procedures are followed by a typical engineer at a large oil company or engineering firm. The variations might have been even larger if some of the smaller or less experienced companies had participated. Thus, while the software available today for performing wave loading and ultimate limit state analyses are very powerful, these state-of-the-art technologies are limited by their necessary human interface, both in their design and their use.

For the wave direction considered in this report, the mean ultimate base shear capacity was 2,446 kips with an associated COV of 22 percent. The minimum and maximum values reported were 1,550 kips and 3,439 kips respectively. The USFOS analysis for this report produced an ultimate base shear of 1,673 kips. Therefore, this analysis resulted in a low estimate of base shear capacity relative to the JIP values. However, this fact is not surprising in light of the fact that this analysis strictly used the non-linear soil modeling procedures from section 6 of API RP 2A.

The authors recognize that the procedures outlined in API RP 2A are based upon a static loading assumption. However, as was previously shown, when dynamic loading is assumed, the strength and stiffness of the foundation can increase significantly (Bea, 1984). This increase can be as high as a factor of 3.0. Using an increase in soil spring strength of 1.41, the platform lateral load resisting capacity increased more than 50 percent to 2,580 kips. Section 7.3 of this report discusses the effects of assuming dynamic loading when modeling the soil springs.

For the same wave direction but with a fixed foundation, the mean JIP ultimate base shear capacity was 3,642 kips with an associated COV of seven percent. The minimum and maximum values reported were 3,374 kips and 4,046 kips respectively. The USFOS analysis for this report produced an ultimate base shear of 3,440 kips. Again, this analysis resulted in a low estimate of base shear capacity relative to the JIP values. However, the range of results is relatively small and the USFOS result is within six percent of the mean JIP ultimate capacity.

The results of the USFOS analysis are reasonable when compared with the PMB JIP results. Thus, the JIP can be viewed as an independent check which validates the USFOS analysis results. However, more important is the fact that even the most sophisticated analysis tools can produce widely scattered results when utilized in industry. This fact ought to be a wake up call to the offshore industry. All results, especially those obtained using complex tools, should be scrutinized under the light of engineering experience. In addition, valid simplified methods should not be discredited due to their lack of sophistication. For while simplified methods may be less powerful and less flexible, they can be more easily understood and usually do not introduce significantly more uncertainty than exists in the more complex methods.

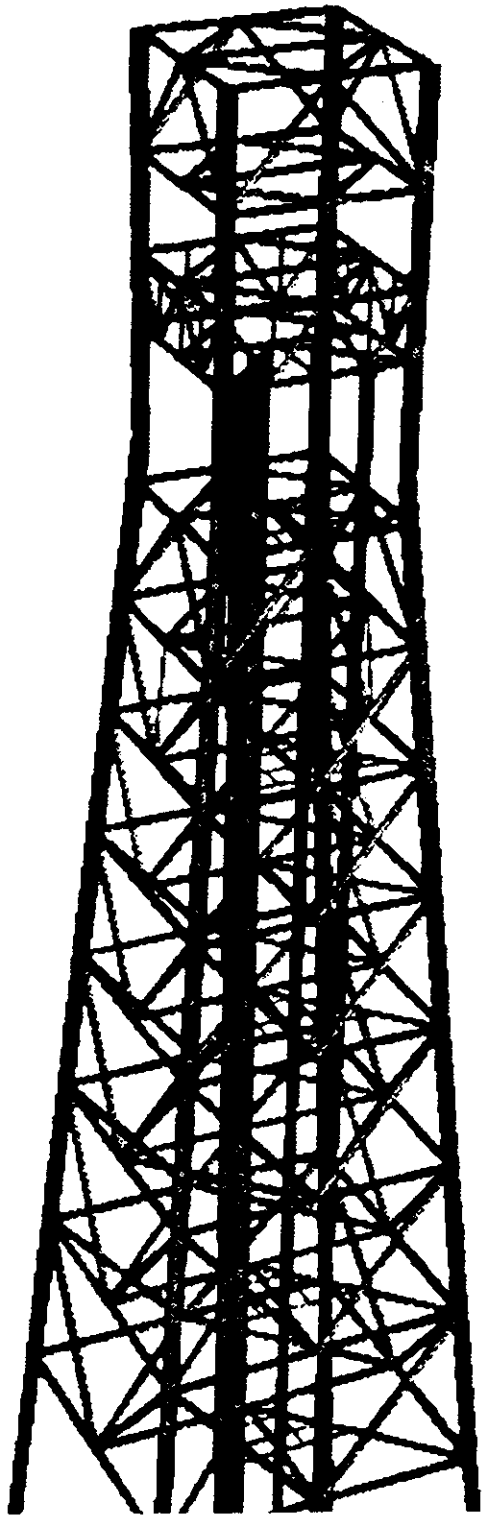

Figure 6.2-1: Platform B Isometric View

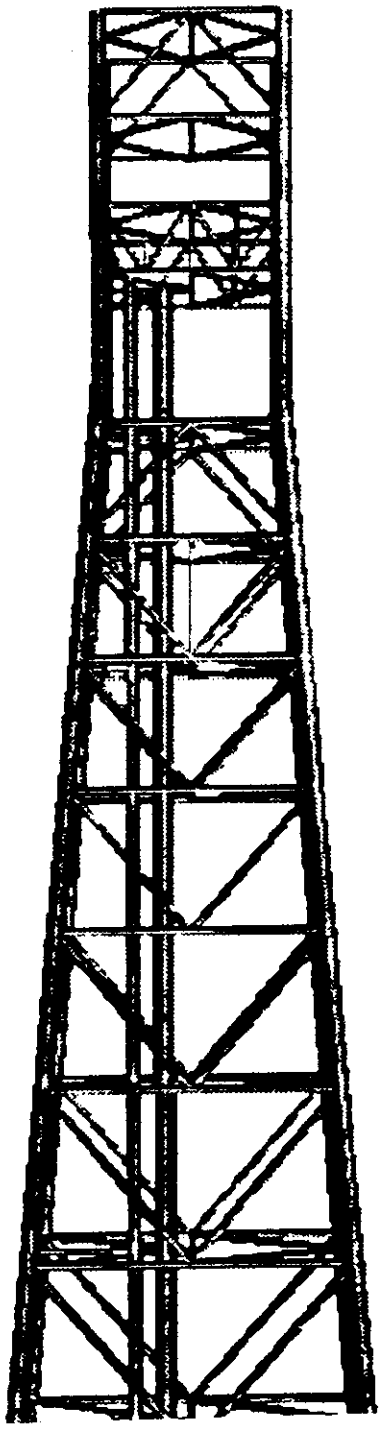

Figure 6.2-2: Platform B Broadside Elevation

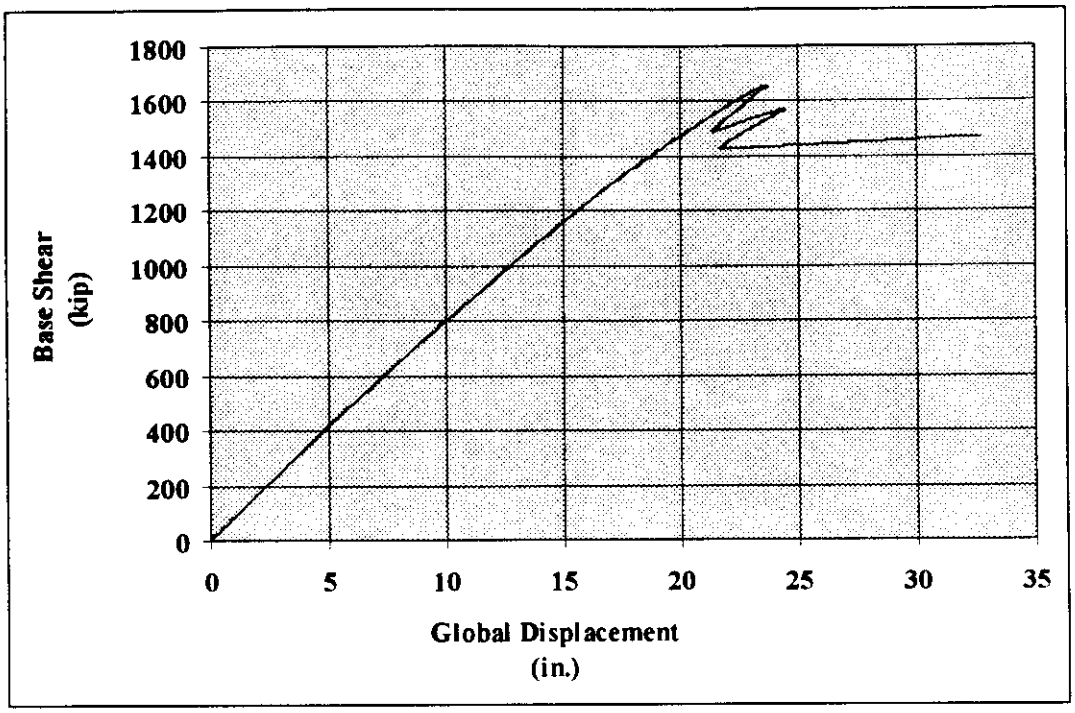

Figure 6.2-3: Platform B Force-Displacement History

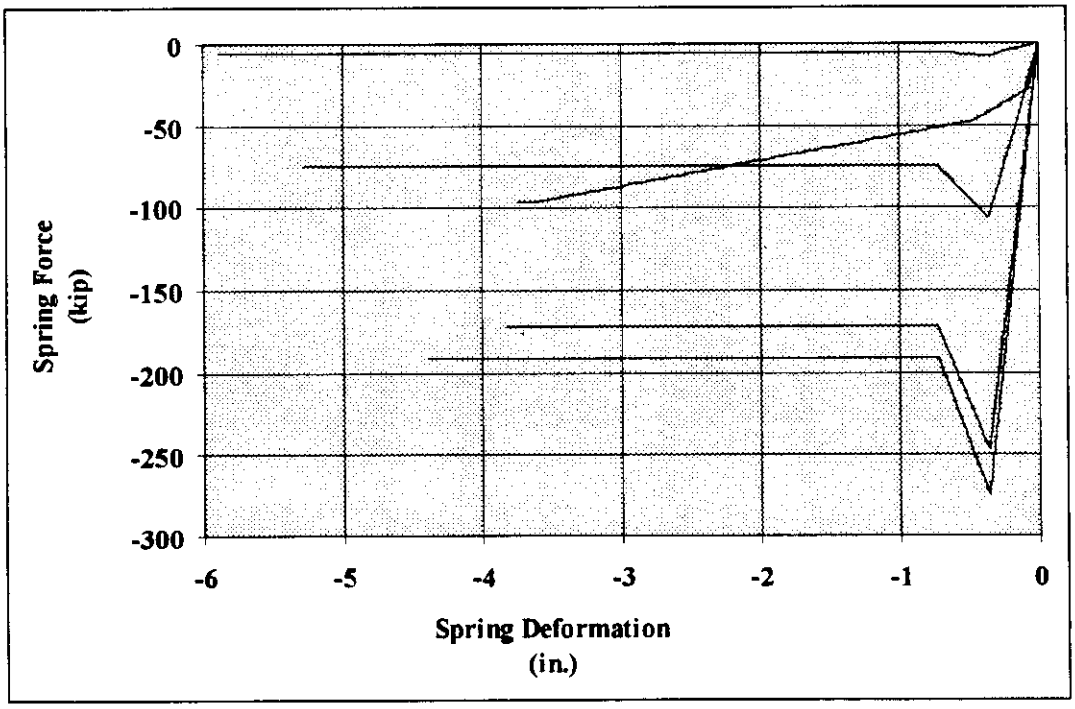

Figure 6.2-4: Platform B Force-Deformation History for Compression T-Z and Q-Z Springs

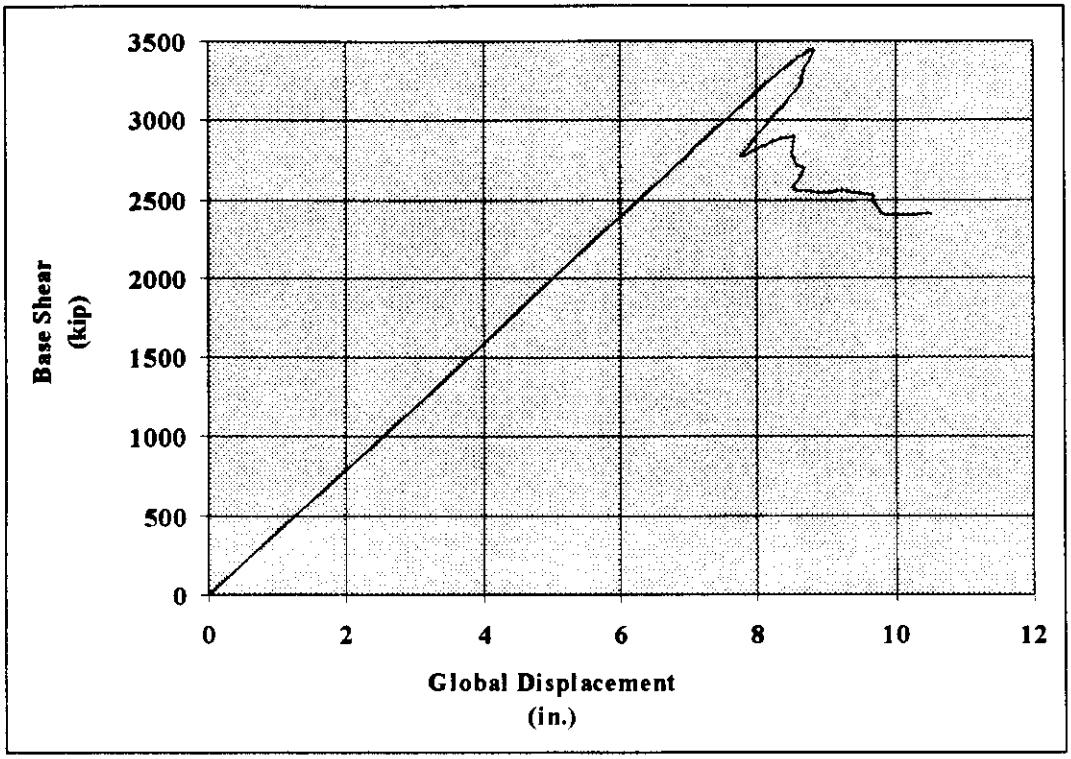

Figure 6.2-5: Platform B Fixed Base Force Displacement History

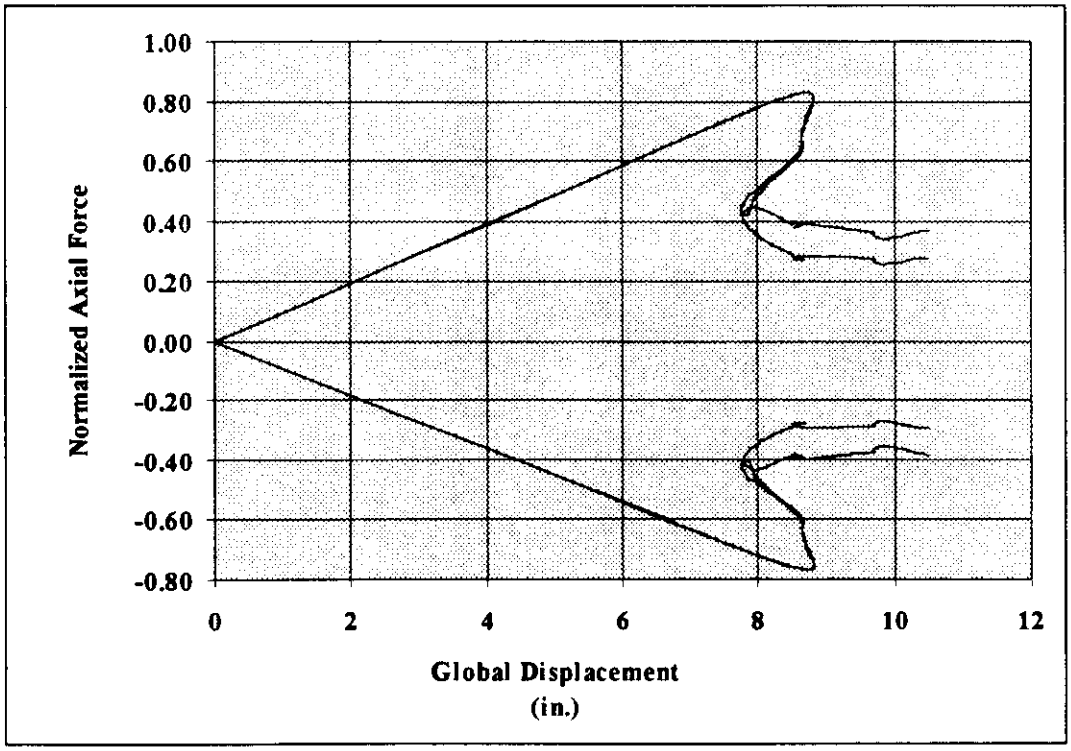

Figure 6.2-6: Platform B Fixed Base Second Bay Brace Axial Force History

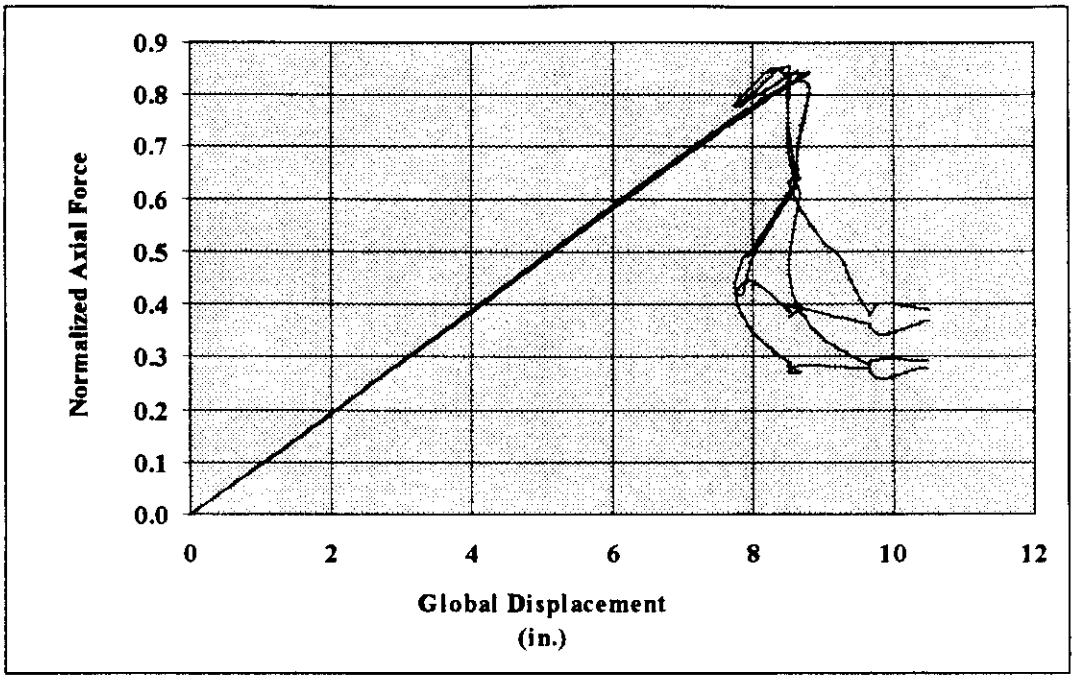

Figure 6.2-7: Platform B Fixed Base Second and Third Bay Compression Brace Axial Force History

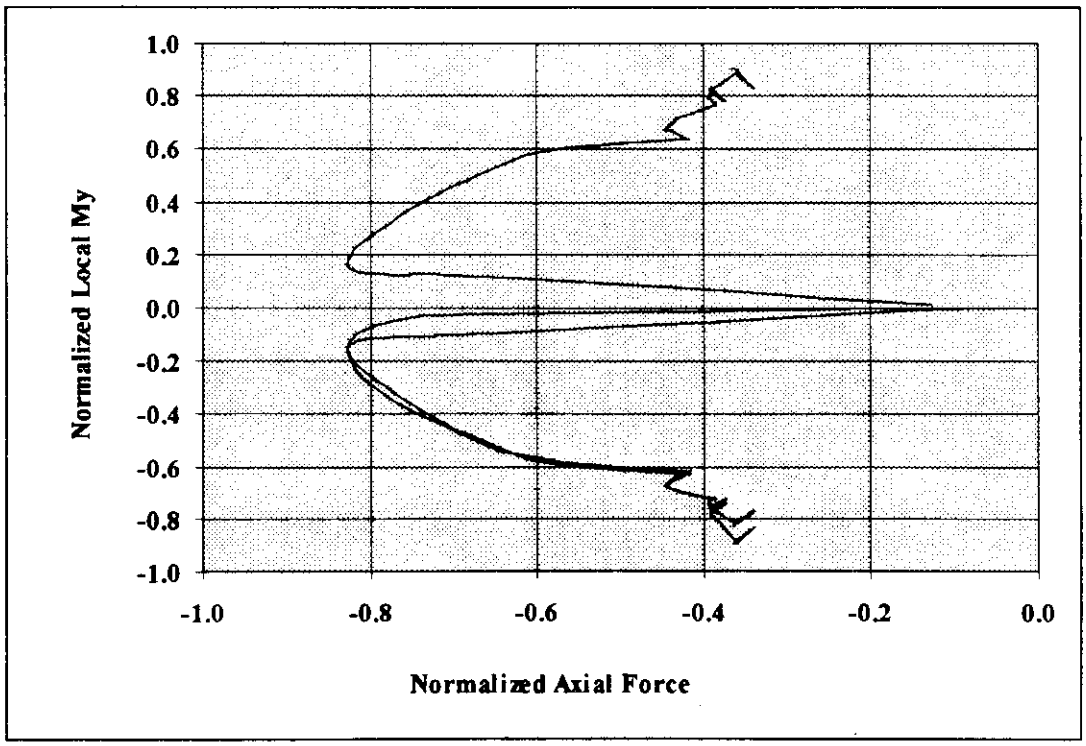

Figure 6.2-8: Platform B Fixed Base Second Bay Compression Brace 361 P-M Interaction at End Nodes and Midpoint

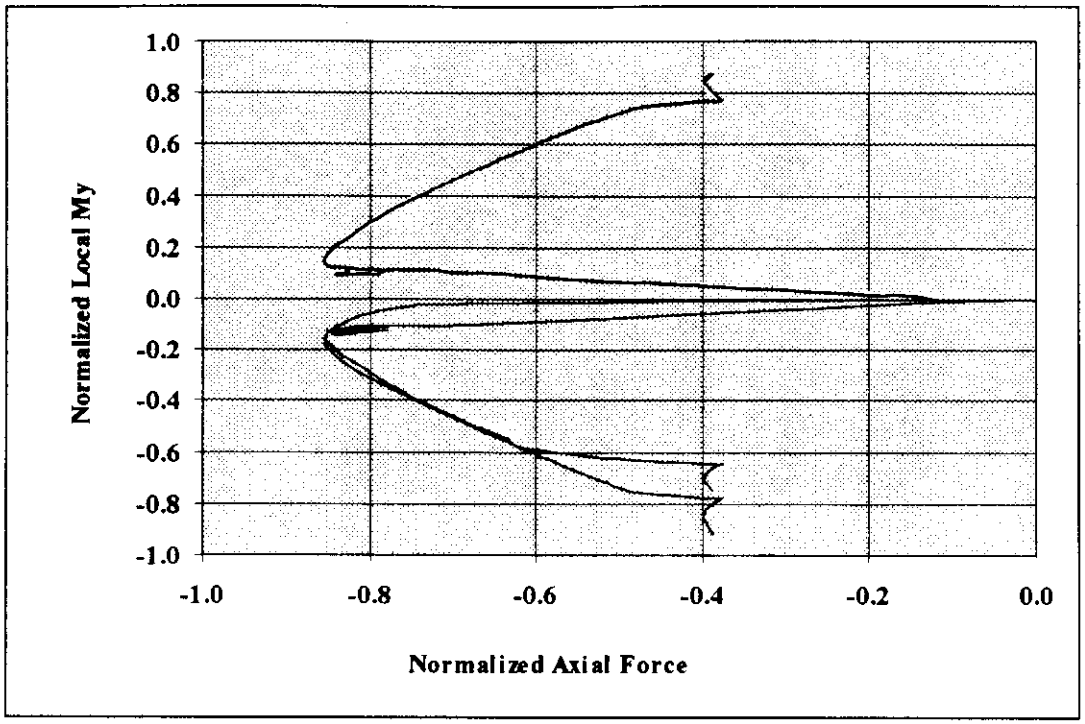

Figure 6.2-9: Platform B Fixed Base Third Bay Compression Brace 461 P-M Interaction at End Nodes and Midpoint

6.3 Platform C

Platform Description

Platform C (PC) is located in the Gulf of Mexico's South Timbalier region. This region was subjected to 100 year wave loads during Hurricane Andrew (Vannan et al., 1994). PC is a eight pile drilling and production platform with eleven 30 in. conductors (figures 6.3-1 to 6.3-3). The platform was designed in 1964 and installed in 137 feet of water. Cellar and main deck elevations are at + 35 ft and +46 ft respectively. The major deck framing is 40 ft x 120 ft in plan, and the jacket legs are battered at one to twelve in both broadside framing. The 30 in. piles extend approximately 180 ft below the mudline through firm to very stiff clay. A dense sand layer lies directly beneath the piles ends.

The 30 in. deck legs are connected to the tops of the 30 in. piles. The 33 in. diameter legs are ungrouted but have thickened joint sections. The broadside braces are 16 in. in all four jacket bays, while the end-on bracing varies from 16 in. to 18 in. The jacket bracing and horizontal framing are made of nominal 36 ksi steel with a mean yield strength of 43 ksi.

Platform Loading

Several trials analyses were performed to find the wave height that caused platform failure with a load factor of unity. It was assumed that the majority of the load causing failure in the platform was due to wave loads, specifically wave-in-deck loads. Therefore, no

attempt was made to exactly correlate the wave height, current and wind to the same return period. Instead, current and wind data from the Andrew hindcast studies were used while the wave height was varied. The broadside wave (loading of end-on bracing) was set to 56 ft while end-on wave was set at 60 ft. The wind forces were calculated using API RP 2A guidelines. The boat landing forces were calculated using their total projected area normal to the wave direction and a similar drag coefficient as was used for the platform. Since the failure mode was not expected to be in the jacket legs or the piles, the broadside and end-on loading scenarios were considered separately.

As before, hydrodynamic coefficients were chosen based on recent test data and engineering judgment. Thus, the drag coefficient, C_d, was taken to be 1.2 for both rough and smooth cylinders. The inertia coefficient, C_m, was taken to be 1.2 for rough cylinders and 1.6 for smooth cylinders respectively (Bea, 1994). A wave kinematics factor equal to 0.88 was used for both the deck and jacket loads. A current blockage factor of 0.80 for broadside loading and 0.70 for end-on loading was also included.

Computer Model

The model for PC contains only the main structural components of the platform. It was assumed that the main and cellar decks were not part of the first failure mode. Therefore, only the main framing members of the decks were modeled. The conductor framing was replaced with sufficiently rigid cross members to simulate their stiffness contribution. All members were given an initial imperfection of 0.003 of their length. Finally, due to

temporary problems in the analysis software and since the legs did have joint cans, this analysis used rigid joints. It should be noted that current API joint checking procedures under-predict mean joint capacities for many joint configurations. This fact has been verified by post-storm investigations of platforms where API procedure predicted joint failure or damage (Vannan et al., 1994). Thus, it is the authors' opinion, that the use of rigid joints does not significantly affect the determination of the failure mechanism or maximum load magnitude.

The non-linear soil springs were developed using section 6 of API RP 2A. These springs were then modified by the factors discussed in section 7.3. In total, the strength of the axial springs was increased by approximately 1.5 and the strength of the lateral springs were increased by approximately 3.0. As with joint capacities, studies have shown that static soil capacities as derived by API RP 2A underestimate the true soil strength (Vannan et al., 1994) (Bea, 1984) (Quiros et al., 1983).

Broadside Loading

The force-displacement curve for broadside loading is shown in figure 6.3-4. This curve indicates that platform PC fails at 0.884 of the reference load pattern or a total base shear of 4,475 kips. The maximum strength is controlled by buckling of the end-on braces in the third bay from the mudline. The axial force histories for the four third bay braces that buckle are shown in figures 6.3-5. The forces shown are normalized by the plastic axial capacity of the members, i.e., the actual axial force divided by the product of the

member's area and yield stress. The normalized interaction curves for two of the four upper compression braces are shown in figures 6.3-6 to 6.3-7.

End-On Loading

The force-displacement curve for end-on loading is shown in figure 6.3-8. This curve indicates that the lowermost broadside braces buckle at 0.623 of the reference load pattern or a total base shear of 2,697 kips. The force-displacement history indicates that there is some reserve strength in the end-on direction. Other analyses performed on PC showed that the braces in the third bay buckle at approximately the same load as those in the first bay. However, one must be cautious of inferring too much from post-buckling behavior. What can be said is that the platform is highly ductile, redundant and robust in the end-on direction.

Detailed force histories for the critical braces are shown in figure 6.3-9. As in the broadside loading case, figures 6.3-10 and 6.3-11 show that the main components of the failure mode, namely the critical compression braces, have a credible interaction relationship.

Observed Behavior and Previous Analysis Results

Platform PC experienced significant loading during Hurricane Andrew. Post-storm investigations revealed that PC collapsed during the storm (Vannan et al., 1994). Based on hindcast data, it is estimated that the platform was loaded between end-on and

diagonally with a maximum wave height of 60 ft. (Oceanweather, 1992). The platform appeared to have failed in the end-on direction.

Previous analyses indicate an ultimate broadside capacity of 4,155 kips and an ultimate end-on capacity of 3,450 kips (Vannan et al., 1994). Thus, the results presented here indicate 12 percent greater strength for broadside loading and 18 percent less strength for end-on loading than the previously published results.

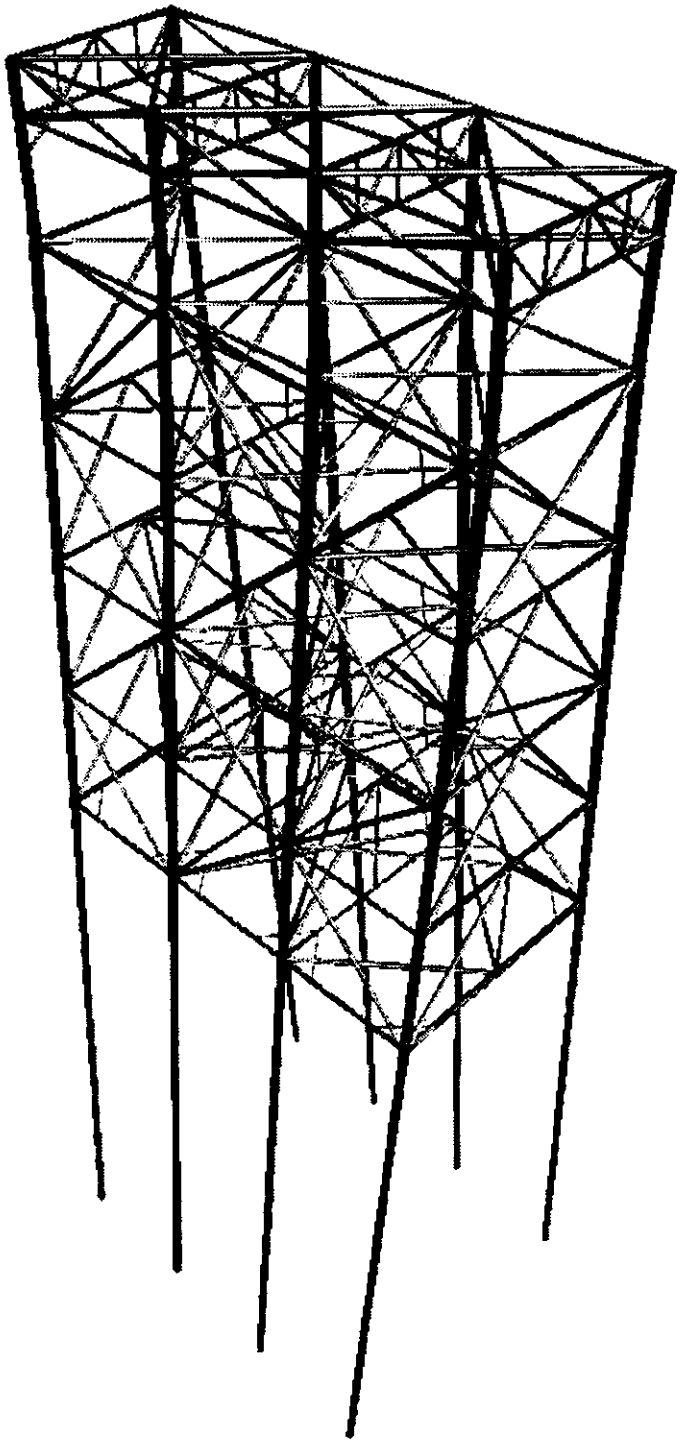

Figure 6.3-1: Platform C Isometric View

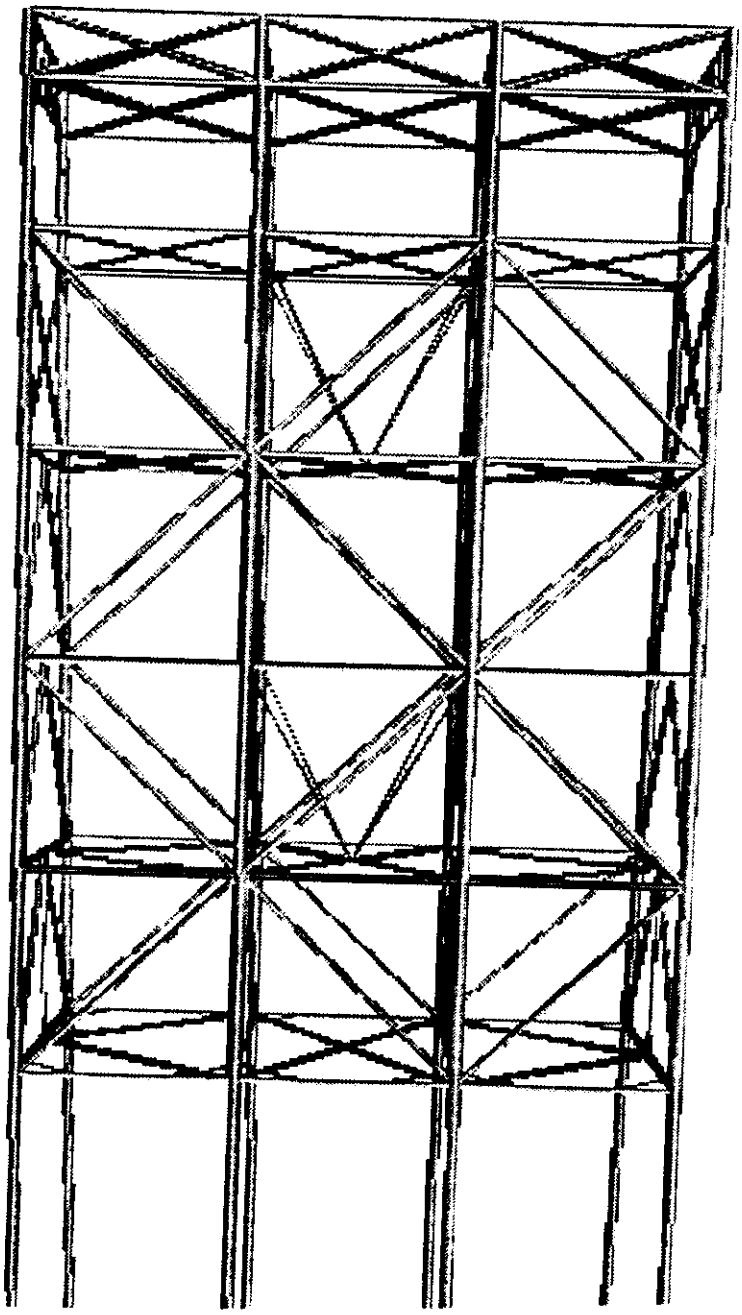

Figure 6.3-2: Platform C Broadside Elevation

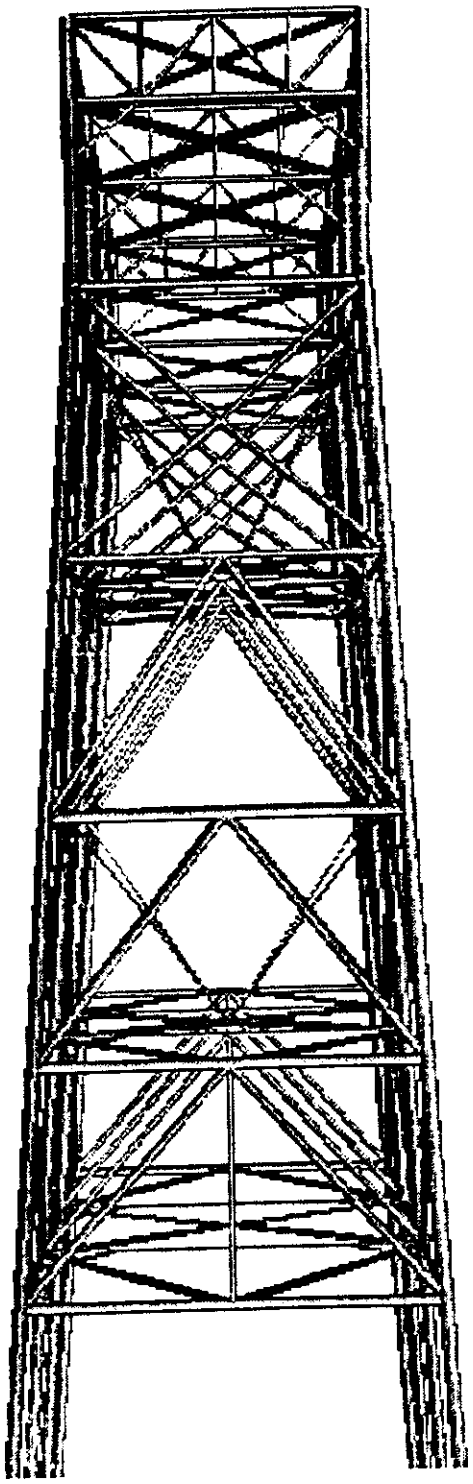

Figure 6.3-3: Platform C End-On Elevation

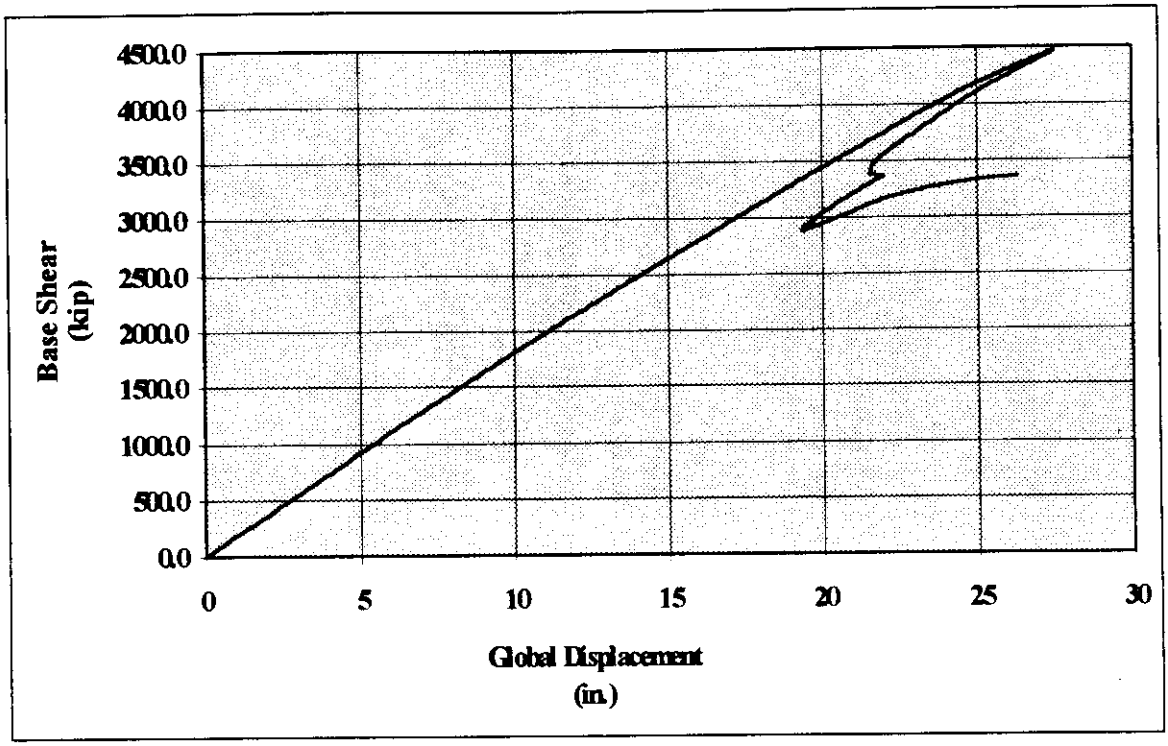

Figure 6.3-4: Platform C Broadside Loading Force-Displacement History

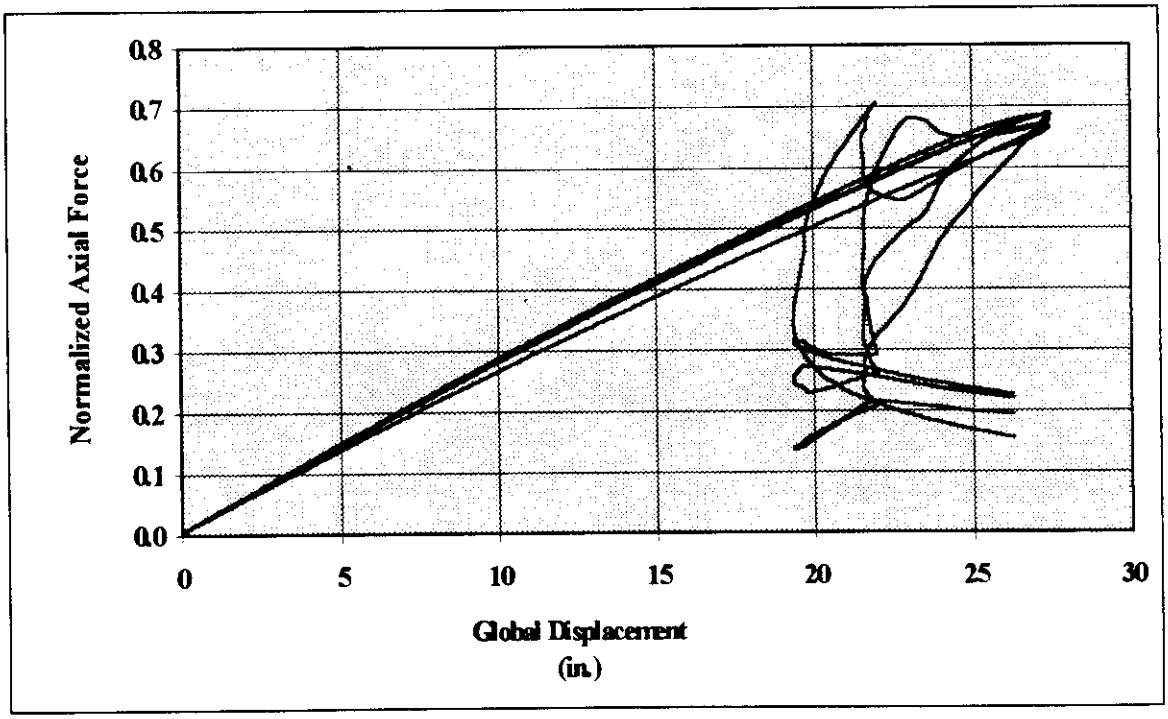

Figure 6.3-5: Platform C Broadside Third Bay Compression Brace Axial Force History

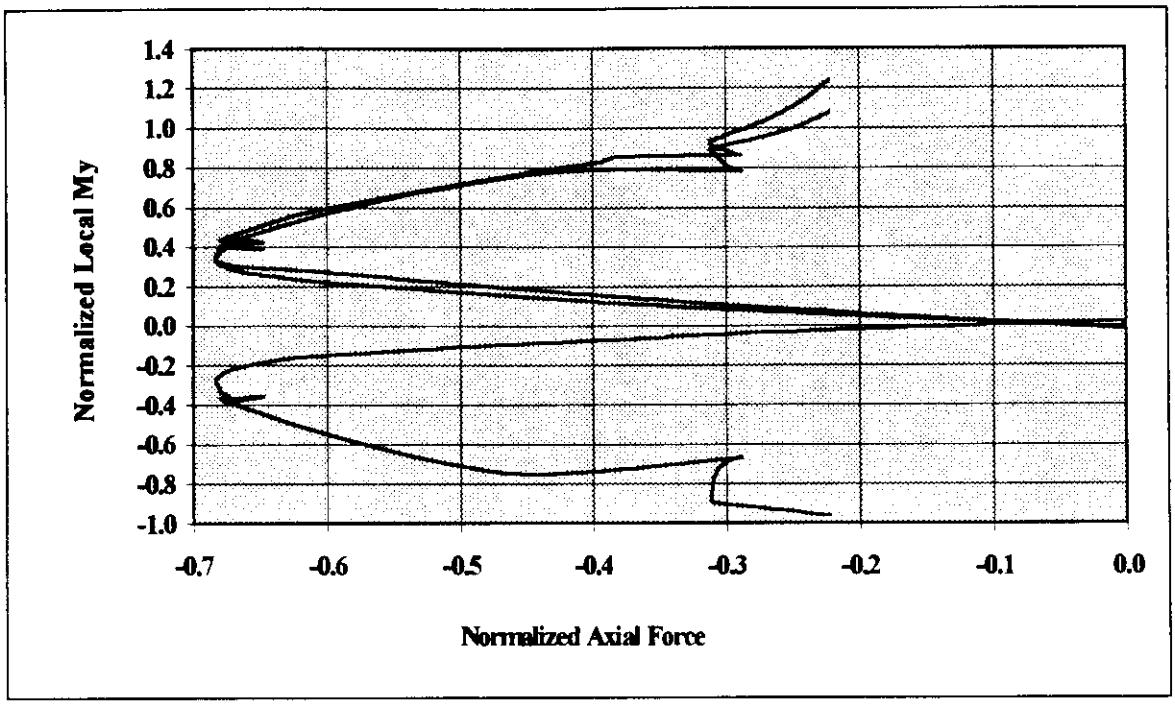

Figure 6.3-6: Platform C Broadside Third Bay Compression Brace 374 P-M Interaction at End Nodes and Midpoint

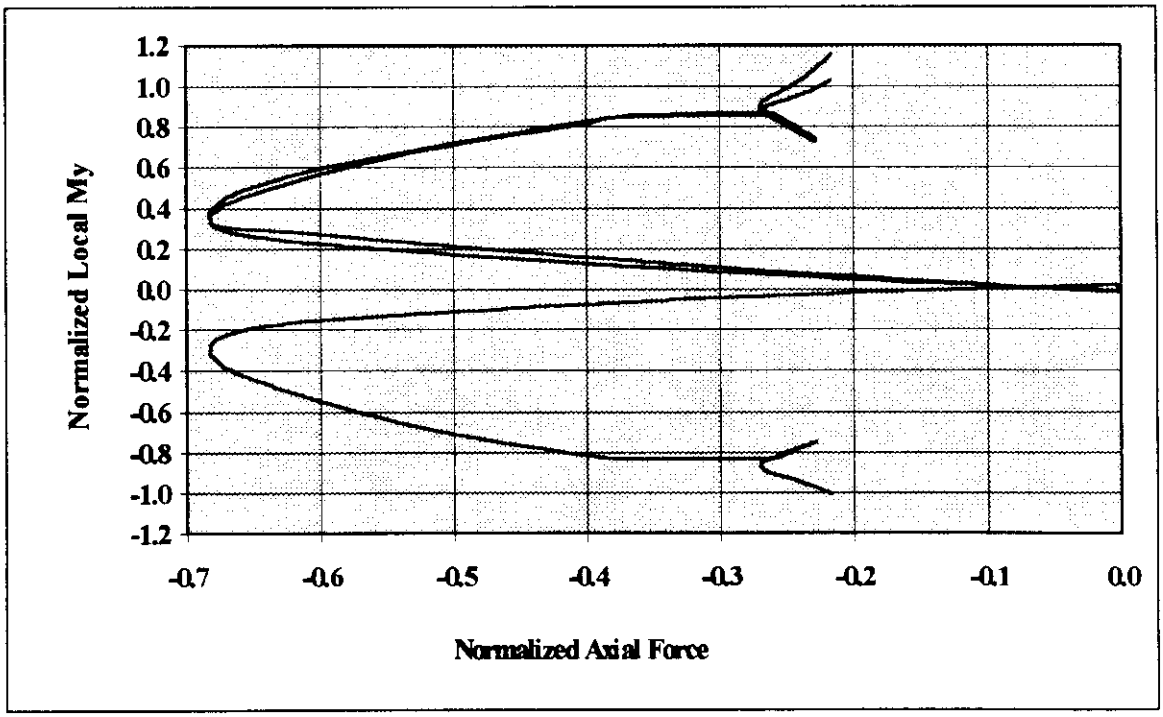

Figure 6.3-7: Platform C Broadside Third Bay Compression Brace 376 P-M Interaction at End Nodes and Midpoint

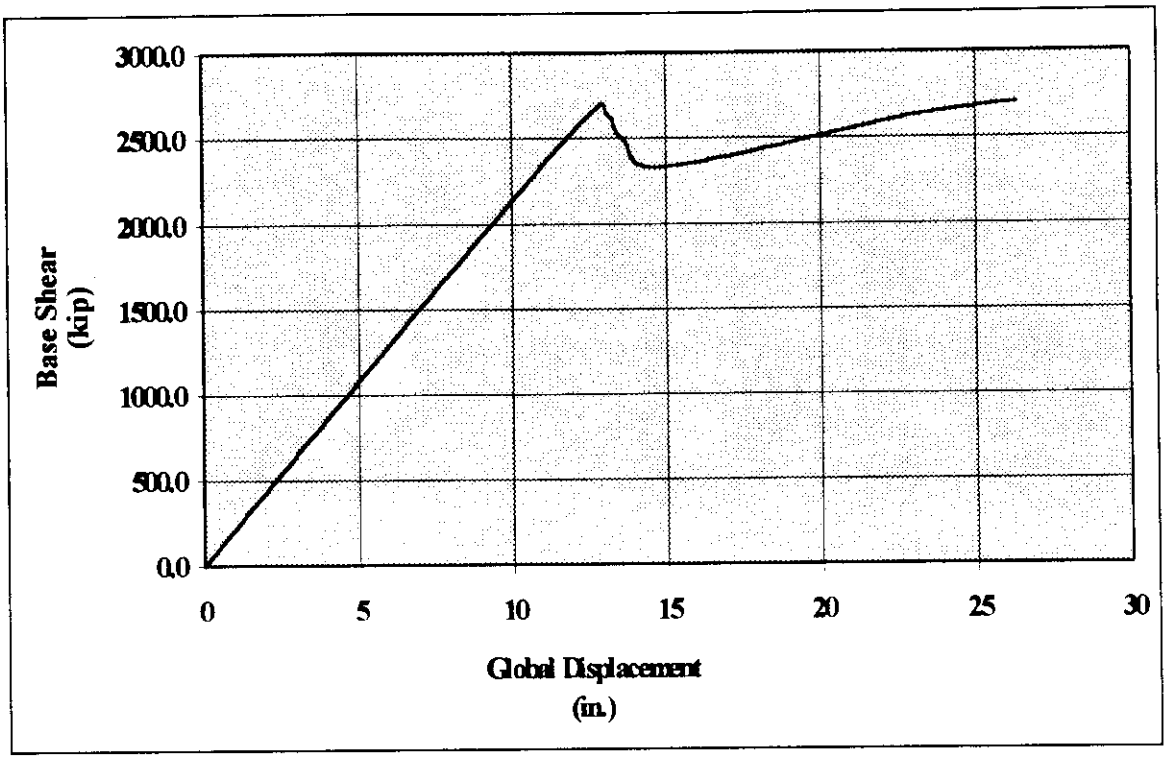

Figure 6.3-8: Platform C End-On Loading Force-Displacement History

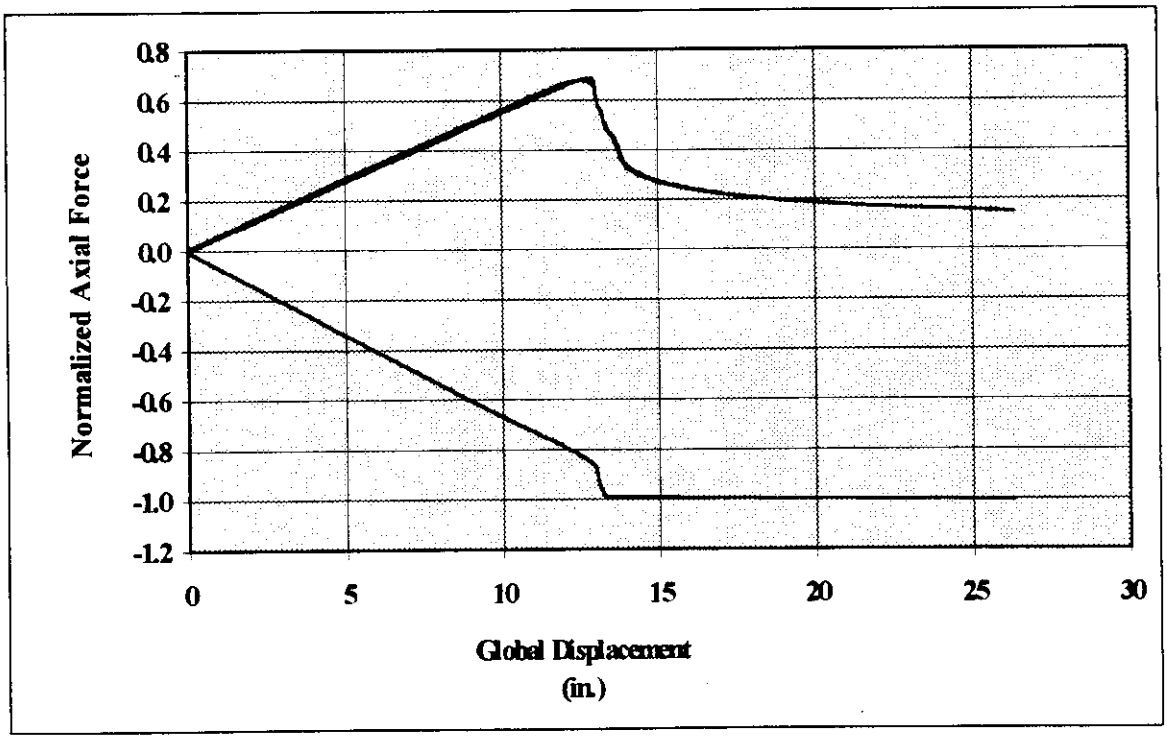

Figure 6.3-9: Platform C End-On First Bay Compression Brace Axial Force History

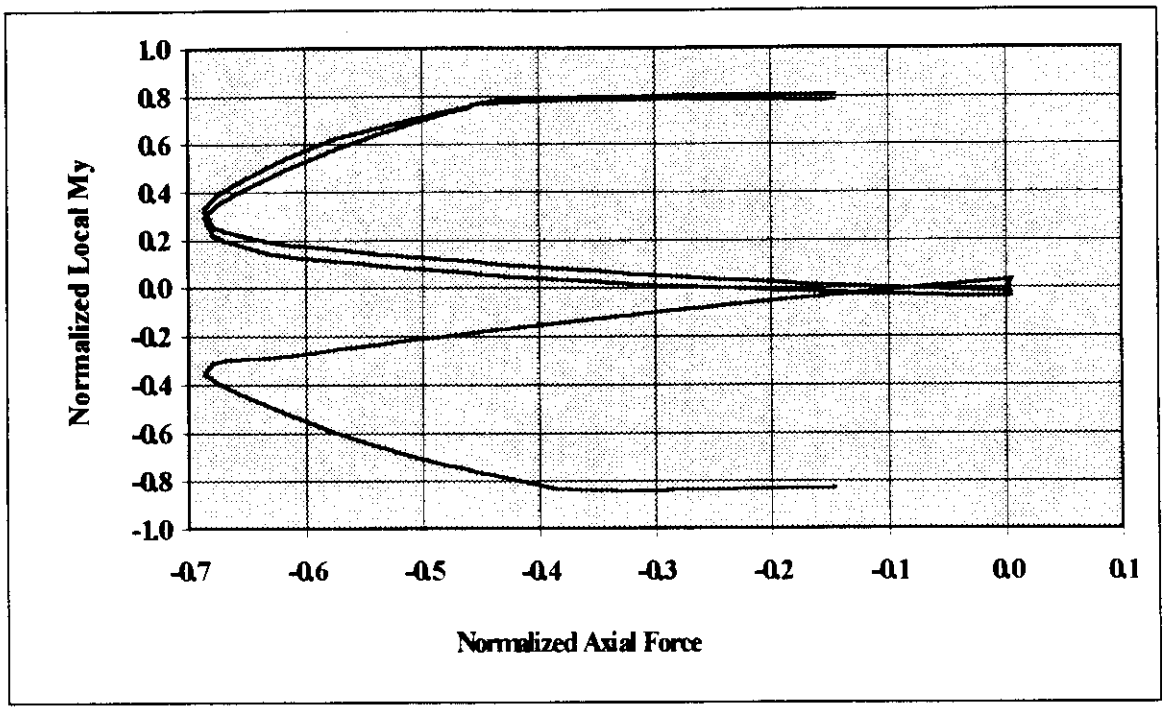

Figure 6.3-10: Platform C End-On First Bay Compression Brace 161 P-M Interaction at End Nodes and Midpoint

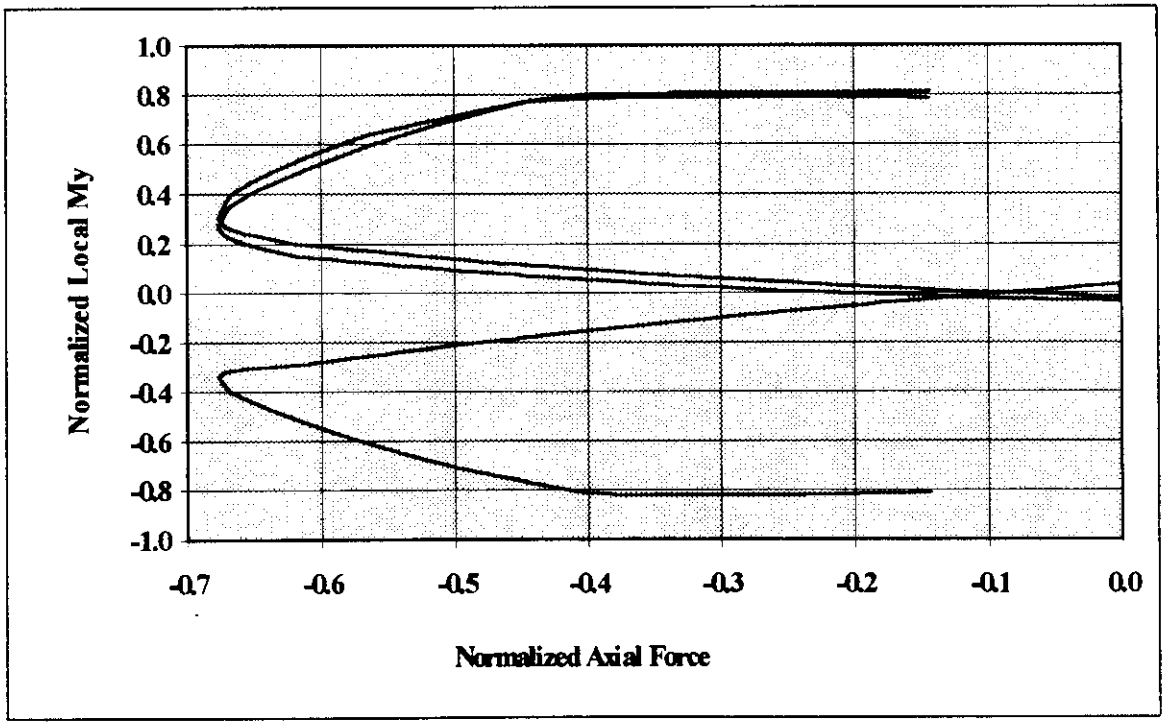

Figure 6.3-11: Platform C End-On First Bay Compression Brace 163 P-M Interaction at End Nodes and Midpoint

6.3 Platform D

Platform Description

Platform D (PD) is located in the Gulf of Mexico's South Timbalier region. This platform is bridge-connected to Platform C. PD is also an eight pile drilling and production platform with sixteen 30 in. conductors (figures 6.4-1 to 6.4-3). The platform was designed with Platform C in 1964 and installed in 137 feet of water. PD is similar in geometry as PC except that PD is battered at one to ten in both broadside and end-on framing. Also, the broadside braces vary from 16 in. in the top bay to 20 in. in the lowest bay. The end-on bracing varies from 16 in. to 18 in.

Platform Loading

The same wave, wind and drag and inertia coefficients for PC were used for PD. However, PD has a much larger base shear for the same storm conditions due to its additional conductors. Again, since the failure mode was not expected to be in the jacket legs or the piles, the broadside and end-on loading scenarios were considered separately.

Computer Model

Similar modeling assumptions were made for PD as were made for PC. All members were given an initial imperfection of 0.003 of their length, and the analysis used rigid joints. Also, as with PC, the soil springs were modified by the factors discussed in section 7.3.

Broadside Loading

The force-displacement curve for broadside loading is shown in figure 6.4-4. This curve indicates that platform PD reaches its maximum capacity at 0.793 of the reference load pattern or a total base shear of 4,709 kips. As with PC, the maximum strength is controlled by buckling of the end-on braces in the third bay from the mudline. The axial force histories for the four third bay braces that buckle are shown in figures 6.4-5. The forces shown are normalized by the plastic axial capacity of the members, i.e., the actual axial force divided by the product of the member's area and yield stress. The normalized interaction curves for two of the four upper compression braces are shown in figures 6.4-6 to 6.4-7.

End-On Loading

The force-displacement curve for end-on loading is shown in figure 6.4-8. This curve indicates that the lowermost broadside braces buckle at 0.879 of the reference load pattern or a total base shear of 4,577 kips. This value is significantly higher than that for PC, which is explained by the difference in first level braces size between the two platforms (20 in. vs. 16 in.). Detailed force histories for the critical braces are shown in figure 6.4-9. As in the broadside loading case, figures 6.4-10 and 6.4-11 show that the main components of the failure mode, namely the critical compression braces, have a credible interaction relationship.

Observed Behavior and Previous Analysis Results

Platform PD also experienced significant loading during Hurricane Andrew. However, unlike it neighbor PC, PD did not collapse (Vannan et al., 1994). Based on hindcast data, it is estimated that the platform was also loaded between end-on and diagonally with a maximum wave height of 60 ft. (Oceanweather, 1992). Previous analyses indicate an ultimate broadside capacity of 3,500 kips and an ultimate end-on capacity of 3,912 kips (Vannan et al., 1994). Thus, the results presented here indicate 25 percent greater strength for broadside loading and 11 percent less strength for end-on loading than the previously published results.

Comparison of Platform C and Platform D Results

Platforms PC and PD are structurally similar and are located adjacent to one another. Both of these platforms experienced significant loading during Hurricane Andrew. Post-storm investigations revealed that PC collapsed during the storm while PD suffered minor damage (Vannan et al., 1994). Based on hindcast data, it is estimated that the platforms were loaded between end-on and diagonally (Oceanweather, 1992). The results of the analyses presented here coincide with these findings.

Specifically, the analyses shows that PC has an ultimate broadside capacity of 4,475 kips while PD is capable of resisting 4,709 kips in broadside loading. Yet, since PD receives significantly more load for the same size wave, PC was found capable of resisting 88.4 percent of the 56 ft wave loading, while PD could only resist 79.3 percent. Thus, PC

should have a slightly greater chance of survival than PD for broadside loading. However, for end-on loading, the analyses indicate that PD has greater capacity than PC. PD was found capable of resisting 87.9 percent of the 60 ft wave loading while PC was only found capable of resisting 62.3 percent of the 60 ft wave loading. This large capacity difference was previously explained by the different sizes of the lower braces for the two platforms. Hence, if the two platforms were loaded primarily in the end-on direction, the results show that PD has a much greater chance of survival that PC.

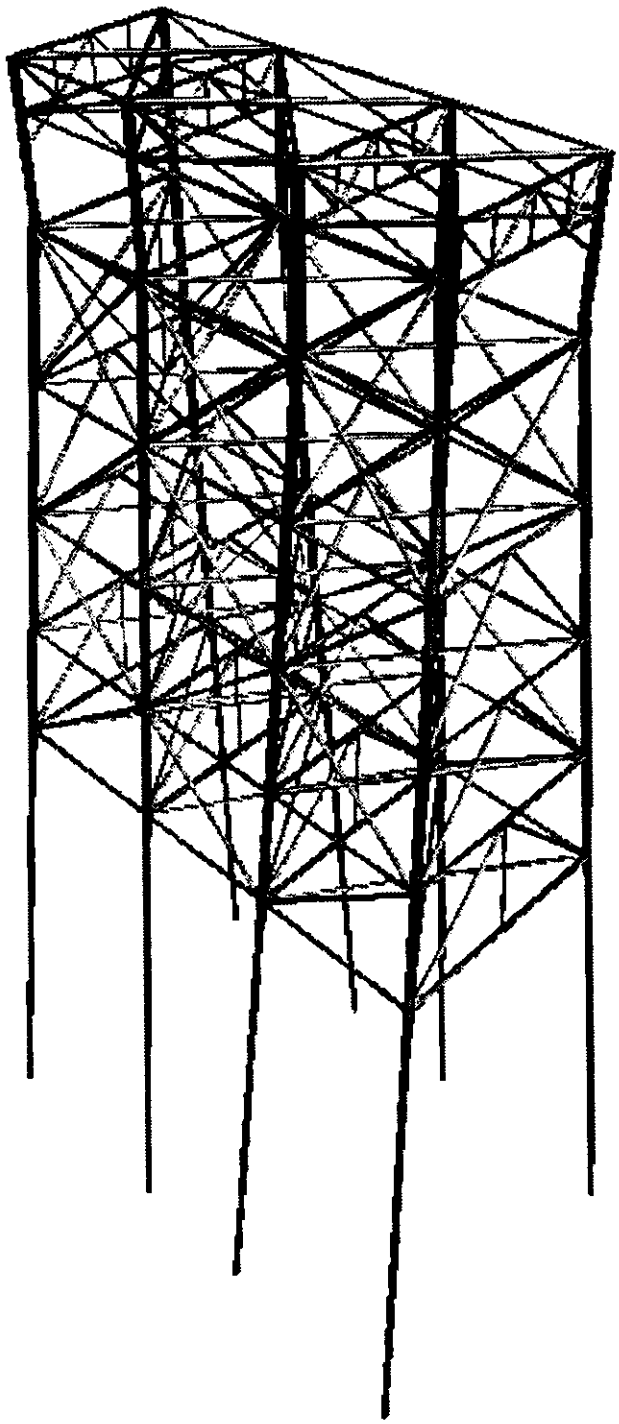

Figure 6.4-1: Platform D Isometric View

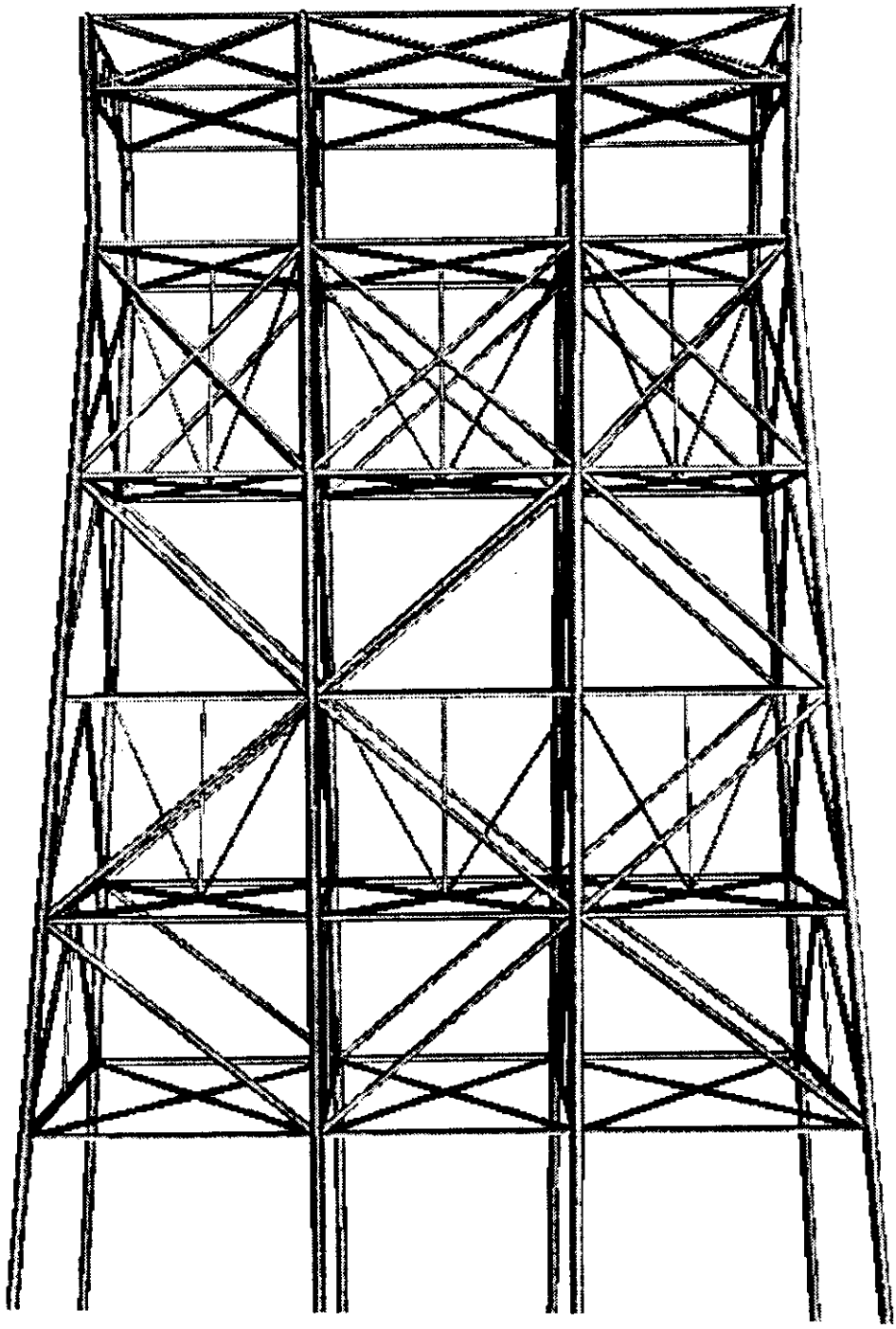

Figure 6.4-2: Platform D Broadside Elevation

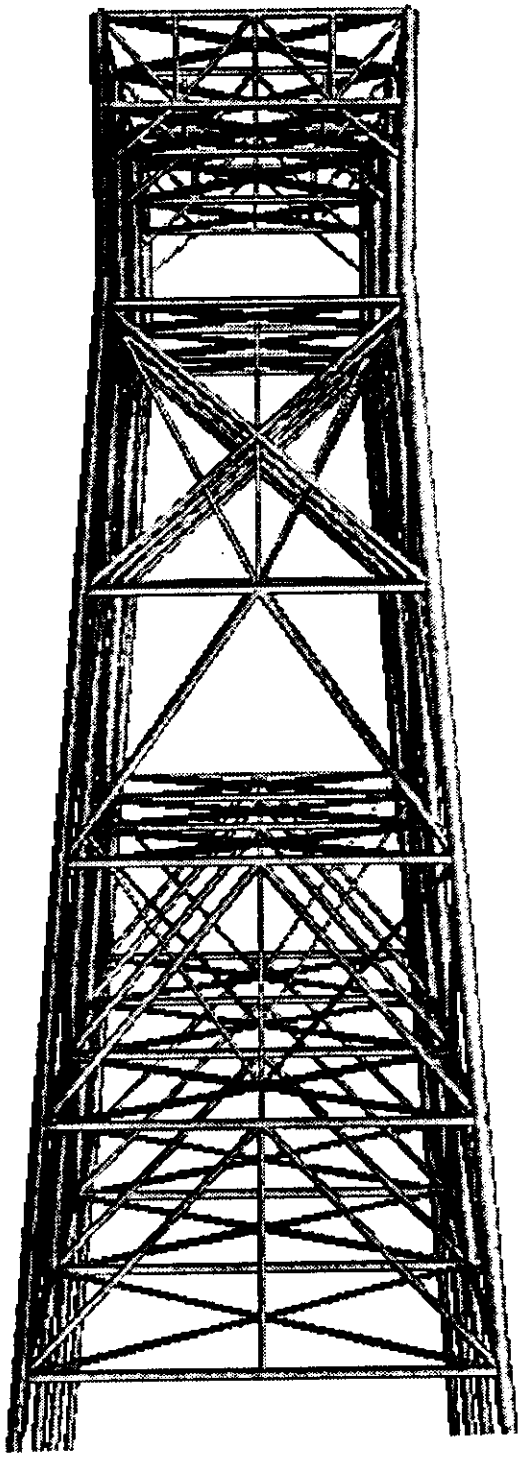

Figure 6.4-3: Platform D End-On Elevation

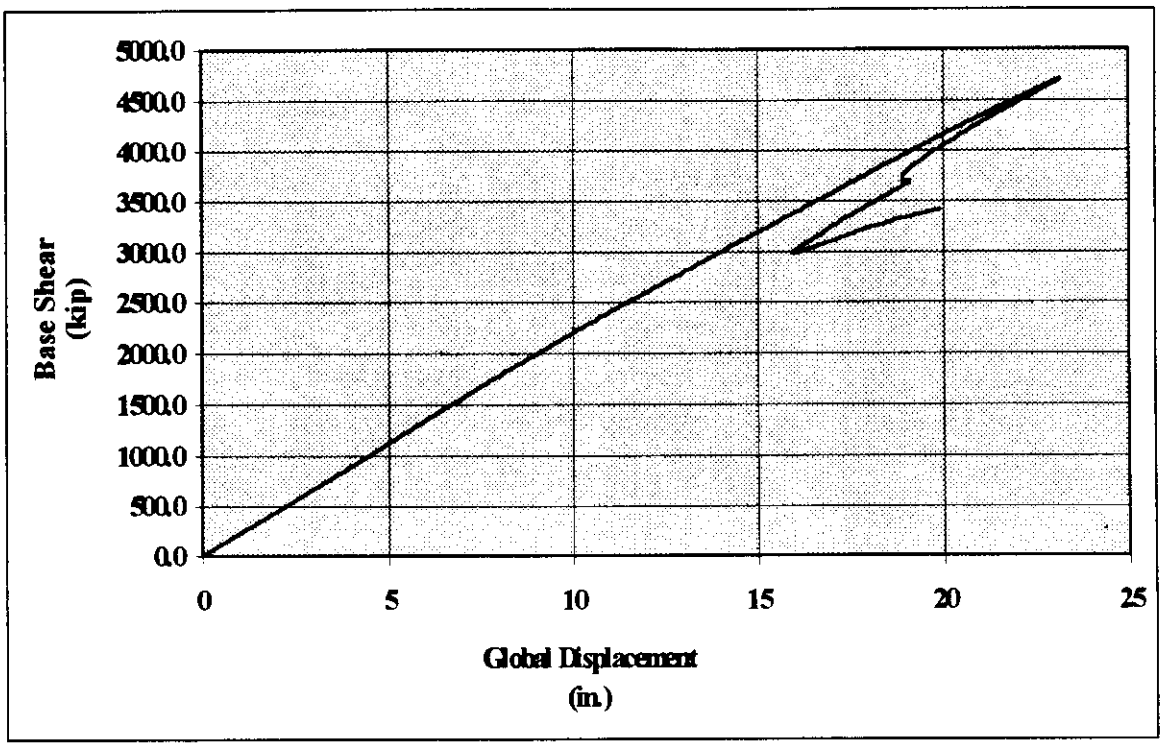

Figure 6.4-4: Platform D Broadside Loading Force-Displacement History

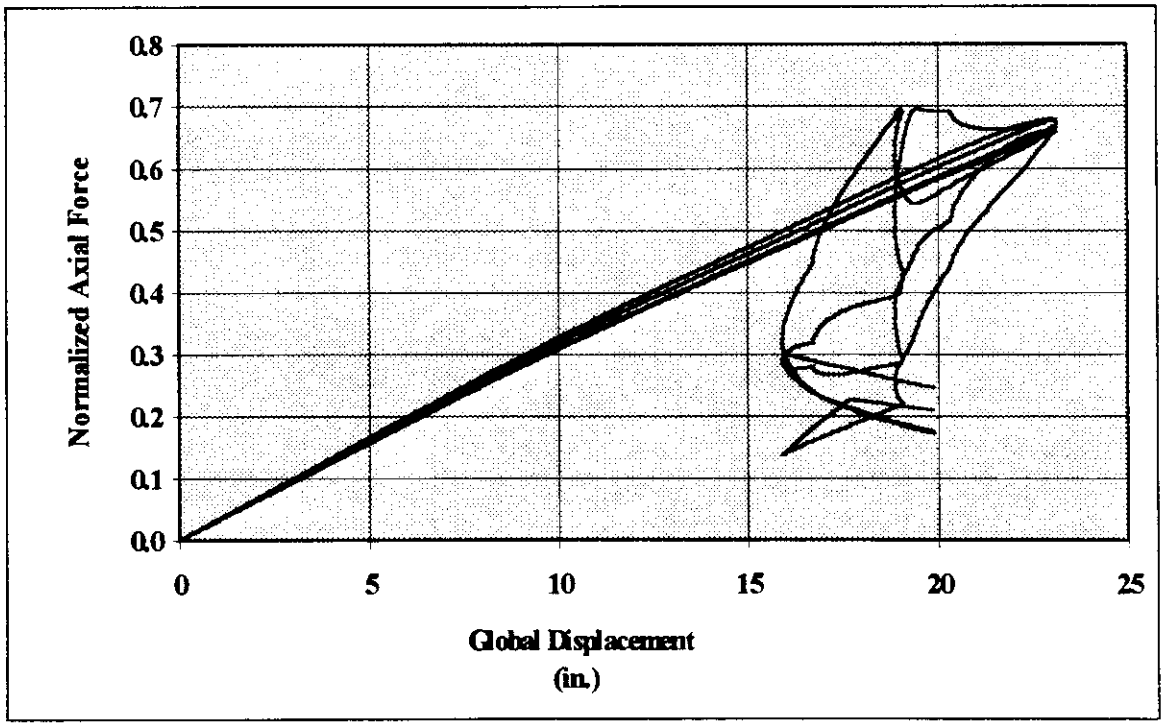

Figure 6.4-5: Platform D Broadside Third Bay Compression Brace Axial Force History

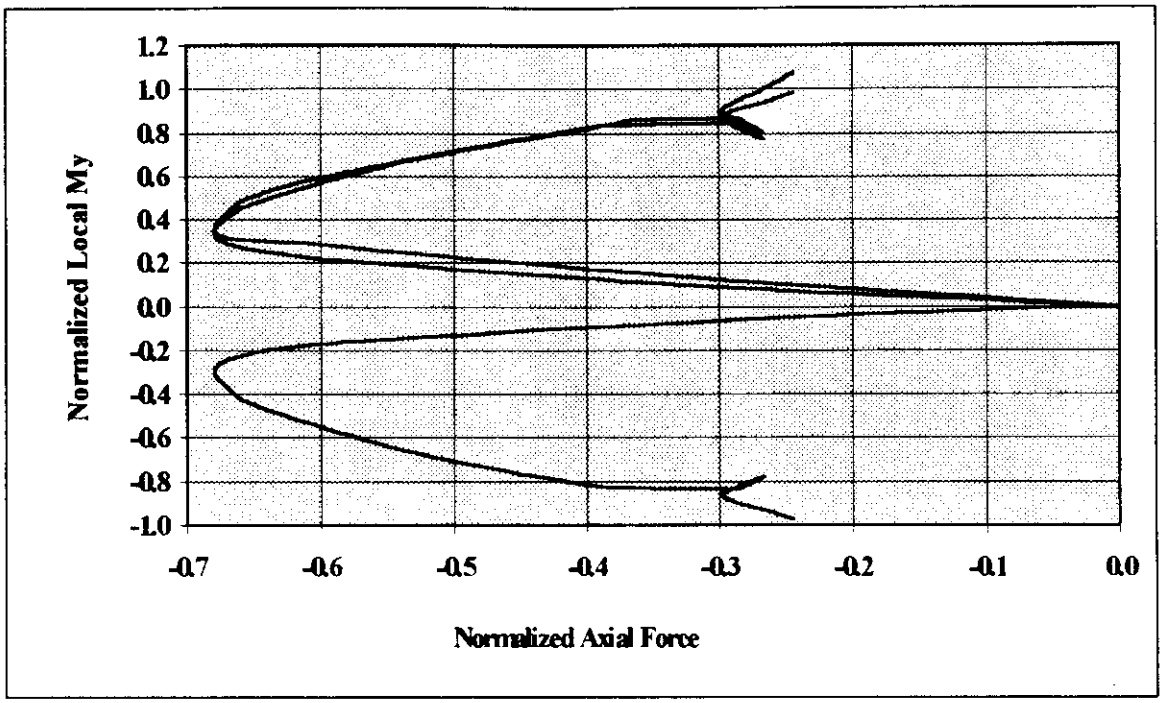

Figure 6.4-6: Platform D Broadside Third Bay Compression Brace 374 P-M Interaction at End Nodes and Midpoint

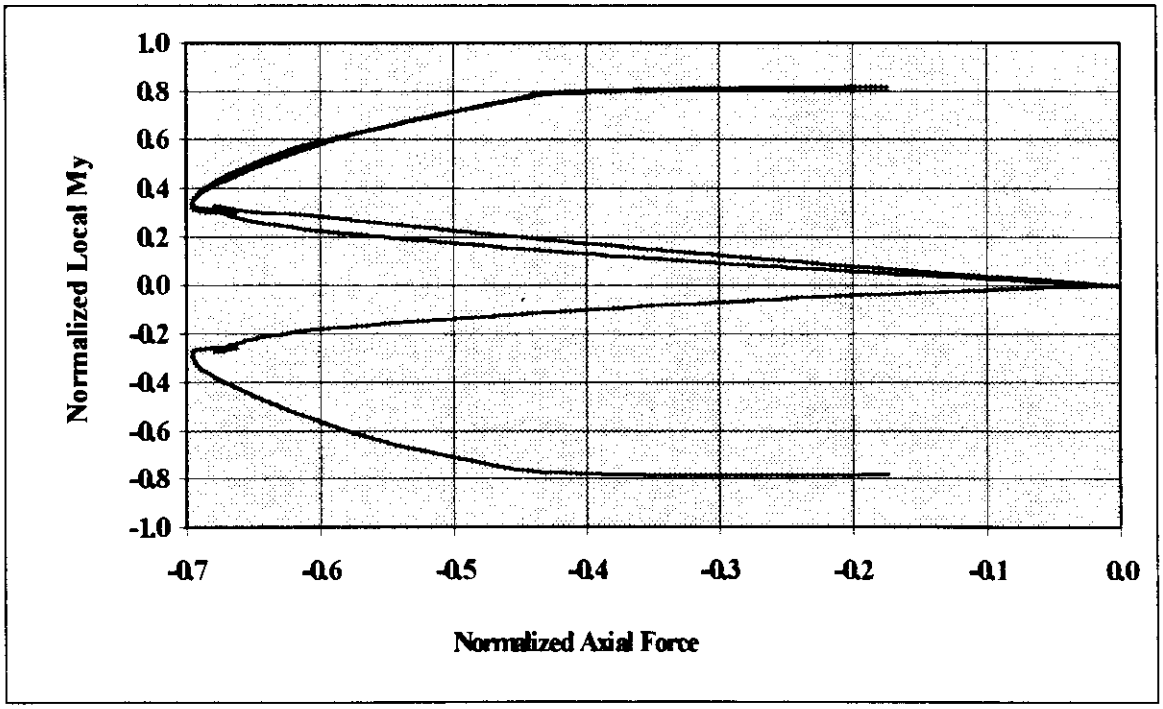

Figure 6.4-7: Platform D Broadside Third Bay Compression Brace 376 P-M Interaction at End Nodes and Midpoint

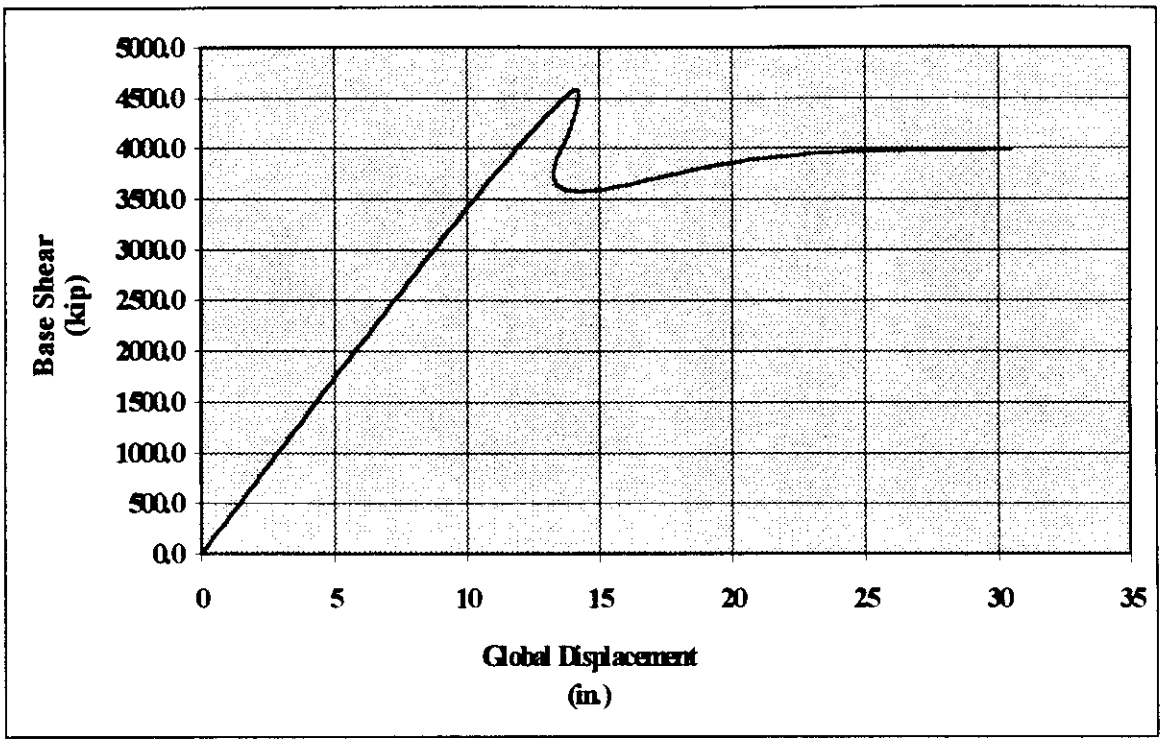

Figure 6.4-8: Platform D End-On Loading Force-Displacement History

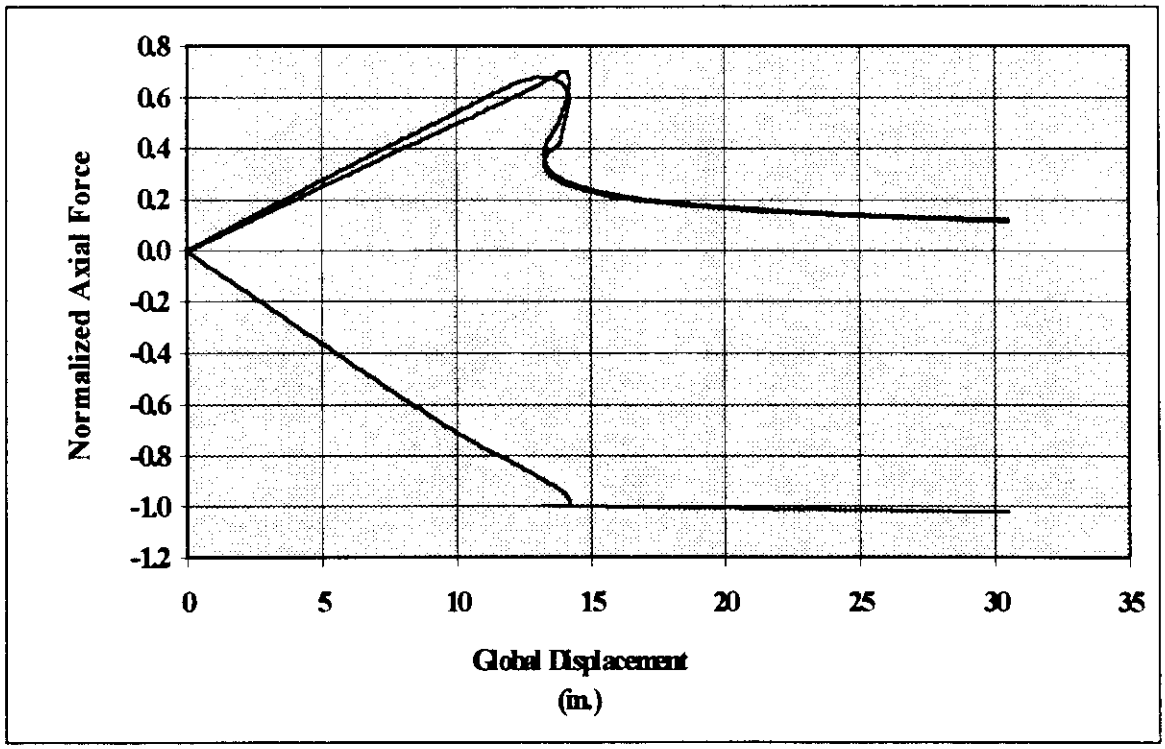

Figure 6.4-9: Platform D End-On First Bay Compression Brace Axial Force History

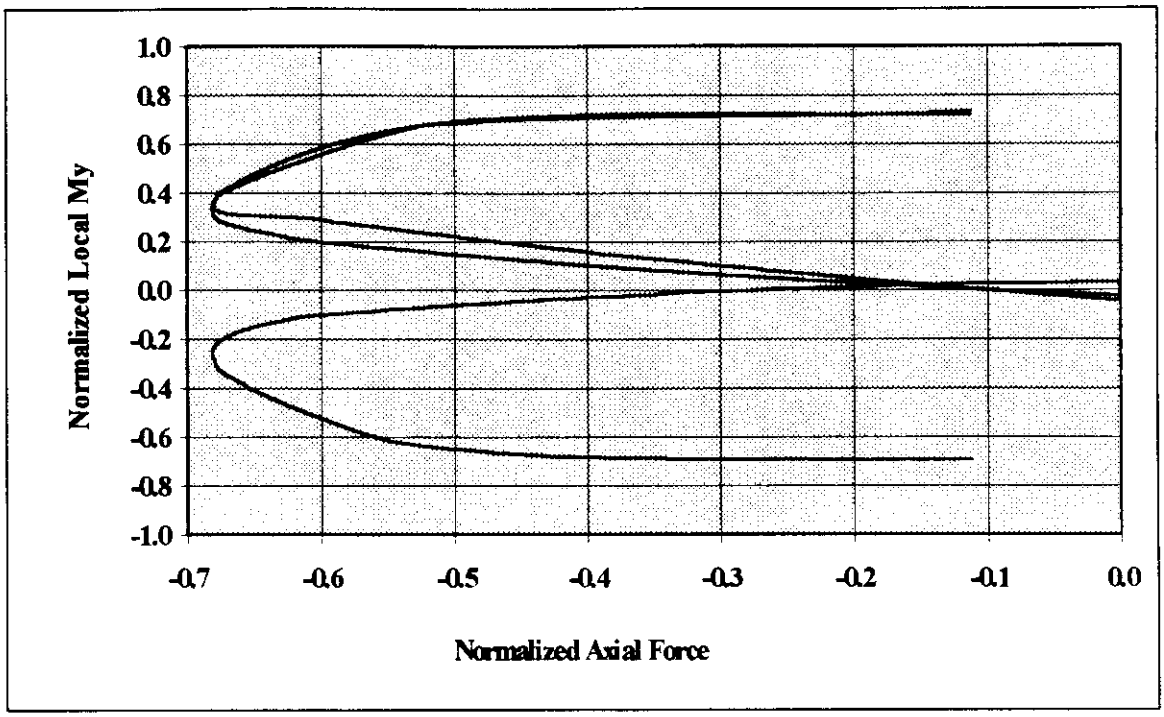

Figure 6.4-10: Platform D End-On First Bay Compression Brace 161 P-M Interaction at End Nodes and Midpoint

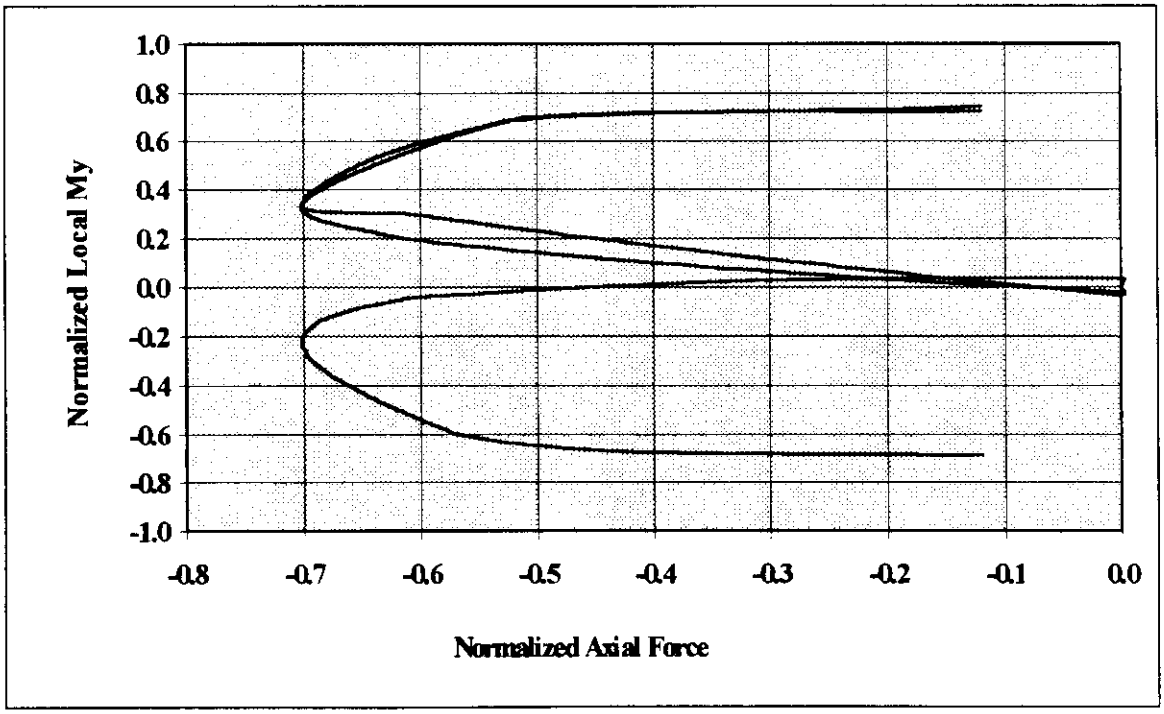

Figure 6.4-11: Platform D End-On First Bay Compression Brace 163 P-M Interaction at End Nodes and Midpoint

7.0 PARAMETER STUDIES

7.1 Wave Induced Vertical Deck Loads

7.1.1 Introduction

Current industry-standard procedures for determining wave induced deck loads are simplified calculations which use a Morison equation approach. Usually, wave induced vertical deck loads are ignored in these calculations. The exclusion of these vertical forces can not only affect the magnitude of the platform's wave load resistance capacity, as determined in the analysis, but also affect the determination of the failure mode itself. In addition, the current industry-standard procedures ignore the effects of dynamics for both vertical and horizontal loads (Bea and Young, 1993).

As stated previously, most older platforms have less lateral wave load resisting capacity than do recently designed platforms. This fact is primarily due to the small, 25-year return period wave heights used in many designs until the mid-1960's. In addition, some existing platforms are subject to subsidence which effectively raises the water level and reduces the existing air gap between the water surface and the bottom the of cellar deck (Broughton and Horn, 1987). Therefore, such platforms may experience potentially large deck loads, both vertical (up and down) and horizontal. Many older platforms were not specifically designed to resist any wave-induced deck forces.

7.1.2 Development of Vertical Forces

As a wave passes through a platform, the surface elevations at all points underneath the decks rise and fall as well as propagate in the wave direction. Consequently, this vertical motion of the wave can create severe impact loads on the bottom of the deck. This is especially true if the deck floor consists of solid steel plating rather than perforated steel grating.

The term slamming force is regularly used to describe the sudden impact of a horizontal member above the still water level (SWL) with the wave surface. The total force on a horizontal member above the still water level is a function of buoyancy and the rate of change in momentum. For a circular cylinder penetrating a fluid surface, the total vertical force per unit length is given as

$$F_v = \rho g A_i + (m_3 + \rho A_i)\ddot{\eta} + \frac{\delta(m_3)}{\delta z}\dot{\eta}^2 \tag{7.1}$$

where,

$$m_3 = \frac{1}{2}\rho r^2\left[\frac{2\pi^3}{3}\frac{(1-\cos(\theta))}{(2\pi-\theta)^2} + \frac{\pi}{3}(1-\cos(\theta)) + (\sin(\theta)-\theta)\right] \tag{7.2}$$

$$\eta = A_{max}\sin\left(\frac{2\pi t}{T}\right) \tag{7.3}$$

and r, θ, z and A_i are defined in figure 7.1-1 and A_{max} is the maximum wave amplitude (Bando et al., 1990). This force equation was developed by Kaplan and Silbert (Bando et al., 1990). Although it appears similar to the MJOS equation, with acceleration and velocity squared terms, the Kaplan-Silbert equation is based on potential flow theory and

not developed empirically (Bando et al., 1990). Sarpkaya rewrote equation 1 in terms of the maximum particle velocity and a slamming coefficient, C_s:

$$F = \frac{1}{2}\rho C_s D L U_{max}^2 \tag{7.4}$$

The theoretical value for the slamming coefficient is (Sarpkaya, 1978) (Bando et al., 1990)

$$C_s = \overline{A}_i \frac{gr}{U_{max}^2} - \left(\overline{m} - \overline{A}_i\right)\frac{r}{A}\sin\left(\frac{2\pi t}{T}\right) + \frac{\delta \overline{m}}{\delta \overline{z}}\cos\left(\frac{2\pi t}{T}\right) \tag{7.5}$$

where $A_i = A_i/r^2$, $m = m/\rho r^2$, $z = z/r$ and $U_{max} = 2\pi A/T$ and A is the maximum wave amplitude.

Taking $z = r(1-\cos(\theta/2))$, it can be shown that C_s is equal to π when the cylinder just touches the free surface and at that point in time is independent of cylinder diameter and flow parameters. After this instant, the slamming coefficient rapidly decreases until it increases again to a second top value of 1.25 just when z/D =1.0. After the cylinder is submerged, buoyancy and drag forces become significant and the slamming force diminishes due to the decreasing rate of change of momentum. Theoretical values of the slamming coefficient as a function of relative submergence are shown in figure 7.1-2 (Sarpkaya, 1978).

Experiments by Sarpkaya and others verify this initial slamming coefficient value (Sarpkaya, 1978) (Faltinsen et al., 1977). However, all experiments concerning slamming coefficients must account for the potential for dynamic amplification. Sarpkaya realized this and subtracted out the inertial force before back-calculating the slamming coefficient. Based on theory, Sarpkaya postulates that an empirically derived slamming coefficient

could be between 0.5 and 1.7 of the theoretical maximum value of π. This conclusion is reasonable since 1.7 is approximately the maximum DAF for both sinusoidal and decreasing triangular impulse loads (Clough and Penzien, 1993). This range was further verified by Sullied who experimentally observed C_s values ranging from 4.1 to 6.4 with an average of 5.3 (Sarpkaya, 1978). This average value is almost exactly 1.7π.

The foregoing discussion and most of the available literature on vertical slamming forces has focused on horizontal cylinders above the SWL. This narrow focus is almost surely due to the ease of mathematical description and consistency in experiments when using a cylinder. Also, there are many platforms which contain exposed cylinders above the SWL. However, the focus of this study is to determine the vertical wave loads on platform decks with solid flooring. This problem is obviously much different than studying a simple cylinder of unspecified length. Yet the background work with horizontal cylinders and the development of the slamming coefficient for cylinders played a major role in the study of vertical wave-in-deck forces.

Most all the research and available literature concerning wave-in-deck forces is focused on the famous Ekofisk platform (Broughton and Horn, 1987) (Bando et al., 1990) (Mes, 1990). In December of 1984 it was discovered that the Ekofisk platform 2/4C was found to be suffering extreme subsidence. Later surveys showed that the subsidence was over 2.6m in the area of the platform 2/4C (Broughton et al., 1987). After much study, the subsidence was attributed to the compression and compaction of chalk layers some

3,000m below the seabed. The problem had been caused by the removal of the hydrocarbons from the area and was extended over an area approximately 6,000m in diameter.

Since the capital investment for the Ekofisk complex was immense and the intent was to continue extracting oil and gas, the problem was considered to be very serious. Hence, a massive engineering study was begun that was headed by the Industrial division of Det norske Veritas and by Veritec, under the supervision of Phillips Petroleum Company Norway (Broughton et al., 1987).

Since the subsidence was not attributable to foundation failure and the problem was not local enough to cause relative displacements between the legs, the most significant concern was wave-in-deck forces. The as-designed air gap for the platform was approximately 2.02m. However, due to less than anticipated jacket leg settlement, the installed air gap was 2.73m (Broughton et al., 1987). It was assumed that the subsidence would continue and therefore, the study considered subsidence between 2.6m and 4.0m.

The study started by developing a theoretical approach and later comparing those results with experiments using a scaled-down model of the platform's cellar deck. The theoretical approach assumed that the vertical force caused by the interaction between the wave surface and the bottom of the platform was proportional to the momentum of the water as it hits the underside of the deck. This led to a theoretical vertical force of

$$F_v = \frac{1}{4}\rho \pi c v B(ct) \tag{7.6}$$

where c is the wave celerity as calculated by Stoke's V wave theory, v is the vertical fluid particle velocity, B is the deck width and ct is the effected length (Mes, 1990). Figures 7.1-3a and 7.1-3b graphically describe these parameters. Later experimental studies using a scale model of the platform decks concluded that the vertical force was approximately 66% of that calculated using the above equation. Also, it was observed that the upward or positive vertical force was in phase with the maximum horizontal force on the deck beam. Of primary interest was the observation of a large downward vertical force as the crest of the wave travels past the backside of the platform. This negative vertical force appears to be caused by suction forces and inertial acceleration forces as the surface comes off the deck underside. The negative vertical force was approximately equal in magnitude to the positive vertical force that occurred moments earlier. This observation was consistent across experiment results.

7.1.3 Case Studies - Description And Test Procedures

Platform B (PB) and Platform D (PD) were re-analyzed considering the effects of vertical wave-in-deck forces. PB was analyzed with a fixed base assumption. Both positive and negative direction loads were modeled in combination with the corresponding horizontal wave-in-deck loads for PB (see figure 7.1.-4), while only the negative or downward direction vertical loads were modeled for PD. PB was subjected to a 70 ft wave, while PD was analyzed for a 56 ft wave in the broadside direction and a 60 ft wave in the end-on direction. The calculations of the deck loads, both vertical and horizontal are included in

Appendix B. It should be noted that, as was done in the Ekofisk study, the vertical loads were based on 66 percent of the vertical loads derived from the theoretical procedure.

7.1.3 Analysis Results

The results of the analyses are best described by figures 7.1-5 through 7.1-10 and partially summarized in table 7.1-2. In general, it can be seen that the inclusion of the positive and negative vertical loads did not significantly affect the global capacity of the structures. This is partly understandable considering the geometry of the test platforms and the manner in which the vertical loads were calculated. First, the test platforms were relatively small. Thus, its plan deck size was also small. An increase in deck size would result in a direct increase in theoretical and empirical vertical forces. In addition, the forces calculated did not account for the large negative vertical force that would result from the water coming up onto the deck as the wave passed through the platform. This negative vertical force would most likely be added to the suction or momentum based vertical force.

Surprisingly, both Platform B and Platform D had nearly equal or slightly higher lateral load resisting capacity when the positive or negative vertical loads were added. Only Platform D end-on loading showed a reduction in capacity with added vertical load. Some positive force redistribution due to the additional vertical loads is possible. However, this result is counter-intuitive and otherwise unexplainable by the authors. More importantly, the results for the three loading cases are extremely similar, differing by less than one

percent. Therefore, the effect of vertical load on the lateral load resisting capacity appears to be insignificant.

It should be noted that dynamics, which could have a potentially significant effect, were ignored in this study. Since the vertical loads are impulsive in nature, there could be important dynamic amplification effects up to approximately 1.7 time the static load for a completely rigid structure. In addition, the results discussed here focus solely on the global response of the structure and do not address local forces in members or plate flooring. The uniformly distributed load on the bottom of the deck could damage the floor and its supports, which in turn could effect the support of the deck mounted equipment.

7.1.4 Conclusions and Recommendations

The results presented here indicate that vertical loads due to deck slamming can possibly be insignificant when determining the ultimate lateral load resisting capacity of a platform. However, as previously mentioned, this study was limited in scope. Thus, with the small amount of available research data to form an explanation of the results, no general conclusions concerning the importance of vertical loads should be drawn. Further study of additional platforms with different deck sizes and shapes with an attempt to include the effects of platform dynamics should shed additional light of the subject. Thus, it is recommended that, as a minimum, vertical loads should be calculated in future platform requalifications and designs whenever the possibility for deck-induced forces exist. These

forces can then be examined in the light of qualified engineering experience and/or used to design or assess the individual deck elements that they load.

Table 7.1-1: Test Case Loading Information

Load Component	Platform B 70 ft Wave (kip)	Platform D B.S. 56 ft Wave (kip)	Platform D E.O. 60 ft Wave (kip)
Jacket	2,359	4,426	4,607
Decks	393	527	330
Boatlanding	82	983	271
Total Horizontal Base Shear	2,834	5,936	5,208
Deck level 1 (pos. vertical)	230	-	-
Deck level 1 (neg. vertical)	-230	-486	-695

Table 7.1-2: Global Analysis Results

Loading Scenario	Maximum Normalized Load	Displace. at Maximum Load (in)
Platform B		
70 ft Wave Base Case	1.16	8.7
70 ft Wave Positive Vertical Load	1.16	8.7
70 ft Wave Negative Vertical Load	1.20	8.8
Platform D Broadside Loading		
56 ft Wave Base Case	0.793	23.1
56 ft Wave Negative Vertical Load	0.824	24.3
Platform D End-On Loading		
60 ft Wave Base Case	0.879	14.2
60 ft Wave Negative Vertical Load	0.857	14.8

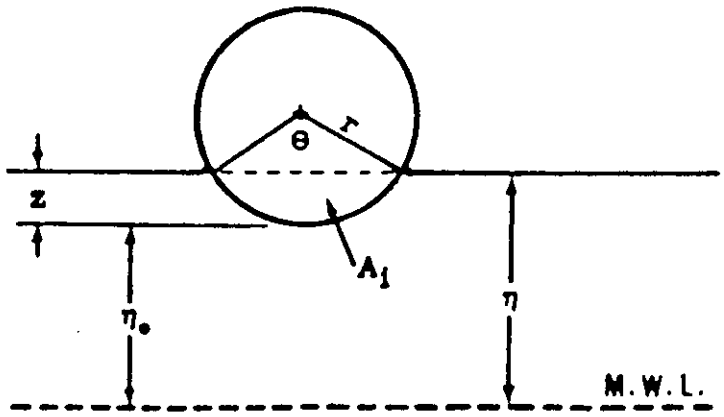

Figure 7.1-1: Surface Impact of a Horizontal Cylinder (Bando et al., 1990)

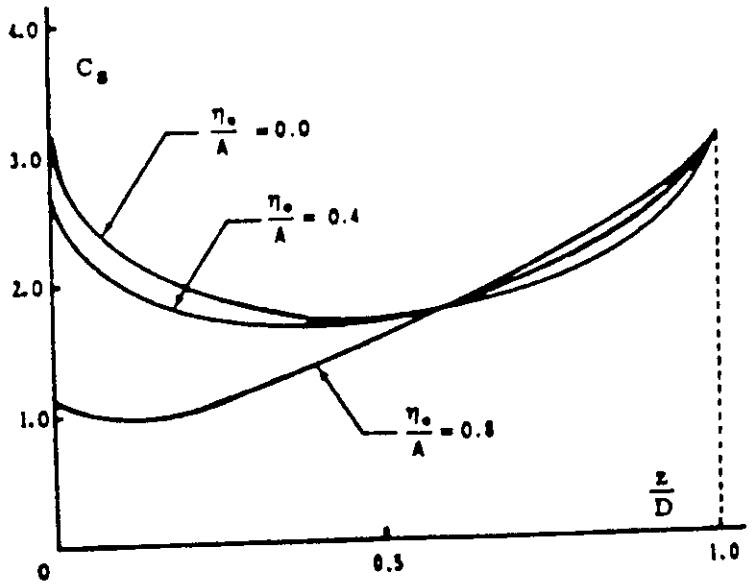

Figure 7.1-2: Theoretical Values of the Slamming Coefficient (Sarpkaya, 1978)

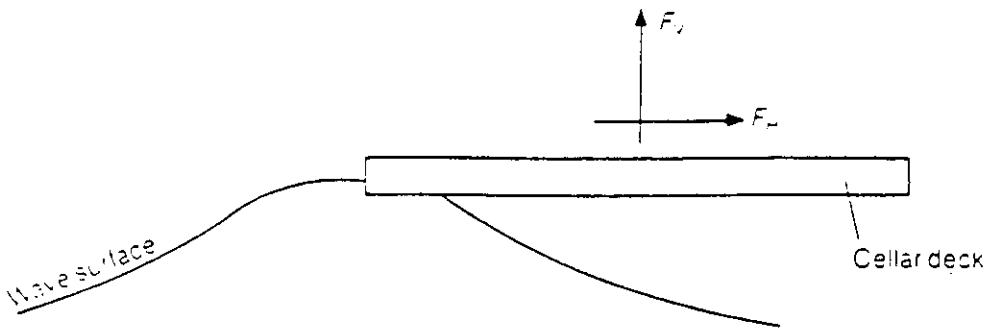

(a)

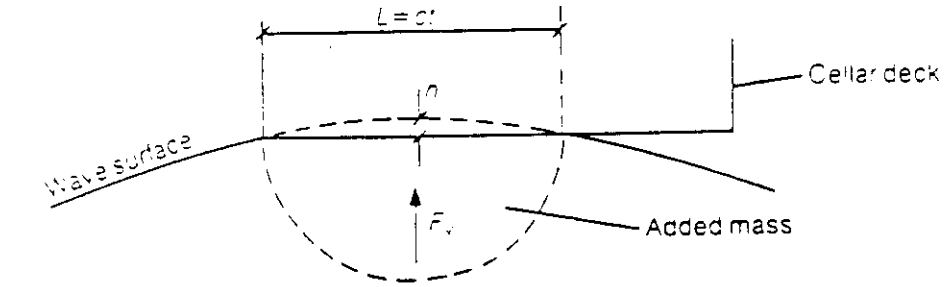

Method:

(b)

Figure 7.1-3: Deck and Wave Surface Interaction: (a) cellar deck-wave interaction; (b) underside of deck and wave interaction providing vertical force (Mes, 1990)

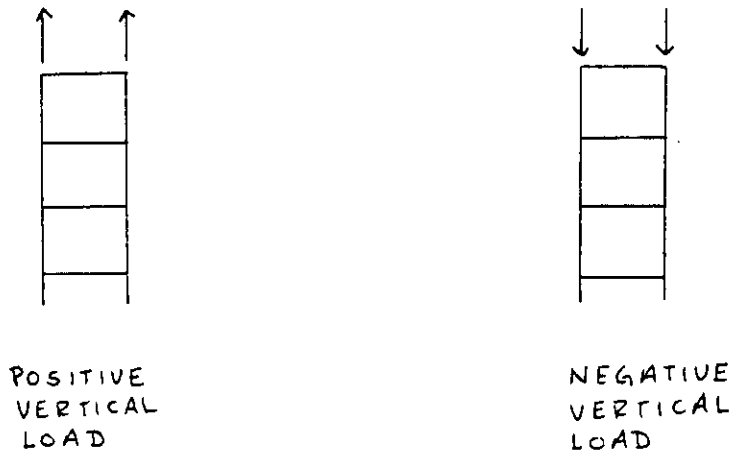

Figure 7.1-4: Positive and Negative Vertical Deck Loads

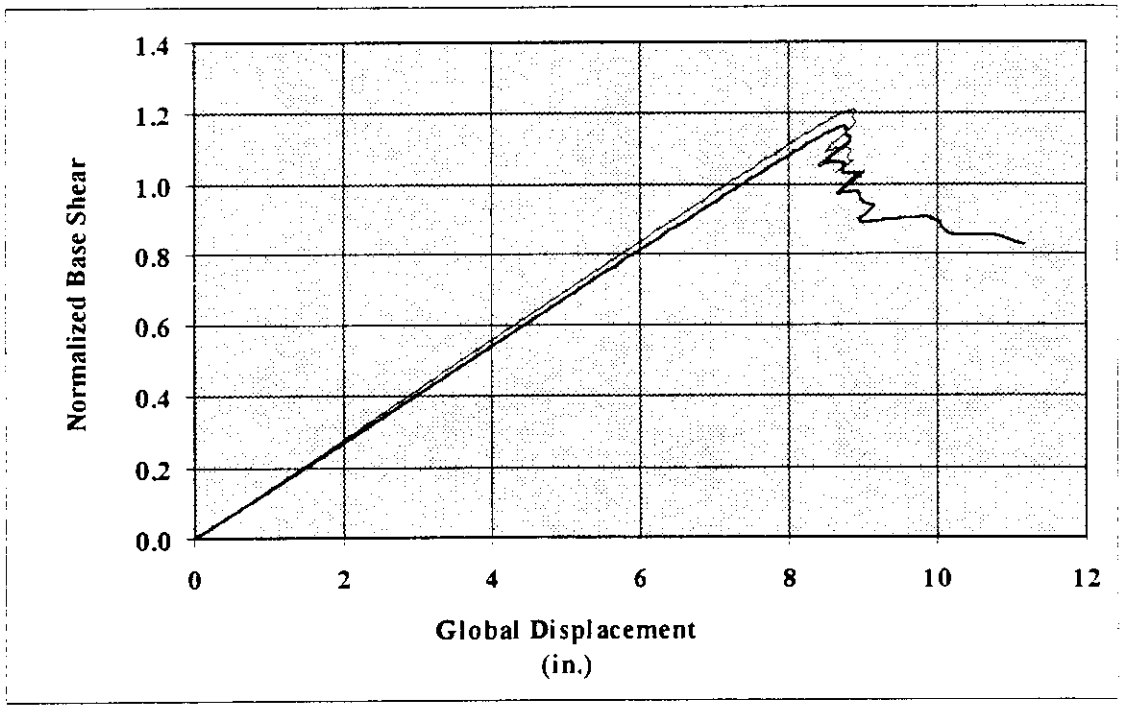

Figure 7.1-5: Platform B - Force-Displacement History for Zero, Positive and Negative Vertical Forces

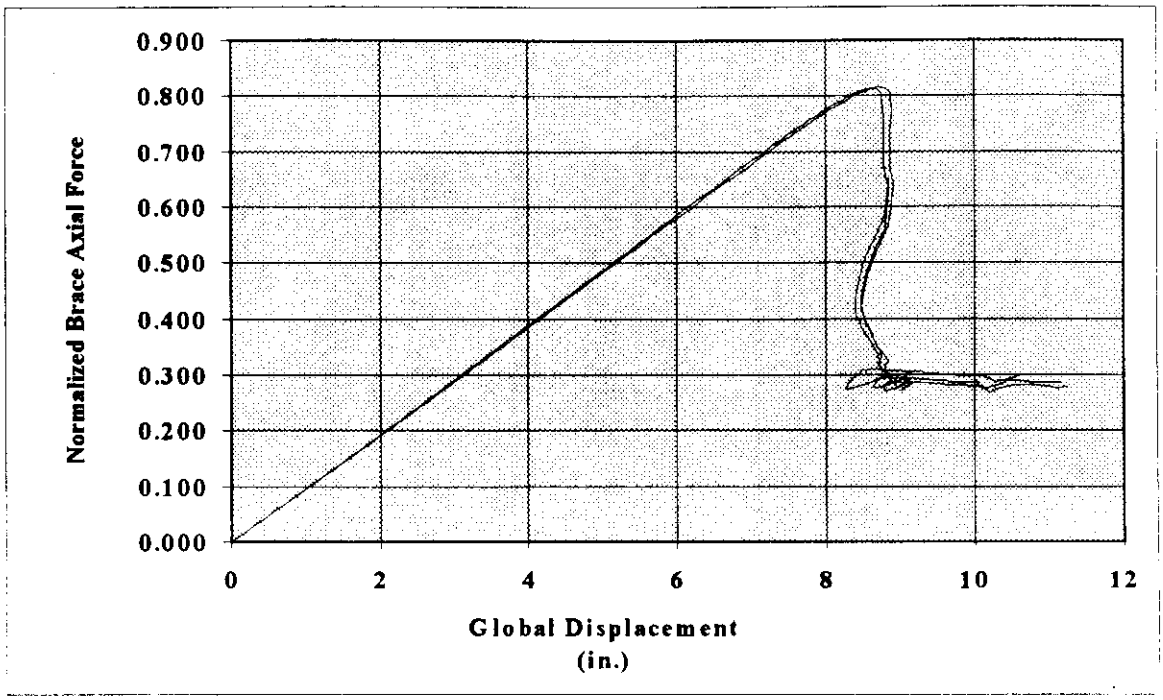

Figure 7.1-6: Platform B - Normalized Axial Force History in Critical Brace for Zero, Positive and Negative Vertical Forces

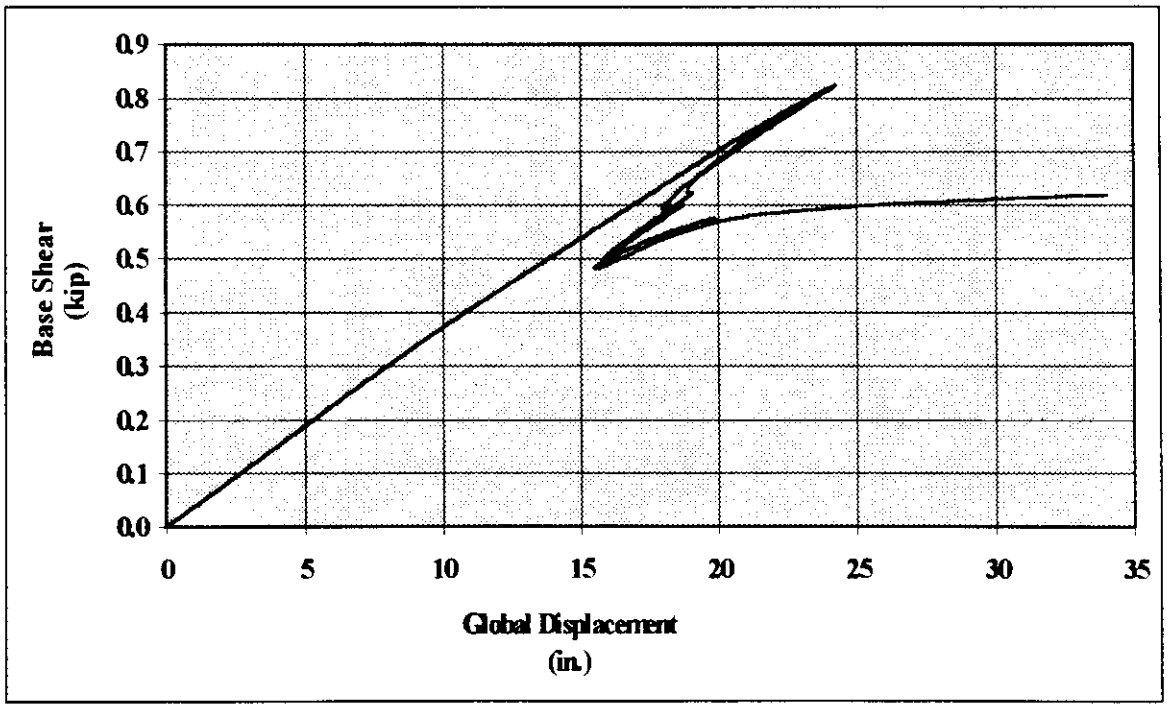

Figure 7.1-7: Platform D - 56 ft Wave - Force-Displacement History for Zero and Negative Vertical Forces

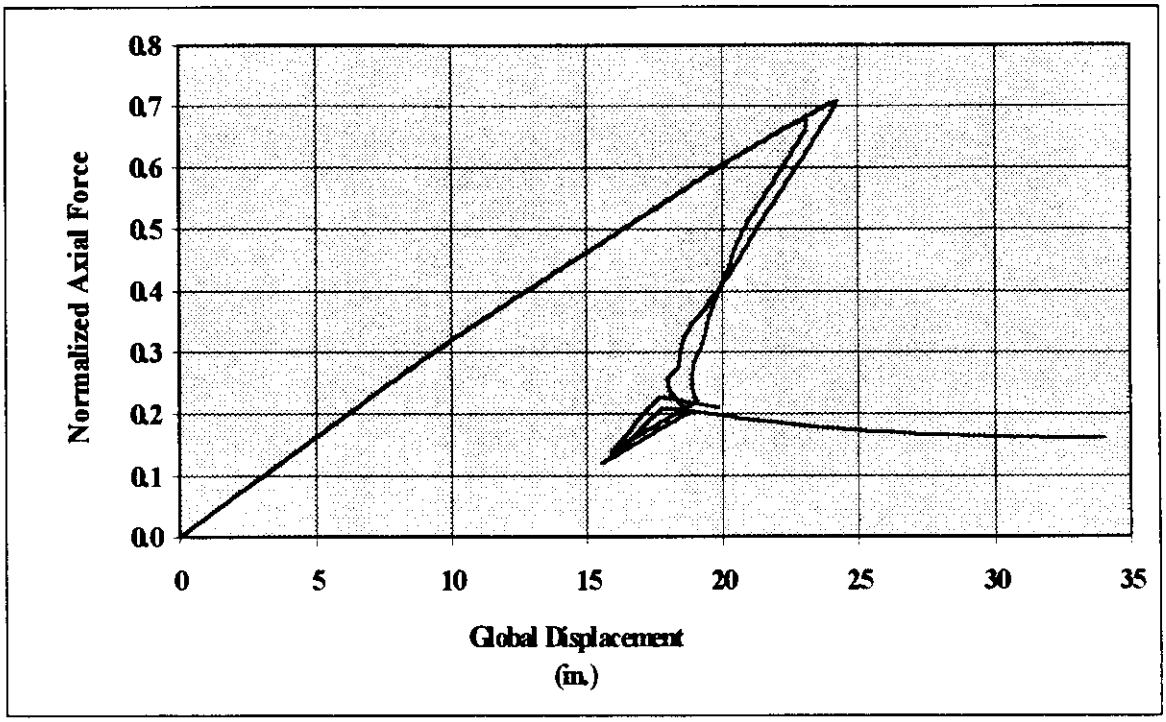

Figure 7.1-8: Platform D - 56 ft Wave - Normalized Axial Force History in Critical Brace for Zero and Negative Vertical Forces

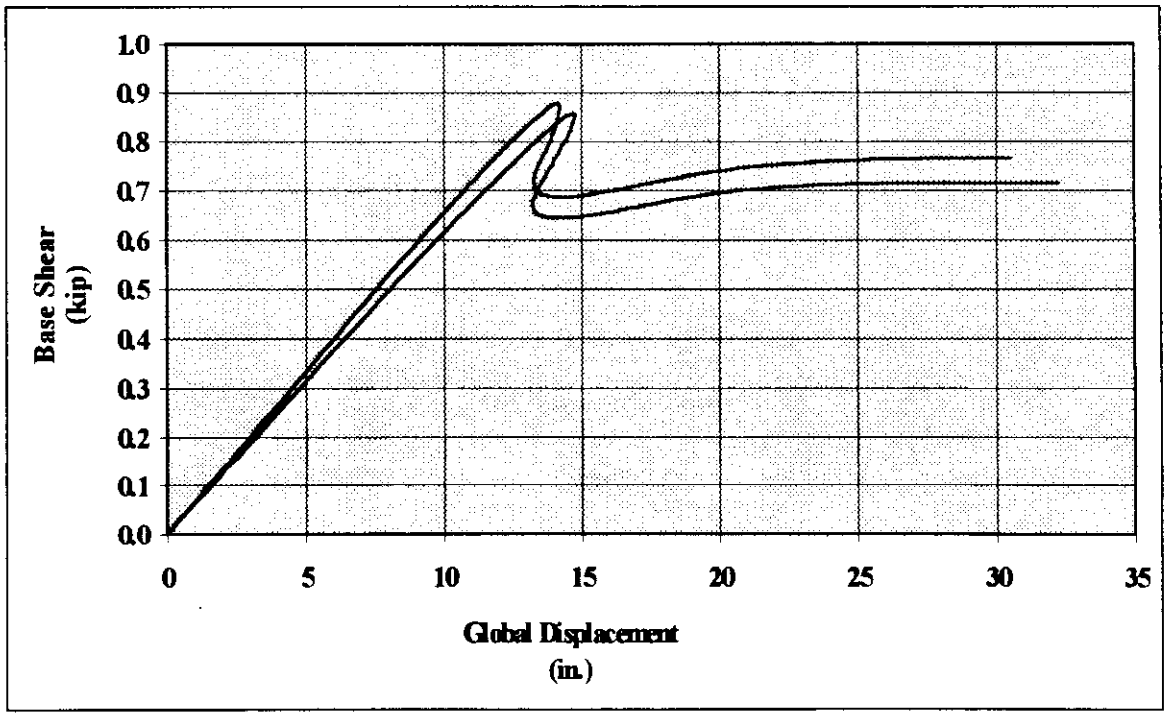

Figure 7.1-9: Platform D - 60 ft Wave - Force-Displacement History for Zero and Negative Vertical Forces

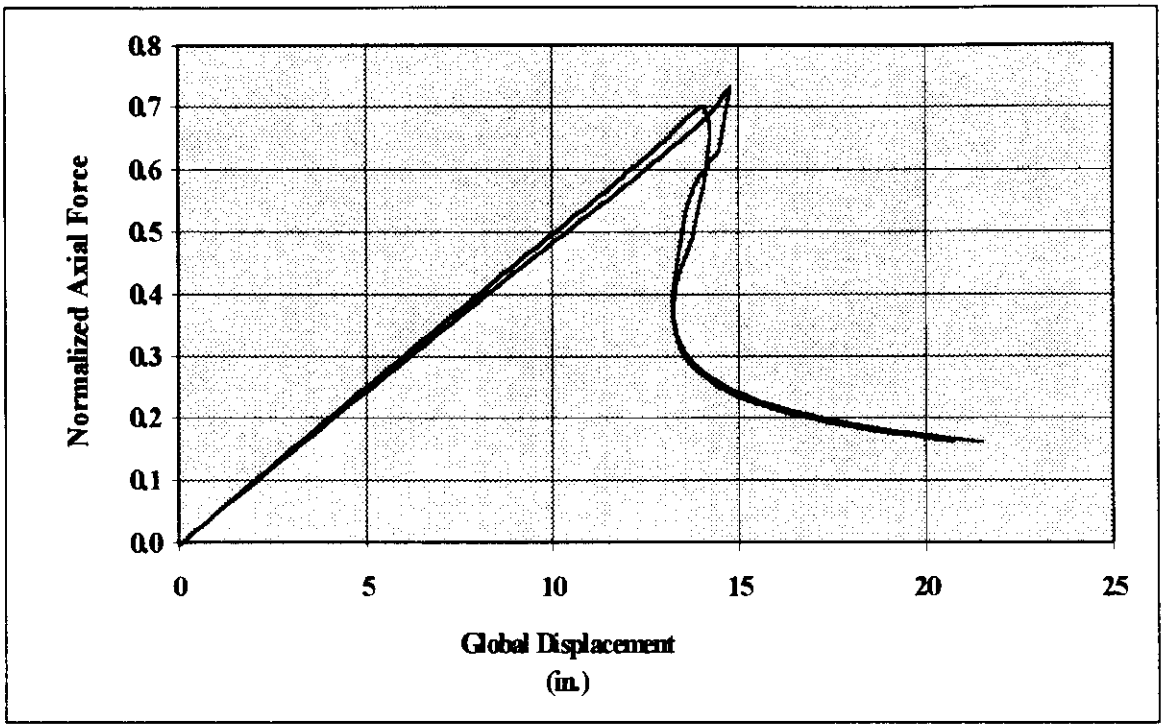

Figure 7.1-10: Platform D - 60 ft Wave - Normalized Axial Force History in Critical Brace for Zero and Negative Vertical Forces

7.2 Initial Member Imperfection and Yield Strength

Offshore platforms are composed of individual members that form a system of load resisting elements. Each of these elements has certain properties that affect its ability to resist a given load. Although platform members are usually completely welded together, giving them "fixed" ends, most steel-frame offshore platforms are designed to behave as a three-dimensional truss. In reality, all the connections are semi-rigid, and most elements exhibit the behavior of a beam-column. However, in the elastic range and even partially into the inelastic range, member axial load capacity is of primary importance. Thus, when designing or assessing platforms, it is important to know the relationship between the member properties and the overall platform load resisting capacity.

Initial member imperfection and member yield stress are two properties that have direct bearing on a member's axial load carrying capacity, and hence the overall platform capacity. In addition, if not carefully selected, these two properties can lead to incorrect analysis results. The remainder of this section documents the results of two parameter studies, which investigate the relationship between these two properties and overall platform load resisting capacity.

7.2.1 Initial Member Imperfection

As noted above, most platform members are designed to primarily resist axial load. Axial load resisting capacity is a function of, among other things, member length, cross-sectional geometry, end restraints, global shape and internal bending moments. Some first order

analyses assume a perfectly straight member and predict buckling at a predetermined load. However, as was discussed in section 5, buckling is actually a non-linear process, dependent upon the axial load/moment combination at various locations along the member.

Member moment comes from three primary sources: end-rotation, local hydrodynamic forces and eccentric axial loading. Obviously, these three sources are interrelated. Specifically, end-rotation and local hydrodynamic forces affect the member shape, which determines the degree of local P-δ or eccentric axial moment. This interrelationship must be investigated and accounted for when performing a non-linear analysis. The moments from these three sources can add together or work against one another, which will effect the maximum axial load a member can resist.

The initial imperfection is included to account for a member's initial out-of-straightness. USFOS allows the user to choose initial imperfections causing either single or double curvature, see figure 7.2-1. This study only considered single curvature, but the discussion presented here is generally applicable to both cases. This study focused on the relationship between initial imperfection and local hydrodynamic forces due to wave action. It should be noted that although not considered in this study, gravity and buoyancy forces have similar relationships with the initial imperfections as do wave loads. Also, this study did not attempt to isolate individual members, and hence, did not investigate the effects of member end rotation. Member end rotation is not a user-defined

quantity but rather a result of the structure model and load input parameters. Therefore, end-rotation of individual members was considered outside the scope of this research.

An initial imperfection has both a magnitude and a direction. The imperfection magnitude will partially determine the extent of eccentric axial moment. The imperfection direction will determine the relationship between eccentric and local hydrodynamic induced moments. These two moments can not be combined using the principle of superposition because the local hydrodynamic forces affect the shape of the member and thus, the total axial eccentricity. This is especially true for relatively long members, since the deflection to due uniform normal loads on non-cantilever members is a function of the length squared.

The extreme combinations of these moments would be an initial imperfection directly in line with the local, normal hydrodynamic load direction and an initial imperfection directly opposite the hydrodynamic load direction, see figure 7.2-2. These two cases were studied with varying imperfection magnitudes for Platforms A and B. For the following discussion, the initial imperfection magnitude is normalized by the member length. USFOS requires this form of imperfection input. In addition, the imperfection to length ratio is a better indicator of axial load capacity reduction than solely initial imperfection. Also, as presented here, positive imperfection is directly in-line with local normal forces while negative imperfection is directly opposite local normal forces.

While not directly considered here, the magnitude of the local normal hydrodynamic forces is also important. The member's location in the wave profile, member orientation, drag and inertia coefficients and wave shape all affect the local normal force magnitude. This study varied the magnitude and direction of the initial imperfection while keeping the hydrodynamic conditions constant.

The relationship between initial imperfection and global platform capacity for platforms A and B are shown in figures 7.2-3 to 7.2-6. The peak of the curves indicates the point where the eccentric axial moment and local normal force moment essentially cancel each other, i.e., they act to resist one another or stabilize the member against the others effects. To the left of the peak, the eccentric axial moment dominates and the member buckles against the direction of the wave forces. To the right of the peak, the local wave forces dominate and the member buckles in-line with the wave direction. Obviously for positive imperfection, the moments add together to weaken the member. Another important observation is that the curve is essentially linear both to the left and right of the peak. There is also no discontinuity around zero imperfection as one might expect. This indicates a linear relationship between initial imperfection and overall platform capacity.

Another important observation is that increasing the magnitude of the imperfection does not always decrease the capacity of a member or the overall platform. Thus, users may unknowingly think that they are being conservative by using an initial imperfection or even by increasing the initial imperfection magnitude, when in reality they may be

unconservatively increasing the capacity of the platform. Figures 7.2-7 and 7.2-8 show the difference in platform load resisting capacity for positive and negative imperfections of various magnitudes. Noting the great difference in results for positive and negative imperfections is very important when working with programs such as USFOS.

USFOS assigns default imperfection directions if they are not specifically assigned by the user. Although it was purely a matter of coincidence, it was noted during this research that the default imperfection directions assigned by USFOS were opposite the proposed wave load for approximately three quarters of the analyses. If one knows the direction of the initial out of straightness, then it can be specified in the input. However, if a general imperfection is specified, the user must pay attention to its direction in order to achieve the desired result.

7.2.2 Member Yield Stress

Member yield stress can affect the overall platform capacity differently depending on the mechanism that controls the critical member(s). However, for most types of inelastic behavior, e.g., tension, compression or bending, "failure" or maximum capacity is directly related to the yield stress. To test this assumption, Platform B was analyzed with different levels of yield stress. All other parameters were kept constant. The initial imperfection was set to e/L=0.001. A coefficient of variation for a yield stress of eight percent was assumed which gave a standard deviation of 3.36 ksi. The test range was taken to be 42 ksi plus or minus two standard deviations. The analysis results shown in figure 7.2-9

verify that for non-linear beam-column members, the overall platform capacity is linearly related to the yield stress.

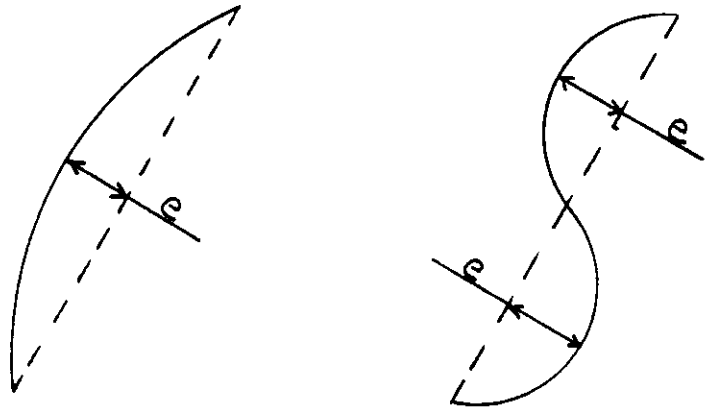

Figure 7.2-1: Single and Double Curvature Initial Imperfections

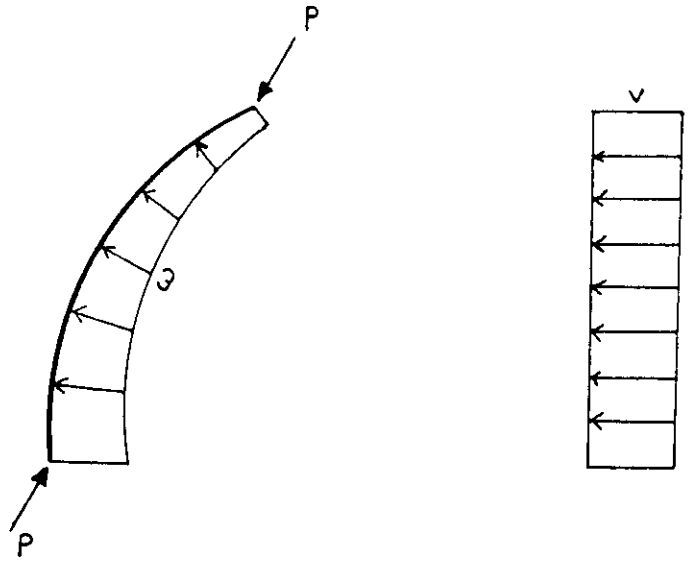

Figure 7.2-2: Local Hydrodynamic Force and Initial Imperfection Interaction

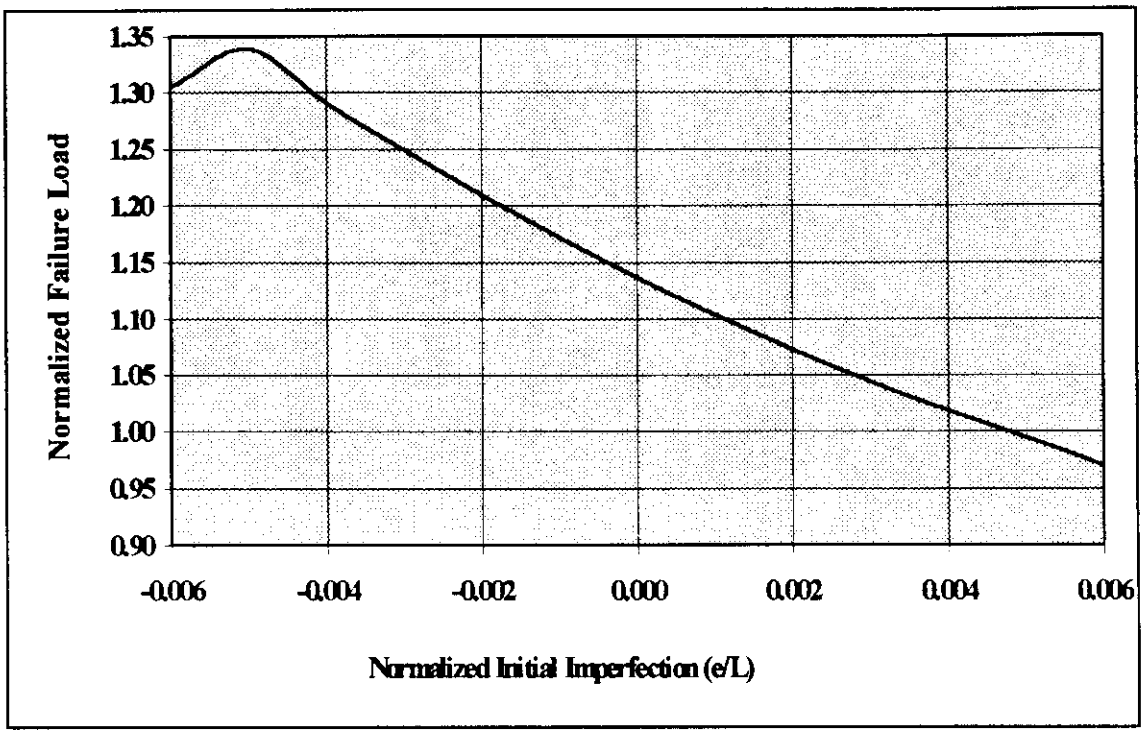

Figure 7.2-3: Platform A - Normalized Failure Load vs. Initial Imperfection

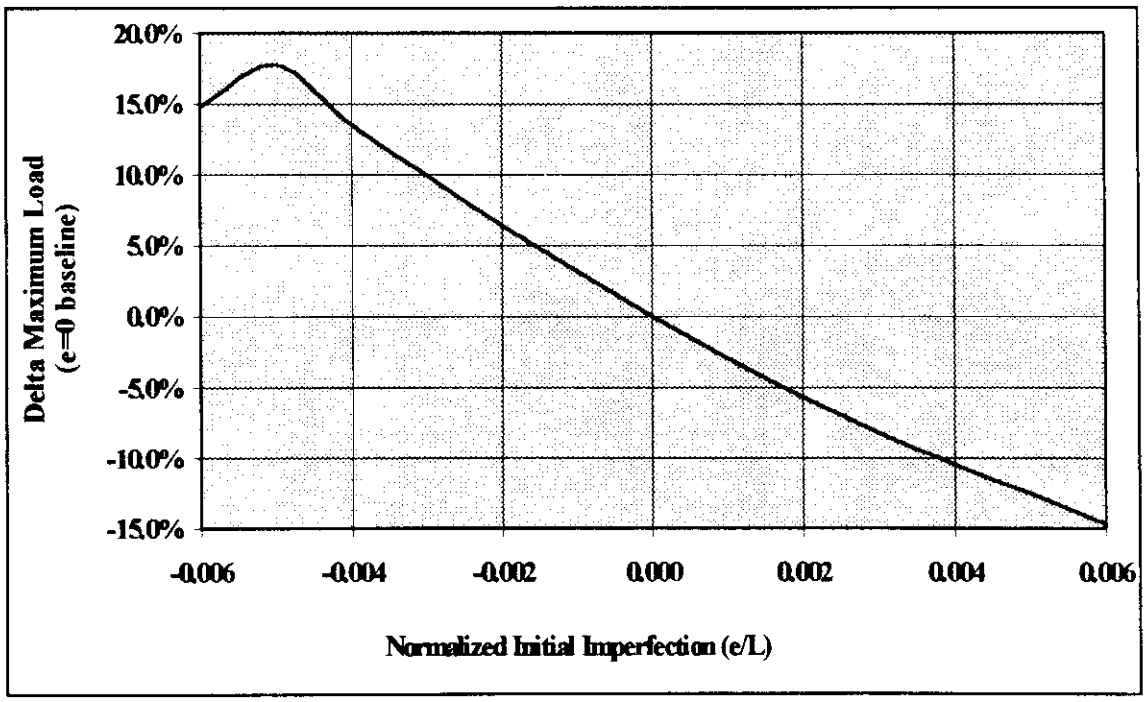

Figure 7.2-4: Platform A - Delta Maximum Load vs. Normalized Initial Imperfection

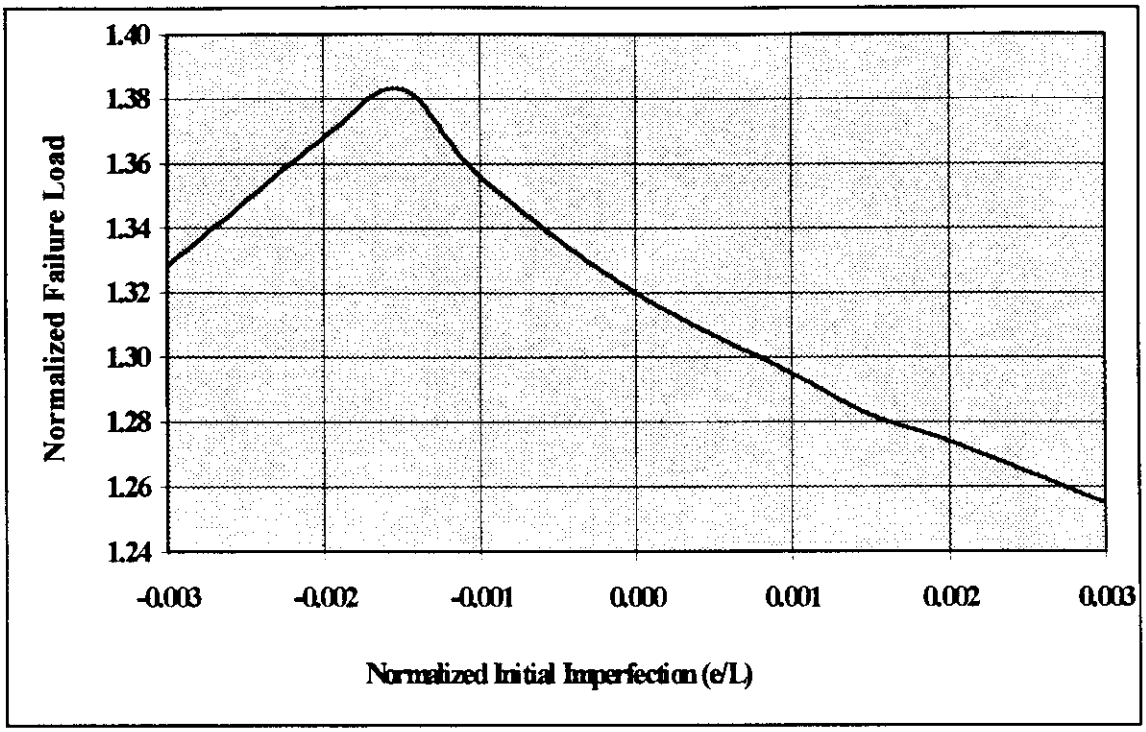

Figure 7.2-5: Platform B - Normalized Failure Load vs. Initial Imperfection

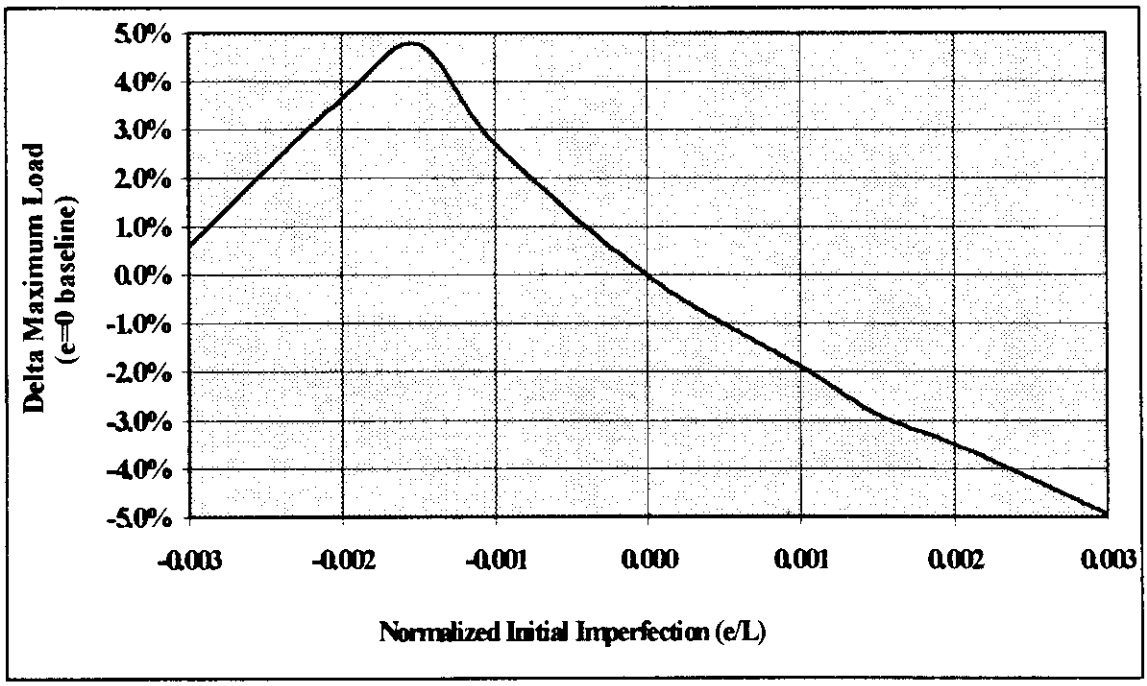

Figure 7.2-6: Platform B - Delta Maximum Load vs. Normalized Initial Imperfection

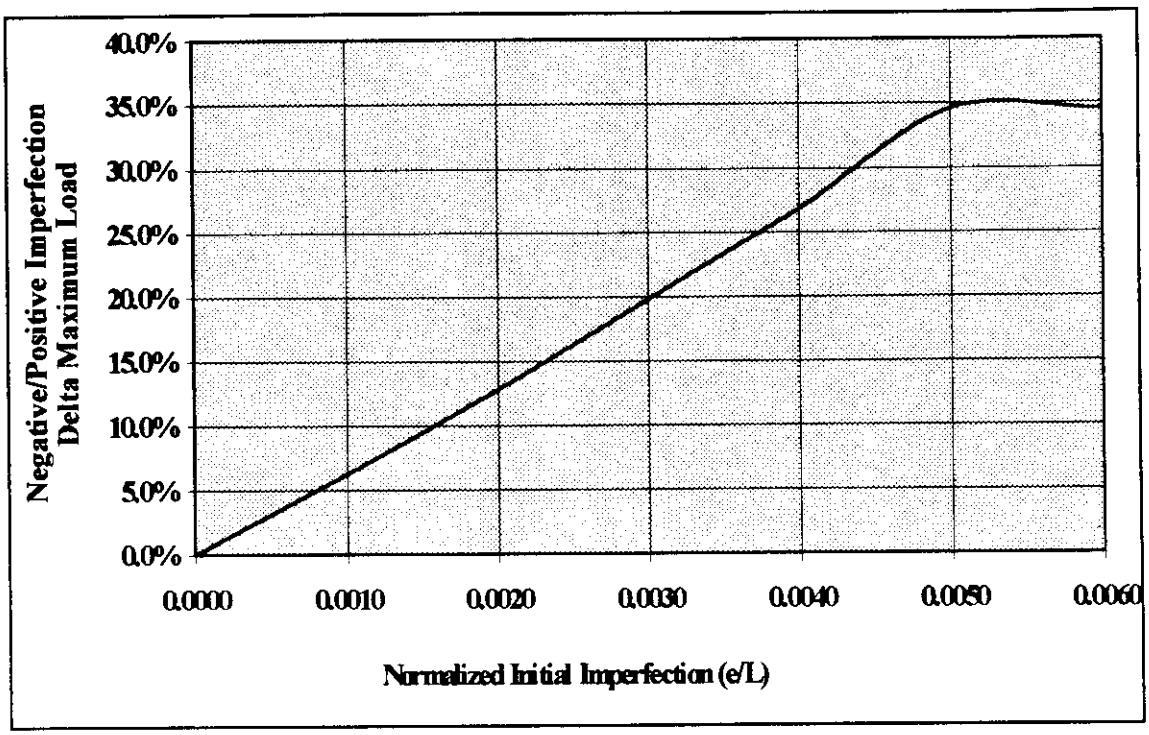

Figure 7.2-7: Platform A - Delta Neg./Pos. Maximum Load vs. Normalized Initial Imperfection

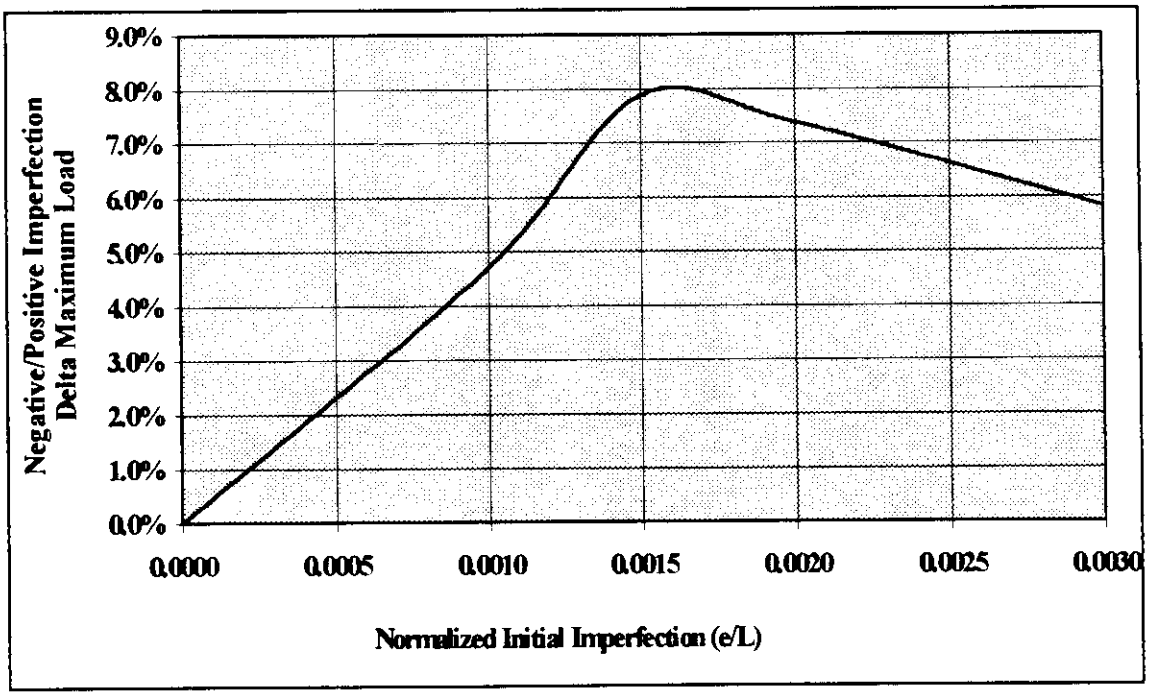

Figure 7.2-8: Platform B - Delta Neg./Pos. Maximum Load vs. Normalized Initial Imperfection

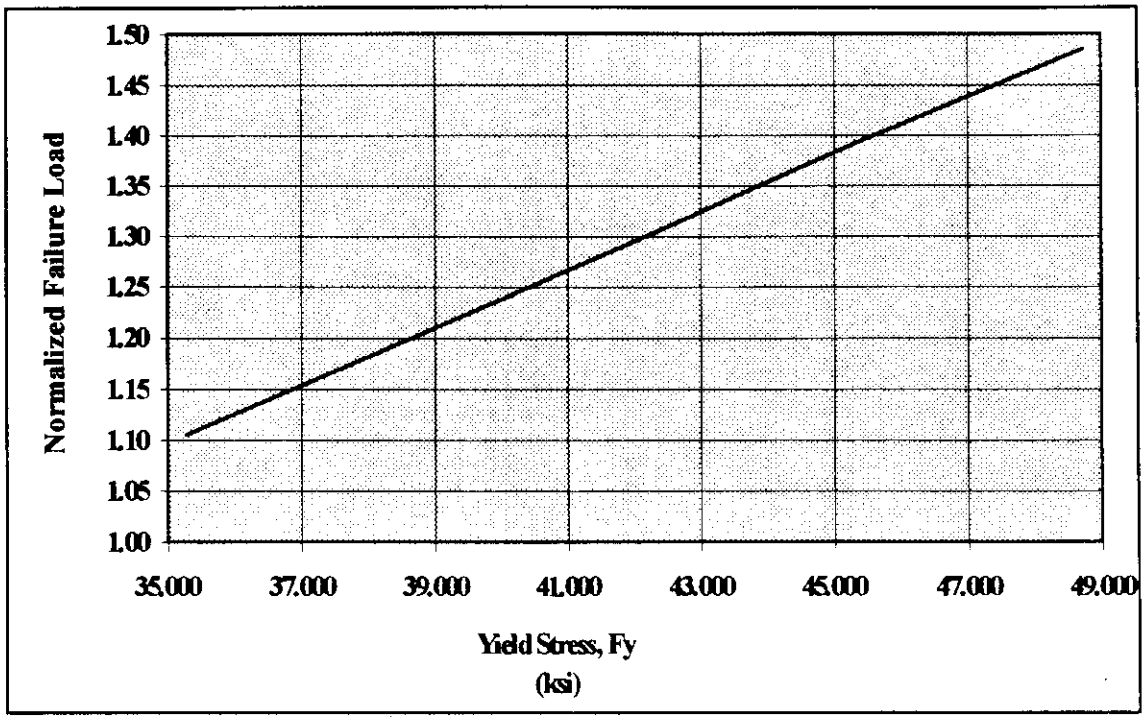

Figure 7.2-9: Platform B - Normalized Failure Load vs. Yield Stress

7.3 Soil Strength and Soil Spring Modeling

One of the most difficult aspects of performing a complete non-linear analysis can be correct modeling of the foundation or platform substructure. More than most other engineering disciplines, geotechnical engineering is an art as much as it is a science. Even under extremely controlled laboratory conditions the coefficient of variation for certain soils properties can reach as high as 100 percent (Bea, 1993). Some sources of uncertainty for foundation modeling are:

- Sampling (pushed vs. driven)
- Testing procedure (mini-vane, triaxial, etc.)
- Analysis (T-Z and P-Y)
- Loading effects (strain-hardening, cyclic degradation)
- Results interpretation

Moreover, correctly determining soil strengths presents only part of the problem. Once soil parameters such as undrained shear strength and effective unit weight are determined or simply chosen, one must correctly use these values to create non-linear soil springs for use in later analyses.

Many engineers face the challenge of creating a non-linear substructure model with little or no soil data. In addition, many times when soil data is available it is old data collected by different methods than employed today, with questionable reliability. Thus, engineers must choose between the high cost of current data collection or the increased uncertainty of using averaged or previously published soil data and conservative code design guidelines. Unfortunately, for most construction projects, immediate costs tend to drive the decision making process, and the future costs caused by inadequate or incorrect data

are not adequately considered. Hence, engineers frequently use the standard code approach (API, 1993) to soil spring development without adequate thought as to its assumptions, applicability and limitations. Standard code approaches to complex problems are to be commended and utilized when appropriate. However, any single approach can not be the best solution to every problem. Thus, code approaches may be a good solution to a wide variety of problems. Yet, to cover as many bases as possible, such solutions usually contain a high degree of conservatism. The remainder of this section discusses three analysis areas that can lead to over-conservative foundation design or modification if not properly considered.

Code Bias

Based on test results (Bea, 1993 and Quiros et al., (1983), the current code approach (API, 1993) to non-linear soil spring development is overly conservative for many situations. Figure 7.1-1 (Bea, 1993) shows test data for an axially loaded pile in cohesionless soil that indicates a code bias approximately equal to two (code underpredicts empirical tests). Table 7.3-1 shows approximate ranges of code bias for axial and lateral loading of cylindrical steel piles in cohesive and cohesionless soils (Bea, 1993).

Soil Sampling Methods

Another source of conservative bias in soil spring modeling comes from the method of data collection and the interpretation of that data. Specifically, for Gulf of Mexico clays,

the values of shear strength vary significantly depending on how the soil core sample was retrieved and how the core was tested. According to Quiros et al. (1983), the common practice of soil collection using a thin-wall tube with a wire-line activated hammer significantly remolds the soil sample, which leads to underestimation of the soil shear strength. Using the same testing procedures, Quiros et al. noted that pushed samples had consistently higher shear strengths than those obtained using a driven tube. Table 7.3-2 presents the ratio of pushed to driven shear strength as measured by unconfined compression (UC) tests, miniature vane test (MV) and undrained unconsolidated (UU) triaxial tests for three sites in the Gulf of Mexico. Insitu field vane tests showed very good agreement with both the MV and UU tests data from the pushed samples; providing further evidence of a data gathering bias.

Foundation Loading Rates

Soil, like other engineering materials, has different strength and stiffness properties depending on the rate and pattern of loading. According to Bea (1984) the dynamic response of the substructure primarily depends on the loading characteristics; specifically, in order of importance:

- Ratio of duration of the dynamic force pulse to the natural period of the system
- Degree of periodicity or randomness of the dynamic force
- Details of the dynamic force (rise times, shapes of pulses)
- Energy dissipated by the system
- Non-linearity developed in the system (effectively increasing response periods and energy dissipation).

This time dependency characteristic is commonly referred to as strain rate effects. Of concern to this discussion is the concept of strain hardening or the ability of a soil to exhibit much higher strengths for brief periods of time (dynamic) than if slowly or statically loaded. Strain hardening is a valuable soil parameter that can increase the capacity of a platform's substructure if properly utilized. Figure 7.3-2 shows the difference in axial pile capacity for both dynamic and static loading (Bea, 1984). This test data indicates a capacity increase of a factor of two for dynamic loading. A similar value can be derived from figure 7.3-3 where the strain rate effects of various materials are plotted (Bea, 1984). From figure 7.3-3 it can be seen that clays, shales and frozen soils all increase in strength from 10 to 50 percent per log cycle change in time of loading to failure. These results can be mathematically described as

$$\beta_R = 1 + F \log \frac{t_r}{t_s} = \frac{R_{md}}{R_{ms}} \tag{7.1}$$

where t_r is the dynamic loading rate, t_s is the static or reference loading rate and F is a material rate factor. Figures 7.3-4 and 7.3-5 respectively show the range of dynamic strength increase for piles in cohesive soils loaded axially and laterally (Bea, 1980 and Bea, 1984).

Moreover, when considering strain hardening effects, it is important to note that peak or maximum loads are of primary concern. It is assumed that during the loading period that there will be only a few load cycles near or at the peak loading. Based on wavestaff and hindcast data, this is a reasonable assumption for most types of ocean storms. Figure 7.3-

6 shows the number of cycles in a typical storm that produce a set level of loading magnitude.

Finally, it should be noted that there are many factors that effect the interpretation of shear strength values. Young et al. (1983) described how soils samples could be disturbed by boat motion, drill pipe movement, drilling operations, sampling technique, sample stress relief, sample extrusion, packaging, transportation procedures, etc. In addition, there are many areas of over-conservatism in foundation design and assessment. Thus, as was previously mentioned, having good data and knowledgeable interpretation experience can significantly reduce the cost of foundation design or assessment recommendations. Considering the large variation associated with soil strength data and the findings presented above, it appears that money spent on high quality geotechnical investigation and the willingness to take educated risks can produce significant financial savings over the life of a platform.

Analysis Results

PB was shown to experience pile pullout if the foundation was modeled with static soil springs. PB was reanalyzed with dynamic soil springs equal to 1.41 times the static strength. Figure 7.3-7 shows the comparison between static and dynamic spring pushover results. Figure 7.3-7 indicates a relatively linear relationship between soil spring strength and overall foundation capacity. Specifically, by increasing the soil spring strength by 1.41, the pile pullout capacity increased by a factor of 1.55.

From section 6.2, it was shown that PB's superstructure reached its maximum capacity at a load factor of 1.3. Thus, by increasing the soil spring strength by approximately 1.3/0.68 or 1.91 the failure mode should move from the foundation to the superstructure. As previously discussed, the combined soil strength increases from rate effects, code biases and sampling methods can be as high as three. Therefore, it is reasonable to assume that PB would experience failure in the superstructure and not in the foundation as the initial analysis results suggest.

Table 7.3-1: Code Bias for Cylindrical Piles (Bea, 1993)

Loading	Cohesive Soil	Cohesionless Soil
Axial	1.5 - 3.0	0.8 - 0.9
Lateral	1.1 - 1.2	0.8 - 0.9

Table 7.3-2: Pushed/Driven Shear Strength Ratios (Quiros et al., 1983)

Test Type	Site 1	Site 2	Site 3	Average
UC	3.3	1.7	2.1	2.4
MV	1.4	1.5	2.0	1.6
UU	1.3	1.3	1.3	1.3
Average	2.0	1.5	1.8	1.8

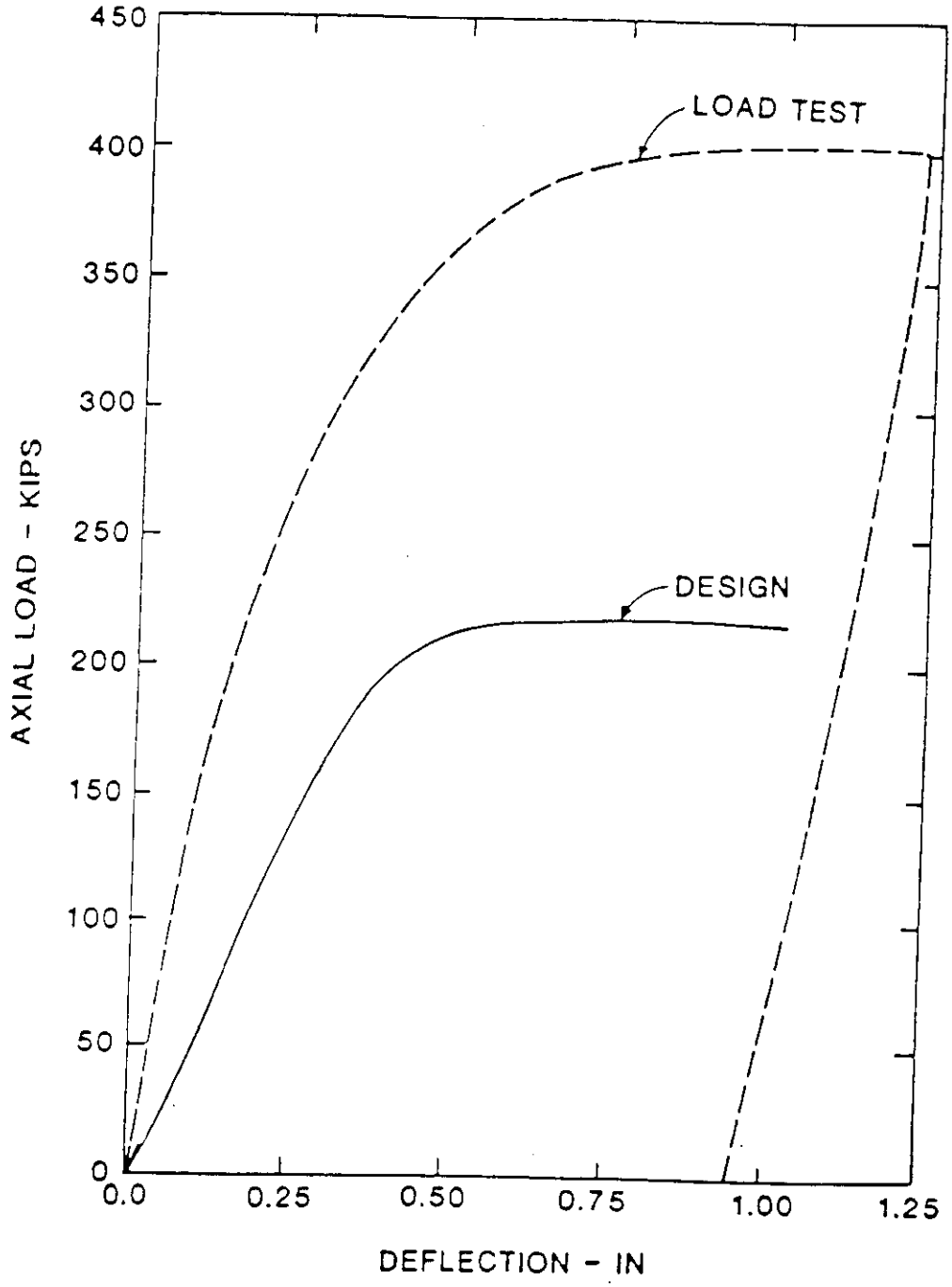

Figure 7.3-1: Comparison of Design and Test Results for an Axially Loaded Driven Pile (Bea, 1993)

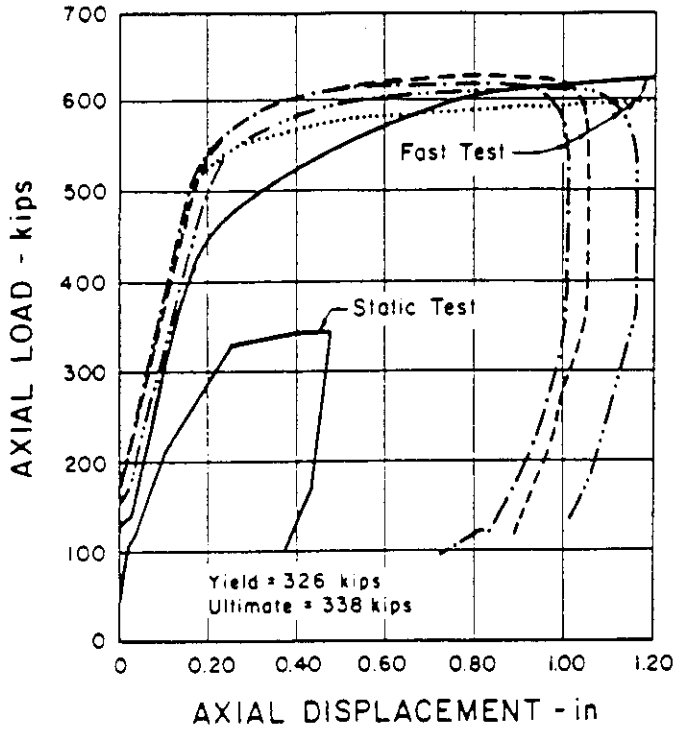

Figure 7.3-2: Static vs. Dynamic Axial Pile Capacity (Bea, 1984)

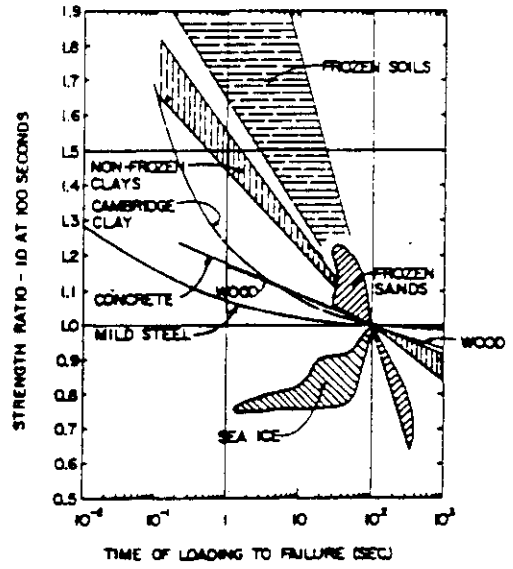

Figure 7.3-3: Strain Rate Effects on Soils and Other Materials (Bea, 1984)

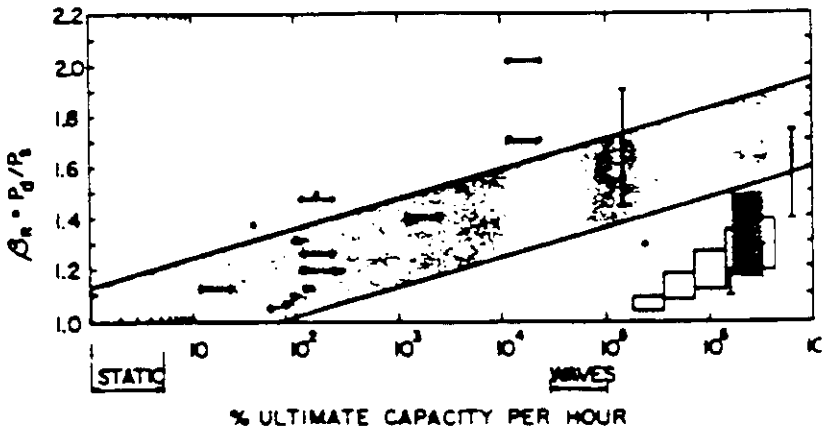

Figure 7.3-4: Rate of Loading Effect on Axial Pile Capacity (Bea, 1984)

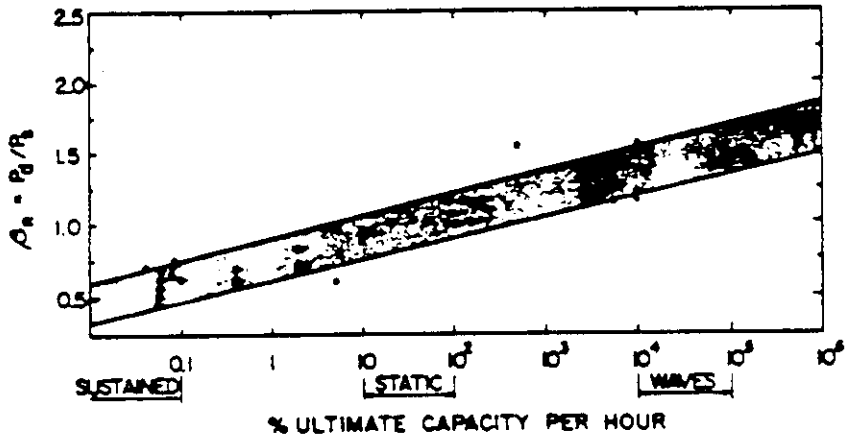

Figure 7.3-5: Rate of Loading Effect on Lateral Pile Capacity (Bea, 1984)

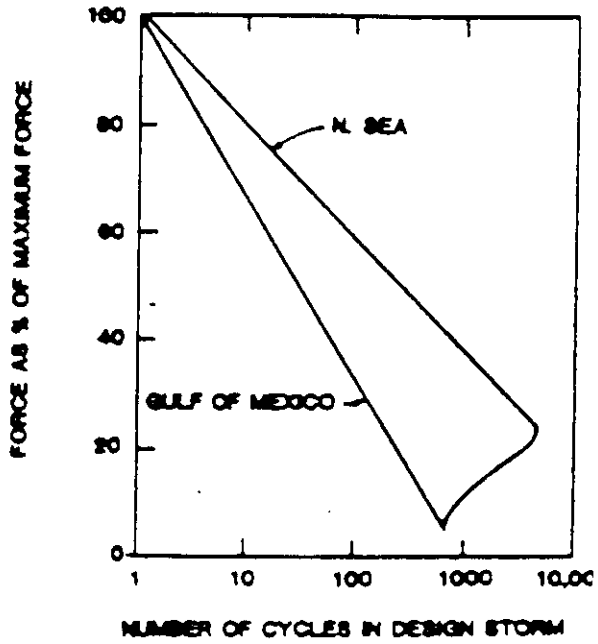

Figure 7.3-6: Cycles of Wave Forces Exerted on Foundations (Bea, 1980)

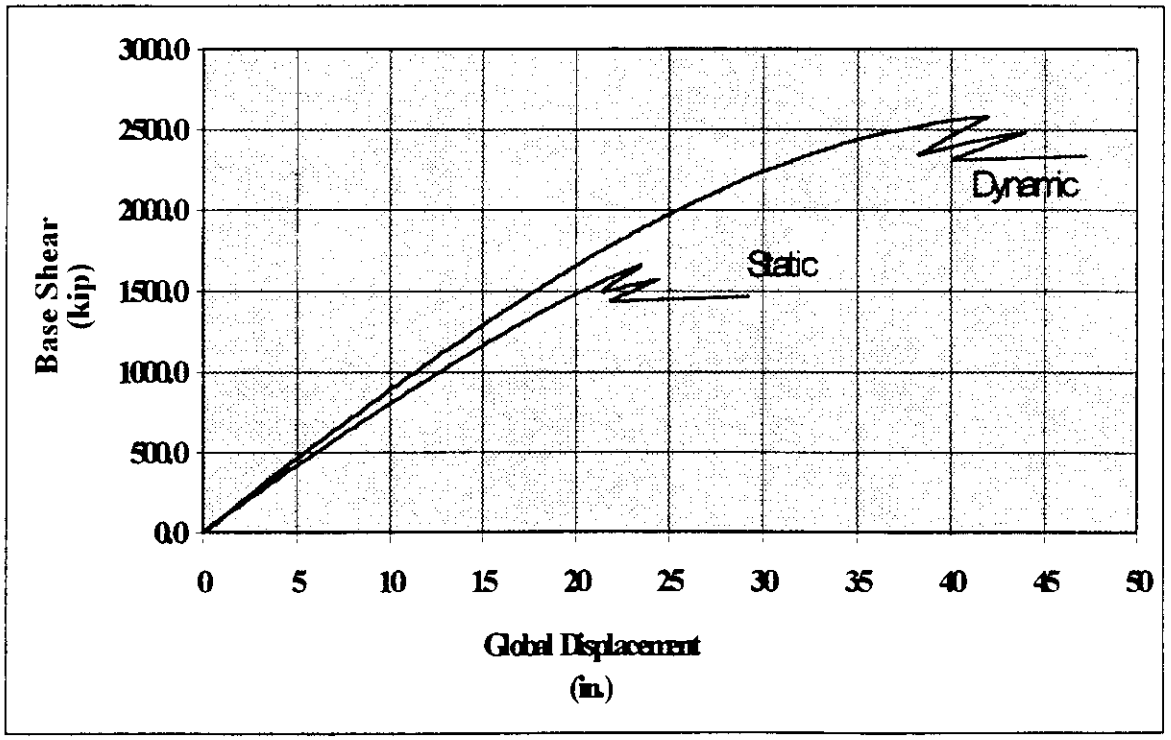

Figure 7.3-7: Static and Dynamic Force-Displacement Histories

8.0 CONCLUSIONS AND RECOMMENDATIONS

8.1 Summary

This report addressed the static pushover analyses of four offshore platforms located in the Gulf of Mexico. All four platforms are steel template type platforms with piled foundations. The results of two platform analyses were compared to actual platform performance during Hurricane Andrew to further evaluate the validity of ULS analyses in predicting platform survival during severe storm conditions. One of these two platforms survived Hurricane Andrew with only minor damage, while the other platform experienced global failure. In addition, one platform was analyzed as part of a JIP lead by PMB Incorporated to determine the variation in results of ULS analyses (PMB, 1994).

Detailed platform information was supplied by the respective platform owners, without whose support this research would not have been possible. The results of the platform analyses are also being used to verify the results of a simplified screening procedure currently being developed at U. C. Berkeley (Bea and Mortazavi, 1995).

The platforms were modeled using DNV's PREFRAME program (DNV, 1994a). The jacket and conductor wave loads were generated using another DNV SESAM program, specifically WAJAC (DNV, 1994b). Deck loads were calculated by hand using the method outlined by API RP 2A Section 17 (API, 1994). The static pushover analyses were performed using a state-of-the-art non-linear analyses program, SINTEF's USFOS

(SINTEF, 1988). Both the loading and analysis programs were run using a IBM RISC 6000 computer, which uses AIX, IBM's version of UNIX, as its operating system.

8.2 Conclusions and Recommendations

As stated in section 2, the purpose of this research was three-fold. First, the validity of ULS results was verified by comparison to actual platform performance during Hurricane Andrew and Hurricane Hilda. Second, the sensitivity of the results to loading, structure and foundation parameters was investigated and discussed. Finally, the methods and procedures used in ULS analyses were assessed, with particular attention being paid to potential pitfalls and oversights. This last topic is discussed in Appendix A.

Platform C and Platform D experienced nearly identical storm conditions during Hurricane Andrew. Platform C collapsed during the storm, while Platform D suffered minor damage. The two platforms are almost identical; yet, they do have some notable differences that could explain their different responses. Platform D is battered in both directions while Platform C is only battered in the end-on framing. Also, the lower braces of Platform D are larger than those of Platform C in both framing directions.

As was shown in section 6.4, for the same wave, Platform C has a slightly greater chance of survival than Platform D. Specifically, Platform C was shown capable of resisting 11 percent more of its base load pattern than Platform D for a 56 ft wave. However, Platform D was shown capable of resisting 41 percent more of its base load than Platform

C for a 60 ft wave in the end-on direction. Thus, if the Hurricane Andrew hit both platforms at a diagonal or end-on direction, the analysis results presented here would agree with the actual platform experience. Hence, Platform C and Platform D verify the accuracy of the USFOS analyses.

Section 7.0 showed that the results of the non-linear analyses are more sensitive to certain input parameters than others. Specifically, section 7.1 showed that for the platforms analyzed, the addition of vertical wave forces in the deck did not significantly change the ultimate lateral load resisting capacity. The additional vertical loads could provide for greater force redistribution of the lateral loads. However, with the limited dataset presented here it is not recommended to make any general conclusions concerning a particular platform.

Section 7.2 showed that the interaction of the initial imperfection and the local hydrodynamic member loads can significantly affect the lateral load capacity. A change in capacity as great as 35 percent could result by changing the direction of the initial imperfection. This effect is significant and should always be carefully considered whenever local hydrodynamic forces can work against those of the initial imperfection. It is recommended that the manufacturer of non-linear software include an option to directly set the degree of interaction between these two forces. In that manner, the user would not be forced to compute three dimensional coordinates to ensure the maximum or minimum interaction.

Section 7.3 discussed the large conservatism that exists for current soil spring modeling procedures as outlined in API RP 2A. While not every foundation can take advantage of all the potential strength increases, it is clear that many substructure systems have much more capacity than current code would predict. This result has been verified by post-storm investigations (Vannan et al., 1994). Hence, current code guidelines for soil spring development do not match well with actual platform performance. Thus, it is recommended that code provision for soil spring modeling be updated to include the potential strength increases that have been widely published and adequately verified. This change would produce significant cost savings for owners and operators of offshore platforms without unduly increasing the risk of failure.

Finally, it should be noted that there are many important and related issues that are not addressed in this report. Of most significance to the authors are the areas of dynamics and material behavior. All analyses performed for this research were static pushover analyses, which did not consider tensile fracture or crack rupture when determining the ultimate platform capacity. Linear and non-linear dynamic loading and capacity effects are clearly presented by Young and Bea (1993). It is the authors' opinion that the results from a static pushover analysis should, as a minimum, be scrutinized in light of these known dynamic effects. In addition, it is recommended that stochastic analyses be performed when warranted to determine the potential effects of material imperfections.

REFERENCES

American Petroleum Institute, Recommended Practice for Planning, Designing and Constructing Fixed Offshore Platforms - Working Stress Design, API RP 2A, Twentieth Edition, API, July 1, 1993.

American Petroleum Institute, "API RP 2A-WSD, Section 17, Assessment of Existing Platforms," API, April 1, 1994.

Astaneh, H. "Design of Steel and Composite Structures," Class notes for CE 247N, University of California, Berkeley, 1994

Bando, Bea, McDonald and Sobey, "Near Surface Wave Forces on Horizontal Members and Decks of Offshore Platforms," 1990

Bea, Pawsey, Litton and PMB Systems Engineering Inc., "Measured and Predicted Wave Forces on Offshore Platforms," Proceedings of the Offshore Technology Conference, OTC 5787, Houston, Texas, May 1988.

Bea and Young, "Loading and Capacity Effects on Platform Performance in Extreme Storm Waves and Earthquakes," Proceedings of the Offshore Technology Conference, OTC 7140, Houston, Texas, May 1993.

Bea and Mortazavi, "Simplified Evaluation of the Capacities of Template-Type Offshore Platforms," 1995.

Bea, R. G., "Dynamic Response of Pile Foundations: Analytical Aspects," 1980.

Bea, R. G., "Dynamic Response of Marine Foundations," 1984.

Bea, R. G., "Reliability Based Criteria for Design and Maintenance of Marine Structures," Class notes for CE 290A, University of California, Berkeley, 1993

Bea, R. G., "Wind and Wave Forces on Marine Structures," Class notes for CE 205B, University of California, Berkeley, 1994

Boresi, Schmidt and Sidebottom' "Advanced Mechanics of Materials," John Weiley and Sons, Fifth edition, 1993

Botelho, Petrauskas, Mitchell and Kan, "A Detailed Study on the Failure Probability of ST130 'A' Platform During the Passage of Hurricane Andrew'" OTC 7472, 1993a.

Botelho, Ullmann, Chancellor and Versowky, "A Survey of the Structural Damage Caused by Hurricane Andrew on Some of the Platforms Located in the South Timbalier Area," OTC 7470, 1993b.

Broughton and Horn, "Ekofisk Platform 2/4C: Re-Analysis Due to Subsidence," 1987.

Campbell III, H. H., "Northridge Fracture: Are We Learning the Right Lessons," ASCE Civil Engineering, March 1995.

Clough and Penzien, Dynamic of Structures, Second Edition, McGraw Hill, 1993.

Davies, R. L., "Wave-Impact Loads on Large-Diameter Horizontal Cylinder Placed Above Still Water Level," OTC 6408, 1990.

Det Norke Veritas, PREFRAME Users Manual, 1994a.

Det Norke Veritas, WAJAC Users Manual, 1994b.

Faltinsen, Kjaerland, Nøttveit and Vinje, "Water Impact Loads and Dynamic Response of Horizontal Circular Cylinders in Offshore Structures," OTC 2741, 1977.

Hellan, Moan and Drange, "Use of Non-Linear Pushover Analyses in Ultimate Limit State Design and Integrity Assessment of Jacket Structures," 1994.

Imm, O'Connor, Light and Stahl, "South Timbalier 161A: A Successful Application of Platform Requalification Technology," 1994.

Kjeldsen and Myrhaug, "Breaking Waves in Deep Water and Resulting Wave Forces," OTC 3646, 1979.

McDonald, Bando, Bea and Sobey, "Near Surface Wave Forces on Horizontal Members and Decks of Offshore Platforms," Coastal and Hydraulic Engineering Department of Civil Engineering, University of California, Berkeley, December 1990.

Mes, M. J., "Wave Crest Forces on Offshore Platforms Using Irregular Wave Theory," OTC 6410, 1990.

Mosaddad and Powell, "Computational Models for Cyclic Plasticity, Rate Dependence and Creep in Finite Element Analysis," UCB/EERC Report, 1982

Oceanweather Inc., "Hindcast Study of Hurricane Andrew (1992) Offshore Gulf of Mexico," November 10, 1992.

Peterson and Rosenberg, "Offshore Platform Steel Specification, " May 1994.

PMB, "AIM III Final Report," September 1988.

PMB Engineering Inc., "Hurricane Andrew - Effects On Offshore Platforms," Joint Industry Project, October 1993.

PMB Engineering Inc., "Draft Final Report - Trail Application of the API RP 2A-WSD Draft Section 17," October 1994.

Quiros, Young, Pelletier and Chan, "Shear Strength Interpretation for Gulf of Mexico Clays," 1983.

Sarpkaya and Isaacson, Mechanics of Wave Forces on Offshore Structures, Von Nostrand Reinhold Company, 1981.

Sarpkaya, T., "Wave Impact Loads on Cylinders," OTC 3065, 1978.

SINTEF, "USFOS - A Computer Program for Progressive Collapse Analysis of Steel Offshore Structures, Tutorial/Course Manual," 1994

SINTEF, USFOS - A Computer Program for Progressive Collapse Analysis of Steel Offshore Structures, Users Manual, 1988a

SINTEF, USFOS - A Computer Program for Progressive Collapse Analysis of Steel Offshore Structures, Theory Manual, 1988b

Thoft-Christensen and Baker, Structural Reliability Theory and Its Applications, Springer-Verlag, 1982

Vannan, Thompson, Griffin and Gelpi, "An Automated Procedure for Platform Strength Assessment," 1994.

White and Hajjar, "Application of Second-Order Elastic Analysis in LRFD: Research to Practice," 1991

Young, C.N., "Loading and Capacity Effects on Platform Performance in Extreme Storm Waves and Earthquakes," Master of Science thesis, University of California, Berkeley, June 1993.

Young, Quiros and Ehlers, "Effects of Offshore Sampling and Testing on Undrained Soil Shear Strength," 1983.

Zarghamee and Ojdrovic, "Northridge Postscript: Lessons on Steel Connections," ASCE Civil Engineering, April, 1995.

APPENDIX A

COMMON ERRORS AND PITFALLS OF

ULTIMATE LIMIT STATE ANALYSES

Performing a Level 4 non-linear pushover analyses of an offshore platform is a large, highly complex process, which is prone to both computer and human error. Such analyses require powerful, sophisticated software and hardware. This process also requires a high degree of human interface, intellect, experience and judgment. Thus, the potential for human error is present before, during and after the actual structural analysis. A partial list of non-linear analysis activities prone to potential human error are listed below.

- Development of non-linear solution scheme
- Development of software
- Development and fabrication of hardware
- Peer review and Beta testing
- Software and hardware installation
- Development documentation of original platform information
- File and information transfer
- Reading and interpretation of original platform information
- Computer/user interface (mouse, keyboard, tape, diskettes)
- Creation of non-linear model
- Development and application of loading condition
- Analysis of platform (initial conditions, analysis parameters, script development)
- Interpretation and verification of results
- Documentation and presentation of results

As can be seen by the size of the above list, human error plays a major role in the success or non-success of a Level 4 non-linear analysis.

The authors caution those who may naively think that they or their associates would never make such errors or could easily recognize and correct them. While admitting error, the authors are not conceding lack of skill or experience in the field of computer modeling and structural analysis. In fact, some errors made during the course of this research were only discovered through the wisdom and experience of multiple researchers and software technicians. Additionally, a recent PMB JIP demonstrated the wide variance of results developed by the leading oil company and offshore consultants when asked to analyze a benchmark platform (PMB, 1994). The PMB and other benchmark studies, as well as the information presented here, should be a wake up call to those who overlook or underestimate the effects of human error.

The purpose of this section is to aid others in avoiding potential pitfalls and to shed light on portions of the tools, i.e., software and hardware, and processes used that could be improved. The purpose of this section is not to discredit or in any way unjustly criticize these tools or their creators. Therefore, the authors hope that all documentation of known or perceived errors in such tools will be viewed with the proper perspective and not be perceived as a negative judgment of their usefulness or applicability. On the contrary, the authors would like to compliment the creators of all the software used for during this research and thank the technical support staff of both SINTEF and DNV for their informative and timely responses when problems and questions arose.

During the course of this research the authors made several errors in analysis and documentation. Some of these errors were self-resolved, some of the errors were found through peer review, and unfortunately it is reasonable to assume that some errors still exist in the final documentation. These errors were not directly beneficial to this research, i.e., they resulted in extended deadlines and increased costs. However, recognition and documentation of these errors is beneficial to the authors and all others who perform research and/or design with similar tools and processes. For only by recognizing and learning from past mistakes can one reasonably expect to mitigate and/or take necessary account of potential future problems. Thus, for the benefit of others in the field of non-linear analysis, the remainder of this section documents the known errors made during this research, and when able, recommends ways the errors could have been avoided.

Case Sensitivity and Input Format

As stated earlier, the analyses for this research were completed using an IBM RISC 6000 AIX system. The three primary pieces of software used were PREFRAME, WAJAC and USFOS. AIX is IBM's version of the UNIX operating systems. Unlike DOS or Microsoft Windows, AIX is case-sensitive. Thus, all operating commands, directory names and file names are case-sensitive.

The requirement for case-sensitivity in the operating system did not actually cause analysis errors. The incorrectly "cased" commands were simply not recognized. In similar fashion, incorrectly cased directory and file names were not recognized. However, the

analyses both required and generated a substantial number of files which had mixed cases. In addition, performing an analysis is an iterative process. Hence, an analysis usually had to be run several times before all the errors could be determined and corrected. Normally, the same output file was specified in order to overwrite the previous analysis output. But if the file name specified was not the exact case of the existing name, then a new file was created, causing later confusion as to which of the two files was the "correct" file. Again, this error was more of a nuisance than a major stumbling block. However, with the amount of files generated, during four to five different analyses for each of the four platforms, the amount of time lost due to backtracking and re-work was noteworthy.

Of the three programs listed above, PREFRAME and WAJAC required the use of FORTRAN input format, i.e., data must be spaced according to a preset interval. This structured input format was the cause of tremendous re-work and trouble shooting. Although the correct spacing for each command line is listed in the documentation, the editor used for file generation did not have column number demarcations. More importantly, certain spacing errors did not cause the software to issue an error message or stop the analysis. Instead, the analysis continued but produced incorrect results, which could only be discovered through a detailed review of the results. Statics, freebody diagrams and visual examination using USFOS's graphical post-processor are just some of the checks used to discover these errors. Once the error was discovered, it took an additional step to discover the source of the error. Such formal and restrictive input formats are unnecessary and can easily be the source of error. Thus, it is recommended

that both PREFRAME and WAJAC change to a free input format to eliminate potential input errors and reduce costly file generation time.

It is important to note that use of ULSLEA led to the discovery of many errors that went undetected by other verification methods. The success which ULSLEA had in discovering analysis errors helped highlight the benefit of using ULSLEA as a sanity check for Level 4 analyses, which was not its original intended purpose.

Inter-Programs Interaction

Using multiple pieces of software led to confusion at times which in turn led to analysis errors. Specifically, the number of input and output files for the different pieces of software required significant effort to organize, edit and maintain. Most design or assessment efforts include several analyses, e.g., broadside and end-on. Hence, a number of files must be used for several different analyses and one must be careful that each analysis is using the appropriate version of the input files.

PREFRAME required one input file and produced approximately five output files. One of these files was the "model" or .fem file which contained each platform's configuration, member and material information. The model file must then be used as the input file for the bandwidth reduction program. The output of bandwidth reduction program then had to be renamed and used as one of two required input files for WAJAC.

The other WAJAC input file contained all the pertinent storm and hydrodynamic information, e.g., unit definitions, water depth, wave description, flood and buoyancy information, drag and inertia coefficients, current details, etc. WAJAC output included three files. One output file could be used for verifying wave kinematics and member loads, while the other two files were used as the analysis "load" files. Deck loads and boatlanding loads were calculated by hand and were applied as joint loads in the "model" file.

A third file, the analysis "control" file, contains all the analysis control information, e.g., initial imperfections, slaving information, maximum load and deflection steps, non-linear soil spring definitions, etc. The "model", "load" and "control" files are used as the input for the non-linear pushover analysis. USFOS produces a number of analysis output files; some of these files can be read, while others files are used to generate reports or graphical post-processing.

Internal Node and Member Numbers

Before a computer model is generated, a user typically creates a description of the model by hand. This description usually contains elevation and plan sections as well as node and member numbers. These numbers can be referred to as external node and member numbers. However, in order to reduce the effective bandwidth and perform the analyses more efficiently, a new model is generated by the computer software that renumbers the

nodes and members. These new numbers may be referred to as internal numbers. This renumbering usually occurs during the bandwidth reduction of the model.

Certain command lines in "model" and "control" file used the internal member numbers, e.g., boundary conditions and joint loads. For large models, the use of internal member numbers is extremely confusing even when the user has a conversion table of external to internal reference list. One must always refer to an outside reference when verifying or modifying these command lines. For large models which can have hundreds or even thousands of node and member numbers, developing a numbering system that has meaning or significance to the user takes considerable effort. To force the user to use a completely different set of node and members numbers is an unnecessary burden. It is recommended that all programs use only the external, user defined numbering system whenever user interface is required. Any conversion to internal numbers should be done, as the name implies, internally by the computer.

Memory Limitations

USFOS is an extremely powerful program that allows the user to obtain a record of almost every conceivable bit of information about the analysis. Due to this high level of power in the software, the input and output files tend to be quite large. USFOS produced the largest output files with the largest being approximately 500 to 600 megabytes for each analysis. Considering all of the other files that were required and generated, it is estimated that a typical analysis required as much as 700 megabytes of hard-disk storage

space. Thus, with a seemingly endless supply of memory, 3 gigabytes, the RISC 600 used to run the analysis could simultaneously store the results of two to three analyses. This hard-disk memory limitation caused careful use of hard-disk space more than actual error. However, there were analyses that were halted by the computer because of insufficient storage space.

The authors discovered another type of memory limitation that had a larger impact on the analyses. During the USFOS analysis, an internal file is generated. During USFOS's creation, this file received a size limitation. For the size of model considered in this research, the analyses frequently exceed this limitation and the analyses were aborted. After discussions with SINTEF concerning the source of this problem, the authors attempted to reduce the file size by eliminating all "unnecessary" members in the model and simplifying the soil spring definitions. This step was difficult, because though all the models were very large, they only contained the major platform members. Thus, the model did not have many unnecessary members. Yet, these efforts usually did not solve the problem.

Through trial and error, it was discovered that the slaving constraints significantly controlled the size of this internal file. Hence, the slaving constraint had to be removed or redefined in another manner. Again, through trial and error, slaving constraint configurations were found that allowed the analyses to proceed. However, in some cases, a "proper" slaving configuration could not be found and the members of concern had to be

restrained in another manner or removed from the model. Specifically, in two of the four platforms analyzed for this research, the conductors were removed and wave loads were manually applied as nodal loads on the platform. Fortunately, according to SINTEF's technical support, this internal memory limitation has been removed in the recently released version of USFOS.

Insufficient Error Message Translation

All three pieces of software used had error messages. Still, many of these messages did not include an adequate explanation of the problem for the user to find the error in the input data. Both SINTEF and DNV technical support were very responsive in deciphering the source of many error messaged received. Although not every error that occurs is simple to explain, many of them have readily definable sources. Therefore, it is recommended that software documentation include specific error message translation or interpretation whenever possible.

Computer Crashes

The IBM RISC 6000 is an extremely reliable machine and never completely crashed during the course of this research. Some analyses were stopped because the computer "hungup", but no data was lost. The most frequent hang-ups occurred during the graphical post-processing. However, computer crashes are possible, so multiple backups were made of important files, both to diskette and to tape. Some of these backup files were occasionally used due to inadvertent overwriting of files. It is recommended to

backup all important files before and after an analysis. Input files are more important to backup, since they are usually generated by the user and would take the most time and effort to reconstruct.

Script Usage

The software used for this research could be run interactively or in batch mode. Since many analyses were run and correctly performing an analysis was an iterative process, the authors ran the programs in batch mode. This was accomplished by developing executable "scripts" in the IBM AIX language. While running scripts made the analysis process much easier, it also introduced another potential source of error. The script-induced errors usually occurred due to incorrectly specifying the input files to be used by the programs. The script must be changed when any of the associated input file names are changed. However, if one forgets to reflect those name changes in the script and the original input file is not erased, then the script will run properly but use the old data.

One potential remedy for this problem is to erase all unnecessary or old files. Also, a "memory jogger" can be put into the script that will note the filenames currently used in the script. If the file names are correct the user must only hit "enter" to continue the script. However, if the files noted are not those intended, then the user can cancel the script and make the appropriate changes before the analysis continues.

Default Local Axes and Potentially Unconservative Initial Imperfections

USFOS has a feature that automatically defines the local coordinate system of each member if it is not specifically defined in the user input. This is a valuable feature, for having to define each local coordinate system by hand would be extremely prohibitive. However, as discussed in Section 7, WAJAC prescribes the wave loads as distributed member loads and USFOS can give members an initial imperfection. Both the local member loads and the initial imperfection are defined in terms of a member's local coordinate system.

Members have bending moments due to the eccentricity caused by the initial imperfection, the local distributed hydrodynamic loads and the rotation of the member ends. Depending on the local coordinate system, these moments can add together or work against each other. Clearly, the case of additive moments will be the most conservative approach, while having the moments counteract one another will increase the capacity of the member over having any of the moments acting alone. It is easy to forget this dependence on local coordinate systems and assume that the moments are acting in a certain manner. Therefore, one must check to ensure that the moments are acting as intended and make modifications if this is not the case.

Most engineers would make the sometimes conservative but always reasonable assumption that the local load moments and the eccentric moments act together. Therefore, it is recommended that analysis software include an option to make these two

moments additive by default. Another option would be to allow the user to specify the initial imperfection direction in terms of the primary local force direction and, therefore, be able to combine the moments as much or as little as desired with one command.

Hand Calculations of Deck Forces

Deck and boatlanding loads were calculated by hand using Mathcad 5.0 Plus. The load calculation method followed API Section 17 and used the hydrodynamic information supplied by WAJAC. Errors were made both in creating and in using the Mathcad worksheet. The errors made in creating the worksheet were corrected before it was used for load calculation. However, the errors made in using the worksheet were sometimes not discovered until after an analysis was compared with ULSLEA results. Primarily, the errors occurred from inputting incorrect fluid particle velocities at the elevations of interest. Other errors came from not updating the worksheet with new or modified information as different analyses were performed. Again, every additional piece of software used added an additional data transfer step that became a source of human error. To correct this problem, it is recommended that the load generation software include a means of calculating Section 17 deck and boatlanding loads. This would allow all load calculations to be performed in one piece of software and would eliminate the need to change two files every time a load modification is required.

Joint Check Malfunction

During the course of this research, it was discovered that USFOS 6.0 could possibly malfunction when attempting to perform a joint check. In the case of Platform A, USFOS 6.0 loaded the structure in the reverse direction and doubled the target load. It is not clear at the present time whether this error occurred consistently within all analyses with version 6.0 or whether certain model input parameters triggered the error. However, according to SINTEF technical support, this error has been corrected in the recently release USFOS 7.0. Thus, this problem should not occur in future analyses.

Incorrect Member Size or Material Specification

With the large amount of nodes and members that exist in most offshore platform models, it is easy to forget the exact numbering system that is set up for the model. Usually, a model's nodes and members are numbered in a meaningful manner, e.g., first level framing is a 100's series, second level framing is a 200's series, etc. Yet, even with such an organized numbering scheme, one can forget the numerical label of a particular member when referring to it in various input command lines. During the course of this research, the authors made errors in specifying the wrong member size or material for certain members because he incorrectly remembered the numbering system of a particular group of members. Sometimes this error was easily detected during graphical post-processing, e.g., when one brace was double the diameter of all other similar braces. However, incorrect member thickness or material property specification are not detected as easily. This type of error can be the most dangerous, because the analysis will still run without

any error messages. Thus, if the results of the analysis seem reasonable to the user and no results verification is performed, the error may go undetected.

One method to avoid such errors is to develop member information tables before the model is created on the computer. Hence, the user will be inputting data from an organized list and will not have to rely on memory. Also, the user should at least perform a cursory review of the critical members, checking their properties and their force/stress histories. While these methods do not guarantee complete error free input, they can uncover basic input and result inconsistencies.

Incorrect Reading or Interpretation of Drawings

Assessment of existing platforms requires a significant amount of platform information. This information is typically retrieved from structural drawings, which have widely varying degrees of quality and/or readability. Old drawings become faded with time and copies are almost always worse than the originals. Errors can easily occur from assuming platform information when it is unavailable or unreadable. In addition, old drawings may have different notation than is currently used, which can result in incorrect interpretation. Thus, one should exhaust all sources of information when initially gathering data. Also, comparing data from different sources can highlight inconsistent data.

Comparing Results with Existing Data

Sometimes, previous analysis results exist which can be used for comparison. While the availability of such information is always valuable, it can also prove to be detrimental to the user. For by reviewing a previous analysis, one may expect certain results and become biased as to the accuracy of the present analysis results. Hence, it is recommended that all previous analysis results be used as comparison only after the analysis has been completed and checked.

Using Existing Model Files for Similar Platforms

Input files for Level 4 analyses are quite large and take considerable effort to create. Sometimes one can save time by modifying an existing input file for a different platform. Even if the platforms are not very similar, time can be saved by using existing input. However, based on the authors' experience, much more time will probably be lost troubleshooting the new file than could ever be gained through file modification.

This inputting shortcut is extremely prone to errors, especially if the user is the creator of the original file. For, by using an existing file, the user is actually starting out with an error-laden file that must be corrected. Trying to remember which sections of the file need to be changed and which sections have already been changed at any given time taxes the intellect much more logically and incrementally creating a file from scratch. Thus, it is recommended that all input files be created as new files, and that very limited information be copied from existing files.

Inefficient Time Constraints

During the course of this research, the author's time availability varied widely. Sometimes the authors were able to work in consistent, large blocks of time. However, at other times the authors' time was quite segmented. At the end of the research, it was obvious that due to the complexity and size of Level 4 analyses, the authors' efficiency and accuracy were indirectly related to the amount of time segmentation. Each time work was begun, there was some of amount of rework or review. Thus, the process was two steps forward and one step back. Yet, when consistent blocks of time were devoted to the work, not only was the time inefficiency reduced, but the amount of user errors also diminished. Consequently, it is recommended that Level 4 analyses be performed over large blocks of time. This time management rule is especially important until the post-processing stage.

Typographical Errors

Lastly, but most commonly, are the ordinary typographical errors. Typos are easy to make and sometimes hard to find. The accidental substitution of a capital O for a zero, 0, can be especially hard to find. Case sensitive command lines that require capital letters frequently cause this error. While, typos represent the classic example of ordinary human error, the user can take steps to lessen their occurrence. First, learning to type instead of "hen-peck" will reduce the amount of typos significantly. Second, working when fully awake and refreshed instead of tired and fatigued also reduces the amount of typos.

Thirdly, using a good, user-friendly editor will reduce typos and allow for easier correction during file creation.

In summary, Level 4 analyses are large, complex, multi-step procedures that are prone to human and software error. By planning ahead and keeping the above points in mind, a user can significantly reduce the number of errors. All analysis results should be viewed with caution and examined under the light of engineering experience. In addition, analysis results should be verified using simple checking procedures or other proven tools such as ULSLEA.

APPENDIX B

DETAILED INFORMATION FOR PLATFORM ANALYSES

WAVE IN DECK CALCULATION

Owner:

Name:

Approximate location:

UNITS

$kip = 1000 \cdot lbf \quad ksi = \frac{kip}{in^2} \quad g = 32.2 \cdot \frac{ft}{sec^2} \quad \rho = \frac{0.064 \cdot \frac{kip}{ft^3}}{g} \quad i = 1,2..4 \quad k = 1,2..3$

ORIGIN = 1

STORM AND PLATFORM INFORMATION (Wave theory: Stokes 5th)

Mean water depth: $d = 137 \cdot ft$

Storm surge: $s = 3 \cdot ft$

Wave height: $h = 56 \cdot ft$

Wave period: $T = 13 \cdot sec$

Wave kinematics factor for X axis: $\alpha x_{wkf} = 0.88$

Wave kinematics factor for Y axis: $\alpha y_{wkf} = 0.88$

Current blockage factor for X axis: $\alpha x_{cbf} = 0.8$

Current blockage factor for Y axis: $\alpha y_{cbf} = 0.7$

Current velocity, X dir.: $U_x = 46.5 \cdot \frac{in}{sec}$

Current velocity, Y dir.: $U_y = 46.5 \cdot \frac{in}{sec}$

Deck drag coefficients (in increasing order of deck elevation):

**Note: if there are less than four decks, use 0.0 for the remaining decks.

$$C_d = \begin{bmatrix} 1.6 \\ 1.6 \\ 0 \\ 0 \end{bmatrix}$$

cellar

top

Absolute deck elevation:

**Note: if there are less than four decks, use the highest deck elevation for the remaining decks.

$$e = \begin{bmatrix} 2063 \\ 2189 \\ 3000 \\ 3001 \end{bmatrix} \cdot in \qquad \begin{matrix} \text{cellar} \\ \\ \\ \text{top} \end{matrix} \qquad E_k = e_{k+1} - e_k$$

Effective Deck Widths

Perpendicular to Platform X Axis

$$b_x = \begin{bmatrix} 120 \\ 120 \\ 0 \\ 0 \end{bmatrix} \cdot ft$$

Perpendicular to Platform Y Axis

$$b_y = \begin{bmatrix} 40 \\ 40 \\ 0 \\ 0 \end{bmatrix} \cdot ft$$

WAVE KINEMATICS

Use the above information to run DNV's WAJAC program in order to determine the wave crest height for the given ocean conditions. Adjust the platform drag coefficients and the current to account for the wave kinematics factor and the current blockage factor. (Multiply the drag coefficient by the square of the w.k.f and multiply the in-line current velocity by the square of (w.k.f./c.b.f).

Crest height: $e_c = 2098 \cdot in$ $\qquad C_k = e_c - e_k$

Wave particle velocity at deck elevations:

X dir. (w/o current):

$$V_x = \begin{bmatrix} 271 \\ 279 \\ 0.0 \\ 0.0 \end{bmatrix} \cdot \frac{in}{sec}$$

Y dir. (w/o current):

$$V_y = \begin{bmatrix} 271 \\ 279 \\ 0.0 \\ 0.0 \end{bmatrix} \cdot \frac{in}{sec}$$

DECK FORCES

Unit wave force factor: (Note: cbf for first deck was included in area determination)

$$f_{x_i} = 0.5 \cdot \rho \cdot C_{d_i} \cdot \left(\alpha x_{wkf} V_{x_i} + \alpha x_{cbf} U_x \right)^2 \qquad f_{y_i} = 0.5 \cdot \rho \cdot C_{d_i} \cdot \left(\alpha y_{wkf} V_{y_i} + \alpha y_{cbf} U_y \right)^2$$

$$f_x^T = (\,0.84 \quad 0.88 \quad 0.00 \quad 0.00\,)\cdot\frac{kip}{ft^2} \qquad f_y^T = (\,0.81 \quad 0.85 \quad 0.00 \quad 0.00\,)\cdot\frac{kip}{ft^2}$$

$$F_{ax_k} = \text{if}\left[e_c < e_k,\ 0\cdot kip,\ \text{if}\left[e_c < e_{k+1},\ f_{x_k}\cdot b_{x_k}\cdot(C_k)\cdot\left[\frac{\left[(E_k) - \frac{C_k}{2}\right]}{E_k}\right],\ f_{x_k}\cdot b_{x_k}\cdot\frac{E_k}{2}\right]\right]$$

$$F_{ax_4} = \text{if}\left[e_c < e_4,\ 0\cdot kip,\ f_{x_4}\cdot\left[b_{x_4}\cdot(e_c - e_4)\right]\right]$$

$$F_{bx_{k+1}} = \text{if}\left[e_c < e_k,\ 0\cdot kip,\ \text{if}\left[e_c < e_{k+1},\ f_{x_k}\cdot b_{x_k}\cdot C_k\cdot\frac{\frac{C_k}{2}}{E_k},\ f_{x_k}\cdot b_{x_k}\cdot\frac{E_k}{2}\right]\right]$$

$$F_{ay_k} = \text{if}\left[e_c < e_k,\ 0\cdot kip,\ \text{if}\left[e_c < e_{k+1},\ f_{y_k}\cdot b_{y_k}\cdot C_k\cdot\left[\frac{\left(E_k - \frac{C_k}{2}\right)}{E_k}\right],\ f_{y_k}\cdot b_{y_k}\cdot\frac{E_k}{2}\right]\right]$$

$$F_{ay_4} = \text{if}\left[e_c < e_4,\ 0\cdot kip,\ f_{y_4}\cdot\left[b_{y_4}\cdot(e_c - e_4)\right]\right]$$

$$F_{by_{k+1}} = \text{if}\left[e_c < e_k,\ 0\cdot kip,\ \text{if}\left[e_c < e_{k+1},\ f_{y_k}\cdot b_{y_k}\cdot C_k\cdot\left[\frac{\frac{C_k}{2}}{E_k}\right],\ f_{y_k}\cdot b_{y_k}\cdot\frac{E_k}{2}\right]\right]$$

$$F_{x_i} = F_{ax_i} + F_{bx_i} \qquad F_{y_i} = F_{ay_i} + F_{by_i}$$

$$F_x^T = (\,252.9 \quad 40.8 \quad 0.0 \quad 0.0\,)\cdot kip$$

$$F_y^T = (\,81.5 \quad 13.1 \quad 0.0 \quad 0.0\,)\cdot kip$$

Owner:

Name:

Approximate location:

Loading direction: broadside

UNITS

$kip = 1000 \cdot lbf$ $\qquad ksi = \frac{kip}{in^2}$

DETERMINATION OF INITIAL IMPERFECTION FOR CRITICAL MEMBERS

Outer diameter: $d_o = 14.0 \cdot in$

Inner diameter: $d_i = 13.25 \cdot in$

Wall thickness: $t = 0.375 \cdot in$

Length: $L = 489.8 \cdot in$

Effective length factor: $K = 0.7$

Yield stress: $F_y = 58 \cdot ksi$

Young's modulus: $E = 29000 \cdot ksi$

Plastic section modulus:

$$Z = \frac{d_o^3}{6} - \frac{d_i^3}{6} \qquad Z = 69.6 \cdot in^3$$

Area:

$$A = \frac{d_o^2 \cdot \pi}{4} - \frac{d_i^2 \cdot \pi}{4} \qquad A = 16.1 \cdot in^2$$

Radius of gyration:

$$r = \frac{\sqrt{d_o^2 + d_i^2}}{4} \qquad r = 4.82 \cdot in$$

Plastic moment:

$$M_p = Z \cdot F_y \qquad M_p = 4.039 \cdot 10^3 \cdot kip \cdot in$$

Critical moment:

$$M_{cr} = \left[0.919 + \frac{0.393}{100 \cdot \left(\frac{d_o}{t} \right)} - 0.545 \cdot \left(\frac{d_o}{100 \cdot t} \right)^2 \right] \cdot M_p \qquad M_{cr} = 3.405 \cdot 10^3 \cdot kip \cdot in$$

Axial yield force:

$$P_y = A \cdot F_y \qquad P_y = 931 \cdot kip$$

Axial force parameters:

$$\lambda = \frac{1}{\pi} \cdot \sqrt{\frac{F_y}{E}} \cdot \frac{K \cdot L}{r} \qquad \lambda = 1.01$$

$$\psi = 1.00 - 0.091 \cdot \lambda - 0.22 \cdot \lambda^2 \qquad \psi = 0.68$$

Critical axial load:

$$P_{cr} = \psi \cdot P_y \qquad P_{cr} = 635.1 \cdot kip$$

Euhler axial load

$$P_E = \frac{\pi^2 \cdot E \cdot A}{\left(\frac{K \cdot L}{r}\right)^2} \qquad P_E = 907.6 \cdot kip$$

Ultimate load (set equal to critical load):

$$P_U = P_{cr}$$

Initial imperfection for USFOS analysis:

$$\Delta_i = \left[\cos\left[\frac{P_U}{2 \cdot \frac{P_y}{\pi}}\right] \cdot M_{cr}\right] \cdot \frac{1 - \frac{P_U}{P_E}}{P_U} \qquad \Delta_i = 0.771 \cdot in$$

$$\frac{\Delta_i}{L} = 0.0016$$

Depth	0-180 ft.	
Effective Density (k/in3):	2.3E-05	
Pile Diameter (in):	30	
J - Dim.less Const.	0.5	
Pushed/Driven Coefficient:		1.75
Code correction Coefficient:		1.33
Dynamic Effects Coefficient:		1.41

P-Y Spring	X (ft)	X (in)	c (ksi)	X.R (in.)	p.u (ksi)	e.c	y.c (in.)
1	0	0	8.51E-03	309.47	6.29E-02	0.04000	3.00
2	8	96	1.03E-02	317.33	1.11E-01	0.04000	3.00
3	16	192	1.09E-02	319.44	1.54E-01	0.04000	3.00
4	24	288	1.15E-02	321.34	2.01E-01	0.04000	3.00
5	32	384	1.22E-02	323.08	2.16E-01	0.04000	3.00
6	40	480	1.34E-02	326.12	2.45E-01	0.04000	3.00
7	60	720	1.56E-02	330.49	2.86E-01	0.04000	3.00
8	80	960	1.82E-02	334.51	3.39E-01	0.04000	3.00
9	100	1200	2.19E-02	338.51	4.11E-01	0.04000	3.00
10	140	1680	2.67E-02	342.22	5.86E-01	0.04000	3.00
11	180	2160	4.25E-02	348.62	3.60E-01	0.04000	3.00

Depth	0-180 ft.	
Effective Density (k/in3):	2.3E-05	
Pile Diameter (in):	30	
J - Dim.less Const.	0.5	
Pushed/Driven Coefficient:		1.75
Code correction Coefficient:		1.33
Dynamic Effects Coefficient:		1.41

P-Y Spring	X (ft)	X (in)	c (ksi)	X.R (in.)	p.u (ksi)	e.c	y.c (in.)
1	0	0	8.51E-03	309.47	6.29E-02	0.04000	3.00
2	8	96	1.03E-02	317.33	1.11E-01	0.04000	3.00
3	16	192	1.09E-02	319.44	1.54E-01	0.04000	3.00
4	24	288	1.15E-02	321.34	2.01E-01	0.04000	3.00
5	32	384	1.22E-02	323.08	2.16E-01	0.04000	3.00
6	40	480	1.34E-02	326.12	2.45E-01	0.04000	3.00
7	60	720	1.56E-02	330.49	2.86E-01	0.04000	3.00
8	80	960	1.82E-02	334.51	3.39E-01	0.04000	3.00
9	100	1200	2.19E-02	338.51	4.11E-01	0.04000	3.00
10	140	1680	2.67E-02	342.22	5.86E-01	0.04000	3.00
11	180	2160	4.25E-02	348.62	3.60E-01	0.04000	3.00

Spring:	1		
Pile Diam. (in):		30.0	
Eff. pile seg. (ft):		8.0	
p.u (ksi):		6.29E-02	
y.c (in.):		3.00	
p/pu	y/y.c	P kip	y in.
0.000	0.00	0.0	0.0
0.500	1.00	90.5	3.0
0.720	3.00	130.4	9.0
1.000	8.00	181.0	24.0
1.000	9.00	181.0	27.0

Spring:	2		
Pile Diam. (in):		30.0	
Eff. pile seg. (ft):		8.0	
p.u (ksi):		1.11E-01	
y.c (in.):		3.00	
p/pu	y/y.c	P kip	y in.
0.000	0.00	0.0	0.0
0.500	1.00	160.0	3.0
0.720	3.00	230.5	9.0
1.000	8.00	320.1	24.0
1.000	9.00	320.1	27.0

Spring:	3		
Pile Diam. (in):		30.0	
Eff. pile seg. (ft):		8.0	
p.u (ksi):		1.54E-01	
y.c (in.):		3.00	
p/pu	y/y.c	P kip	y in.
0.000	0.00	0.0	0.0
0.500	1.00	222.3	3.0
0.720	3.00	320.1	9.0
1.000	8.00	444.6	24.0
1.000	9.00	444.6	27.0

Spring:	4		
Pile Diam. (in):		30.0	
Eff. pile seg. (ft):		8.0	
p.u (ksi):		2.01E-01	
y.c (in.):		3.00	
p/pu	y/y.c	P kip	y in.
0.000	0.00	0.0	0.0
0.500	1.00	289.8	3.0
0.720	3.00	417.4	9.0
1.000	8.00	579.7	24.0
1.000	9.00	579.7	27.0

Spring:	5		
Pile Diam. (in):		30.0	
Eff. pile seg. (ft):		8.0	
p.u (ksi):		2.16E-01	
y.c (in.):		3.00	
p/pu	y/y.c	P kip	y in.
0.000	0.00	0.0	0.0
0.500	1.00	310.9	3.0
0.720	3.00	447.7	9.0
1.000	8.00	621.8	24.0
1.000	9.00	621.8	27.0

Spring:	6		
Pile Diam. (in):		30.0	
Eff. pile seg. (ft):		20.0	
p.u (ksi):		2.45E-01	
y.c (in.):		3.00	
p/pu	y/y.c	P kip	y in.
0.000	0.00	0.0	0.0
0.500	1.00	880.9	3.0
0.720	3.00	1268.5	9.0
1.000	8.00	1761.8	24.0
1.000	9.00	1761.8	27.0

Spring:	7		
Pile Diam. (in):		30.0	
Eff. pile seg. (ft):		20.0	
p.u (ksi):		2.86E-01	
y.c (in.):		3.00	
p/pu	y/y.c	P kip	y in.
0.000	0.00	0.0	0.0
0.500	1.00	1028.9	3.0
0.720	3.00	1481.7	9.0
1.000	8.00	2057.9	24.0
1.000	9.00	2057.9	27.0

Spring:	8		
Pile Diam. (in):		30.0	
Eff. pile seg. (ft):		20.0	
p.u (ksi):		3.39E-01	
y.c (in.):		3.00	
p/pu	y/y.c	P kip	y in.
0.000	0.00	0.0	0.0
0.500	1.00	1221.4	3.0
0.720	3.00	1758.8	9.0
1.000	8.00	2442.8	24.0
1.000	9.00	2442.8	27.0

Spring:	9
Pile Diam. (in):	30.0
Eff. pile seg. (ft):	40.0
p.u (ksi):	4.11E-01
y.c (in.):	3.00

p/pu	y/y.c	P kip	y in.
0.000	0.00	0.0	0.0
0.500	1.00	2961.0	3.0
0.720	3.00	4263.8	9.0
1.000	8.00	5922.0	24.0
1.000	9.00	5922.0	27.0

Spring:	10
Pile Diam. (in):	30.0
Eff. pile seg. (ft):	40.0
p.u (ksi):	5.86E-01
y.c (in.):	3.00

p/pu	y/y.c	P kip	y in.
0.000	0.00	0.0	0.0
0.500	1.00	4219.4	3.0
0.720	3.00	6076.0	9.0
1.000	8.00	8438.9	24.0
1.000	9.00	8438.9	27.0

Spring	Top Depth	Bottom Depth	True Length	Unit Skin Friction kips/sf	Friction Capacity kip
1	0.0	8.0	8.03	0.800	50.44
2	8.0	16.0	8.03	0.850	53.59
3	16.0	24.0	8.03	0.950	59.90
4	24.0	32.0	8.03	1.000	63.05
5	32.0	40.0	8.03	1.000	63.05
6	40.0	60.0	20.07	1.000	157.63
7	60.0	80.0	20.07	1.000	157.63
8	80.0	100.0	20.07	1.000	157.63
9	100.0	140.0	40.14	1.500	472.89
10	140.0	180.0	40.14	2.000	630.52
			180.63		1866.33

Spring 1 Diam. Pile: Shear Cap.	30.00 50.44	inches kips	
Z/D	t/tmax	t kip	Z in.
0.0000	0.00	0.00	0.00
0.0016	0.30	15.13	0.05
0.0031	0.50	25.22	0.09
0.0057	0.75	37.83	0.17
0.0080	0.90	45.40	0.24
0.0100	1.00	50.44	0.30
0.0200	0.70	35.31	0.60
0.5000	0.70	35.31	15.00

Spring 2 Diam. Pile: Shear Cap.	30.00 53.59	inches kips	
Z/D	t/tmax	t kip	Z in.
0.0000	0.00	0.00	0.00
0.0016	0.30	16.08	0.05
0.0031	0.50	26.80	0.09
0.0057	0.75	40.20	0.17
0.0080	0.90	48.23	0.24
0.0100	1.00	53.59	0.30
0.0200	0.70	37.52	0.60
0.5000	0.70	37.52	15.00

Spring 3 Diam. Pile: Shear Cap.	30.00 59.90	inches kips	
Z/D	t/tmax	t kip	Z in.
0.0000	0.00	0.00	0.00
0.0016	0.30	17.97	0.05
0.0031	0.50	29.95	0.09
0.0057	0.75	44.92	0.17
0.0080	0.90	53.91	0.24
0.0100	1.00	59.90	0.30
0.0200	0.70	41.93	0.60
0.5000	0.70	41.93	15.00

Spring 4 Diam. Pile: Shear Cap.	30.00 63.05	inches kips	
Z/D	t/tmax	t kip	Z in.
0.0000	0.00	0.00	0.00
0.0016	0.30	18.92	0.05
0.0031	0.50	31.53	0.09
0.0057	0.75	47.29	0.17
0.0080	0.90	56.75	0.24
0.0100	1.00	63.05	0.30
0.0200	0.70	44.14	0.60
0.5000	0.70	44.14	15.00

Spring 5 Diam. Pile: Shear Cap.	30.00 63.05	inches kips	
Z/D	t/tmax	t kip	Z in.
0.0000	0.00	0.00	0.00
0.0016	0.30	18.92	0.05
0.0031	0.50	31.53	0.09
0.0057	0.75	47.29	0.17
0.0080	0.90	56.75	0.24
0.0100	1.00	63.05	0.30
0.0200	0.70	44.14	0.60
0.5000	0.70	44.14	15.00

Spring 6 Diam. Pile: Shear Cap.	30.00 157.63	inches kips	
Z/D	t/tmax	t kip	Z in.
0.0000	0.00	0.00	0.00
0.0016	0.30	47.29	0.05
0.0031	0.50	78.81	0.09
0.0057	0.75	118.22	0.17
0.0080	0.90	141.87	0.24
0.0100	1.00	157.63	0.30
0.0200	0.70	110.34	0.60
0.5000	0.70	110.34	15.00

Spring 7 Diam. Pile: Shear Cap.	30.00 157.63	inches kips	
Z/D	t/tmax	t kip	Z in.
0.0000	0.00	0.00	0.00
0.0016	0.30	47.29	0.05
0.0031	0.50	78.81	0.09
0.0057	0.75	118.22	0.17
0.0080	0.90	141.87	0.24
0.0100	1.00	157.63	0.30
0.0200	0.70	110.34	0.60
0.5000	0.70	110.34	15.00

Spring 8 Diam. Pile: Shear Cap.	30.00 157.63	inches kips	
Z/D	t/tmax	t kip	Z in.
0.0000	0.00	0.00	0.00
0.0016	0.30	47.29	0.05
0.0031	0.50	78.81	0.09
0.0057	0.75	118.22	0.17
0.0080	0.90	141.87	0.24
0.0100	1.00	157.63	0.30
0.0200	0.70	110.34	0.60
0.5000	0.70	110.34	15.00

Spring 9 Diam. Pile: Shear Cap.	30.00 472.89	inches kips	
Z/D	t/tmax	t kip	Z in.
0.0000	0.00	0.00	0.00
0.0016	0.30	141.87	0.05
0.0031	0.50	236.44	0.09
0.0057	0.75	354.67	0.17
0.0080	0.90	425.60	0.24
0.0100	1.00	472.89	0.30
0.0200	0.70	331.02	0.60
0.5000	0.70	331.02	15.00

Spring 10 Diam. Pile: Shear Cap.	30.00 630.52	inches kips	
Z/D	t/tmax	t kip	Z in.
0.0000	0.00	0.00	0.00
0.0016	0.30	189.15	0.05
0.0031	0.50	315.26	0.09
0.0057	0.75	472.89	0.17
0.0080	0.90	567.46	0.24
0.0100	1.00	630.52	0.30
0.0200	0.70	441.36	0.60
0.5000	0.70	441.36	15.00

End Bearing Spring

Pile Diameter 30.00 inch

End Area 707.83 sq. inches

Bearing Cap. 172.04 kips

Z/D	Q/Qp	Q kip	Z in.
0.000	0.00	0.00	0.00
0.002	0.30	212.35	0.07
0.013	0.50	353.92	0.47
0.042	0.75	530.88	1.51
0.073	0.90	637.05	2.63
0.100	1.00	707.83	3.60
0.500	1.00	707.83	18.00